UNIVERSITÀ DEGLI STUDI DI PADOVA

DIPARTIMENTO DI TECNICA E GESTIONE DEI SISTEMI INDUSTRIALI

RHEINISCH-WESTFÄLISCHE TECHNISCHE HOCHSCHULE AACHEN

GIESSEREI INSTITUT

Master-Thesis

Optimization and simulation of the directional solidification in an industrial scaled Bridgman furnace for a eutectic NiAl-(CrMo) alloy

Presented by: Mattia Piron B.Sc.

Supervisor: Prof Dr.-Ing. Andreas Bührig-Polaczek
Prof. Ing. Franco Bonollo
Dipl.–Ing. Samuel Bogner
Thomas Vossel M.Sc.

Aachen, summer semester 2015

Statement of Authorship:

I, Mattia Piron, hereby declare that this thesis has been composed in sole authorship by the undersigned with no other help by third-parties and sources other than indicated in the thesis itself.

_____ _____

Place, Date Name

Acknowledgement

Firstly, I would like to express my sincere gratitude to Prof. Dr.-Ing. Andreas Bührig-Polaczek, and Prof.-Ing. Franco Bonollo, for giving me the great opportunity to write the thesis at RWTH Aachen University.

Then, I would like to thank my supervisors Dipl.-Ing Samuel Bogner and Thomas Vossel M.Sc. for having trained me about all the work done, for the continuous support, patience, and for their knowledge that helped me a lot. Their guidance helped me in all the parts of my thesis.

I'm also grateful to Romuald Laqua for his truly important assistance with the simulation software Star-CCM+, simulation that cannot be done without him, to Elke Schaberger, Elke Zimmermann and Martina Thönnißen for help me during all stages of preparation and analysis of the specimens, and in general a big thanks to all the Access staff.

A special thanks to my parents, which made possible all my studies and this special opportunity to study abroad and overall a big thank you to all my family to support me in all moment of my life.

Last but not least, thank you to all the friends meet here in Aachen, that helped to make these six months the best time of my life, and a really special thanks to Angelica and Salvatore, for their friendship and for the unforgettable moments spent together. I cannot imagine this time without them, thank you!

Table of contents:

1 Abstract ... iii

2 Motivation ... 1

3 Theory & Literature Review ... 3

3.1 Solidification ... 3

3.1.1 Eutectic growth ... 10

3.1.2 Directional solidification ... 15

3.2 Ni Al Alloy ... 25

3.2.1 Ni Al 28Cr 6Mo ... 28

3.3 Investment casting ... 29

3.4 Simulation ... 32

4 Experimental ... 35

4.1 Physical experiment ... 36

4.2 Simulation ... 46

5 Results and discussion ... 53

5.1 Physical experiment ... 53

5.1.1 Undercooling ... 53

5.1.2 Directional solidification ... 57

5.2 Simulation ... 66

6 Conclusion and outlook ... 77

7 Bibliography ... 81

8 Compendio ... 83

8.1 Motivazione ... 83

8.2 Teoria e letteratura ... 84

8.2.1 Solidificazione ... 84

8.2.2 Solidificazione eutettica ... 84

8.2.3 Solidificazione direzionale ... 85

8.2.4 Leghe nickel-alluminio ... 86

8.2.5 NiAl 28Cr 6Mo ... 86

8.2.6 Investment casting ... 86

8.2.7 Simulazione ... 86

8.3 Sperimentazione 87
8.3.1 Sperimentazione fisica 87
8.3.2 Simulazione 89
8.4 Risultati e discussione 90
8.4.1 Sperimentazione fisica 90
8.4.2 Simulazione 94
8.5 Conclusioni e prospettive future 96

1 Abstract

One of the most interesting engines for power production and aerospace industry is the turbine engine, because of its high power to weight ratio. The major problem of these engines is that, in order to give an interesting value of efficiency, the working temperature must be very high. NiAl is an interesting intermetallic alloy because of its low density and high thermal conductivity, compared to the nickel-based superalloys usually used for these applications, that can raise the efficiency of the engine and lower the weight, which can give an important improvement in performances.

The major problem of this alloy is its brittleness at ambient temperature that could be very problematic and can lead to a breakage of the turbine blade. In order to solve this problem a composite material can be used, in order to improve the fracture toughness. This is because the fracture mode of a composite material is very complicated, the presence of the matrix and fibers disturbs the propagation of the crack and then the fracture behavior is much better compared to the single components properties.

During this work, a solidification of the NiAl 28Cr 6Mo alloy was investigated, in order to obtain an in-situ composite material. An in-situ composite material is a composite formed during the solidification, working with eutectic or near eutectic alloy. During the solidification of these materials, two (or more) phase growth together, a matrix as first phase and a fiber as second phases. With the appropriate control on the solidification, it's possible to create an aligned fibrous second phase.

The work was completed in two parts done simultaneously. During the first part, a physical model was produced and analyzed with an optical and electronic microscope. In the second part the same model was reproduced using CAD software, and then the entire process was simulated with the FEM CFD software STAR CCM+. The first simulation was conducted with the same parameters used for the physical experiment, in order to check that the results are comparable and, if not, to adapt the model. When the model is ready the process can be simulated with various configurations. The goal is to obtain a planar front of solidification, in order to obtain well aligned lamellae of the second phase in the material.

For the analysis of the experimentally obtained specimen, there are two effects observed, that influence the alignment of the Cr(Mo) lamellae. On the microscopic scale a planar solidification morphology with a stable eutectic growth leads to high alignment of Cr(Mo), while on the macroscopic scale a plain solidification front without any curvature maintains a high Cr(Mo) orientation parallel to the directional solidification.

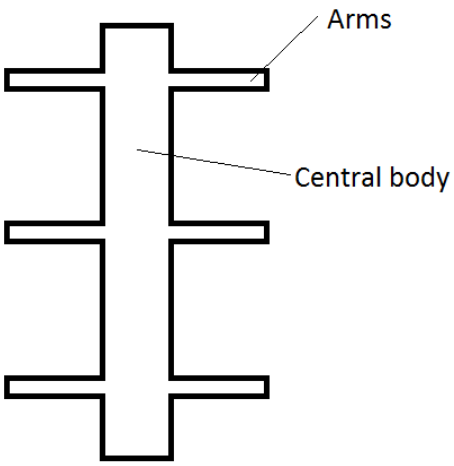

Figure 1-1: Shape of the used specimen

During the analysis of the sample, it is clear that with the parameters derived from the experiment the simulated solidification is directional, but the lamellae are not perfectly aligned in all the section of the specimen. In the central body of the specimen the microscopic shape of the front of solidification is in cells form, instead of being planar. This fact leads to curved lamellae, instead of a flat solidification front. Where there is a change of shape the structure becomes disordered and a directional growth is not visible. Moreover, the lamellae are not only curved, but also present some zones with dendritic growth. During the simulation, it can be seen that the macroscopic front of solidification in the central body is almost planar, but in the arms it is not. With this information, the first improvement of the process should be towards the shape of the solidification front.

With lower withdrawal velocity and higher temperature gradient, the front of solidification becomes planar in both central body and arms, instead of only in the central body. This means that it is possible to obtain a macroscopic planar front of solidification in all areas of the specimen, and this can lead to a regular structure. To ensure the achievement of the desired microstructure, the microscopic shape of the solidification front must be investigated, with a second physical test. In fact the correct pair of withdrawal velocity and temperature gradient that led to a planar macroscopic solidification front could lead to a cellular or dendritic microscopic shape of the solidification front. This could happen, for example, if the withdrawal velocity is too high. Moreover, a mushy zone is present due to the presence of a range of solidification temperature. Because of that, dendrites can grow leading to a non-regular structure. The used alloy must be eutectic, but is not, due to the difficulties to reach a high grade of control of the composition, so an improvement of the process can be a better control of the alloy composition. Moreover there is a difference in the temperature gradient in the arms, where there is change of cross-section, compared to the body. This probably is due to the big change of cross-section in this specimen; so that a better design of the shape, for example the use of filleted corner or more graduated change of section, can lead to a better solidification behavior.

In conclusion, it is possible to obtain a planar front of solidification, but not with the used furnace. This furnace in fact can reach a maximum temperature of 1620 °C but the

simulation done with the software are all at higher temperature, cannot be reached in a new physical experiment. There is a necessity of a furnace that can reach a higher temperature. With these new physical experiments, the microscopic front of solidification could be investigated.

2 Motivation

The continued search of increased thrust or improved efficiency of gas turbines has led to a necessity of materials with high resistance at higher temperature for critical components, such as turbine blades. In fact, the efficiency of all heat engines is directly related to the upper temperature of the thermodynamics cycle. Then, progress in gas turbine is due to the progress in material of blades. The target of material requirements depends on the field of applications of the turbine. For military aero-gas turbines where the life can be relatively short and the focus is in maximizing the thrust, the chief objective is in developing materials that retain their strengths at higher temperatures. For improving the fuel consumption a higher compression ratio is necessary, but the turbine entry temperature can be lowered. In case of gas turbines for marine, commercial or industrial applications, where long live and low fuel consumption are essential, improvements in high temperature corrosion should be aimed for rather than mechanical behavior (McLean, 1983).

Since the invention of gas turbines in 1930, the turbine entry temperature has been progressively raised with a combination of improvements in materials and design (like air-cooled blades). With the introduction of investment casting rather than machining of blade the materials development is attributed directly to the alloy and process selection. Each turbine blade is subjected to a centrifugal force and high temperature as such the creep fracture strength and thermal fatigue strength are important. Creep fracture and thermal fatigue are associated to the grain boundaries transverse to the applied stress. By reducing the density of transverse grain boundaries it is possible to increase ductility and inhibit grain fracture, as seen by VerSnyder and co-workers (Shank, 1970). This is possible with directional casting procedure which produces elongated grains, as demonstrated by Northcott in 1930 (Northcott, 1938). Then, the directional solidification has been the actual state-of-art in turbine blades. The next step is the casting of single-crystal rather than columnar grain structures, and composite materials made by eutectic or near-eutectic alloys (McLean, 1983).

The standard alloys used right now for this purposes are all Nickel-based alloy because of its exceptional combination of high temperature strength, toughness and oxidizing resistance. The creep resistance is dependent on slowing the speed of dislocation motion within a crystalline structure, the γ’ cubic-like precipitates (Figure 2-1) present within the structure act as a barrier to dislocation motion.

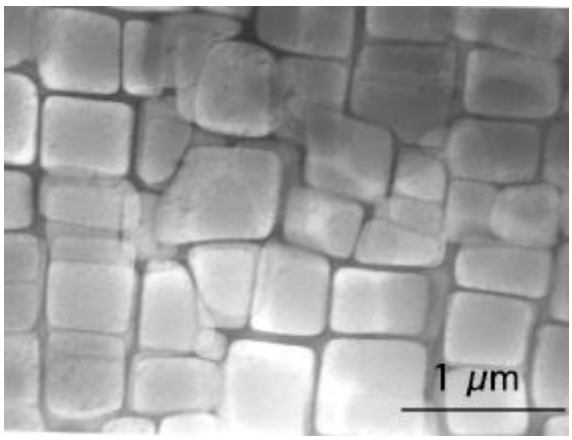

Figure 2-1: Transmission electron micrograph showing a large fraction of cuboidal γ' particles in a γ matrix. (Hillier, 1984)

The properties of the Ni-based alloy can be tailored by addition of both metallic and non-metallic elements, like chromium, iron, cobalt, tantalum, titanium, carbon and so on. Chromium and aluminum are essentials for oxidation resistance, boron and zirconium are grain boundary strengthening elements, and many other elements works as carbide formers, that precipitate at grain boundaries and hence reduce the tendency for grain boundary sliding.

As said before the goal is to raise the working temperature of these alloys. At these temperatures, corrosion and oxidation are important, for this reason coating was studied. Coatings are designed to protect the alloy from high temperature oxidation and corrosion. Initially, the NiAl alloy was used as coating, because of its highly oxidation resistant.

Other advantages of the NiAl alloy, compared to the other Nickel-based alloy, are its low density and high thermal conductivity. For these reasons create an entire turbine blade with this alloy, instead of using only as coating, can lower the weight and raise the turbine entry temperature, because the higher thermal conductivity lead to a better cooling. The mainly problem is that this alloy is very brittle at ambient temperature.

By using a eutectic alloy and directional solidification, it is possible to create during the solidification an in-situ composite that can raise the strength of the material and thus a brittle fracture can be avoided.

3 Theory & Literature Review

In this chapter I will discuss a general theory of all the aspects used during this work. A directionally solidified investment casting specimen will be produced physically and re-produced via software, thus a theory of solidification, casting production and software-simulation will be discussed.

3.1 Solidification

Solidification is a phase transformation from liquid to solid, that start from a nucleation point in the liquid, where one single particle became solid, until the complete solidification of the all melt. Nowadays, cast metal products can be economically produced from alloys having melting points as high as l660°C. (W. Kurz, 1992)

The main advantages of the melting process is that the liquid metal has a very low viscosity, then also complicate shape can be formed with low effort, compared to other process like forging or similar. Moreover, from starting to a liquid metal with different technique of cooling the microstructure can be changed in order to obtain the desired properties of the material.

In most of the alloy the solid and liquid temperature is different. These values depend on which components there are in the alloy, and in which percentage, and the exact value can be found on phase diagram (Figure 3-1).

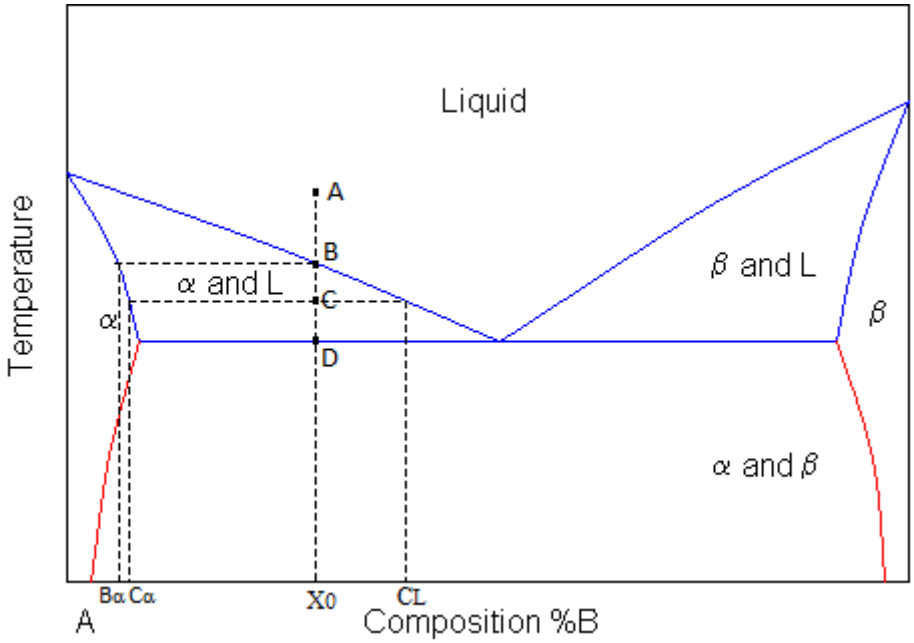

Figure 3-1: Typical binary phase diagram, (Cambridge)

These diagrams show the equilibrium states of an alloy, so with a given composition between the two mixtures and a temperature it is possible to find which phases is formed. It is possible also to know which phases with which composition is forming during the solidification. As example, composition X was taken (see Figure 3-1). At point A, this alloy was completely liquid. Lowering the temperature, at point B the first particles at composition B_α nucleate. In this point all the material was liquid, but with lowering again the temperature these particle growth. In every parts of the diagram it is possible to calculate the quantity of the two phases. For example, at point C the solid part of the melt is at composition C_α, while the liquid part is at composition C_L, and the weight percentage of the two phases can be calculated with the lever rule (eqn 3.1 and 3.2).

$$X_S = \frac{C_L - X_0}{C_L - C_\alpha} \tag{3.1}$$

$$X_L = \frac{X_0 - C_\alpha}{C_L - C_\alpha} \tag{3.2}$$

Then it is clear that for an alloy a single solidification temperature does not exist, but there is a of solidification temperature interval. This is true for almost all compositions, except for eutectic compositions, where there is only. The eutectic solidification will be treated later.

As said before, the solidification begins with nucleation, which is a process of formation of stable crystallization centers of a new phase. The nucleation can be homogenous or heterogeneous, depending on the value of undercooling of the liquid phase.

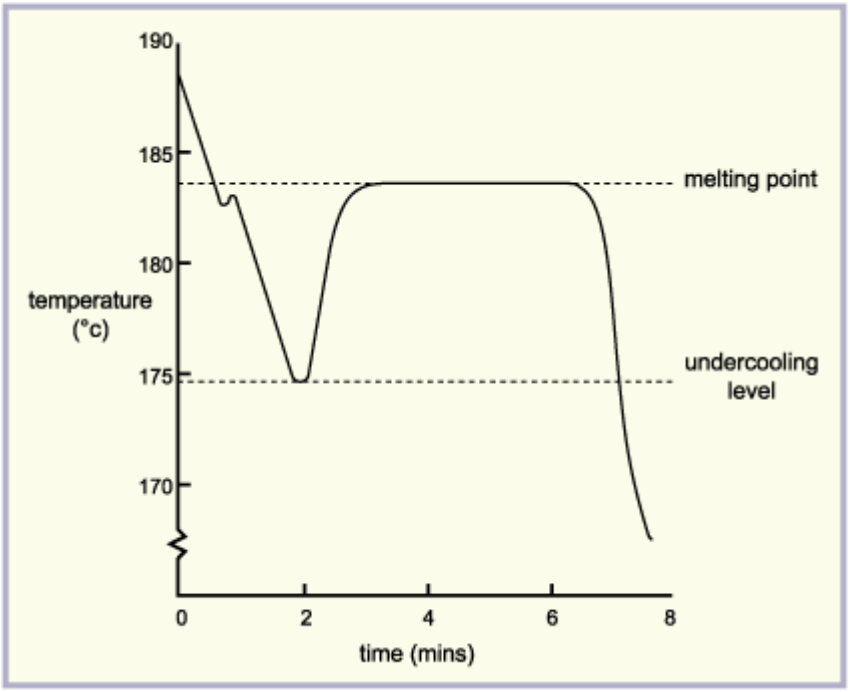

Figure 3-2: Partial cooling curve, showing the undercooling required to nucleate the primary crystals, (mtarr.co.uk, 1988)

The precipitation of the crystal is not spontaneous, but requires some activation energy. This is usually supplied thermally, by the undercooling effect (Figure 3-2). Heterogeneous nucleation begins from impurity in the melt, existing nuclei or from nucleation site like the mold wall. The activation energy is here lower compared to homogeneous nucleation. If in the melt there aren't other solid particles, then homogeneous nucleation occurs. During solidification in conventional casting or ingot, near the mold wall the temperature gradient is high, especially if the mold is cooled, and there is probably the presence of nucleation site in the mold wall. For these reason the solidification began from the mold wall and growth toward the center of the ingot. At the beginning the solidification is then from the wall to the center and it's similar to a directional solidification, with the formation of columnar zone (Figure 3-3).

It's clear that the nucleation don't happen only in one part of the melt and then growth until all the liquid metal become solid. In the melt there is a lot of nucleation site, that

growth at the same time, creating a lot of solid particles in the melt. When the material is completely solidified, all these growth particles form the grain, small crystals with random orientation of the crystal-lattice. The material formed during conventional casting, then, is not a unique grain, but is formed by a lot of grain attached together. The interface between these grains is called grain boundary that are defects of the material with pros and cons. The main advantage of these grains boundary is that can block dislocations with a strengthening of the material at low temperature, but this fact is not important for the purpose of this thesis.

The disadvantages of these grains are that tend to decrease electrical and thermal conductivity, can be promoting the corrosion and lowered the creep-strength of the material, at both low and high temperature. This last effect is called Coble creep that occurs through the diffusion of atoms in a material along the grain boundaries, which produces a net flow of material and a sliding of the grain boundaries. For this reason, for component (like the turbine blade) that must work with high stress along one direction and high temperature, the creep strength is very important and then the grain boundaries are to be avoided. They can be avoided with directional solidification, described later.

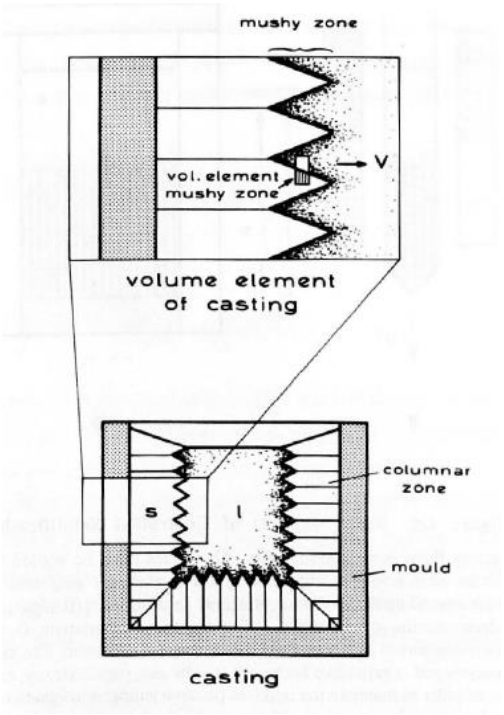

Figure 3-3: Solidification in Conventional Castings and Ingots (W. Kurz, 1992)

During the growth of the columnar zone, three regions can be distinguished. These are the liquid, the liquid plus solid (so-called mushy zone), and the solid region. The mushy zone is the region where all of the microstructural characteristics are determined, e.g. the shape, size, and distribution of concentration variations, precipitates, and pores. An infinitesimally narrow volume element which is fixed in the mushy zone and is perpendicular to the overall growth direction permits a description of the microscopic solidification process and therefore of the scale and composition of the microstructure. (W. Kurz, 1992)

Beyond a certain distance from the wall, some parts of the columnar zone can detached and growth independently. In these solid parts the heat it's extracted radially, and then the growth is equiaxed. This happens when nucleation

occurs in the liquid ahead of the columnar zone. The solidified region containing them is called the inner equiaxed zone (Figure 3-4). The transition from columnar to equiaxed growth is highly dependent upon the degree of convection in the liquid. In continuous casting machines, electromagnetic stirring is often used to promote this transition and lead to superior soundness at the ingot center. (W. Kurz, 1992)

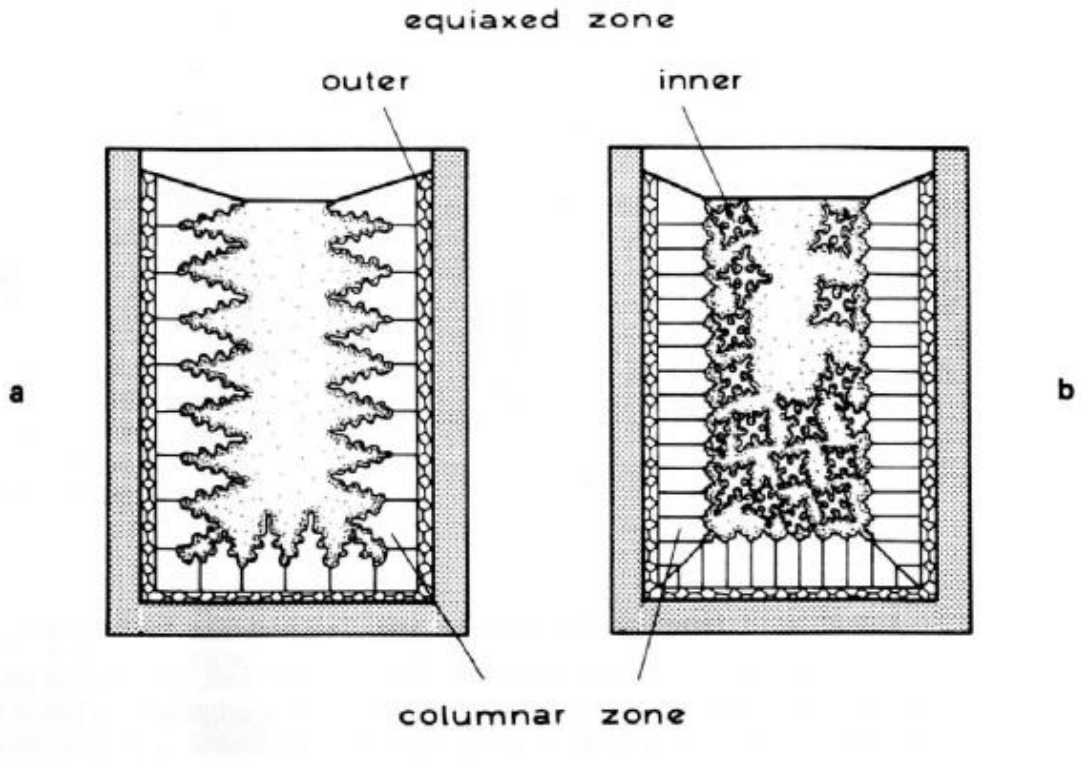

Figure 3-4: Structural Zone Formation in Castings (W. Kurz, 1992)

It is possible to find the growth rate of the melt during a conventional casting, with some boundary condition. The first, in case of ceramic shell mold, is that the thermal conductivity K_m of the shell mold is lower than the thermal conductivity of the metal (both solid and liquid). Then, the principal temperature gradient is in the mold wall. For simplicity, was considered a cylindrical mold with internal radius *a* and thickness *d*.

Flemings (M.C., 1974) considered the heat flow resulting from pouring a charge of liquid metal at its melting point T_m (i.e. no superheat) into a mould at temperature T_0 and, for mathematical simplicity, assumed that T_0 was maintained at the outside surface (Figure 3-5). The heat flow must satisfy the time-dependent Laplace equation:

$$\frac{\partial^2 T}{\partial r^2} + \frac{1}{r}\frac{\partial T}{\partial r} = \frac{1}{\alpha_m}\frac{\partial T}{\partial t} \tag{3.3}$$

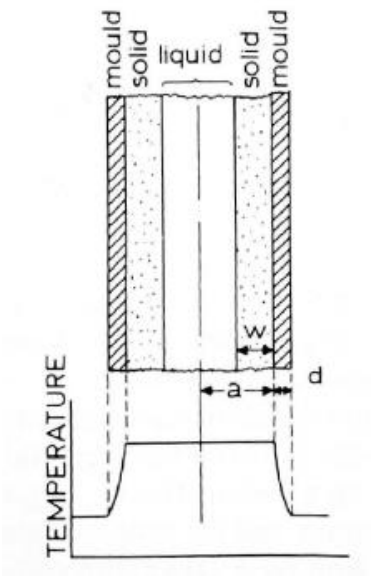

Figure 3-5: Mold configurations and temperature distribution during conventional casting (McLean, 1983)

Where $\alpha_m = K_m/\rho_m C_m$ is the heat diffusivity, ρ_m= mould density, C_m= specific heat of mould, t is time and r is the radial distance from the cylinder axis. The equation 3.3 was solved with an appropriate boundary condition, and the expression for the thickness of the solidified was found.

$$w = \left(\frac{T_m - T_0}{\rho_m L_f}\right)\left[\frac{2}{\sqrt{\pi}}\left(\frac{K_m}{\rho_m C_m}\right)^{1/2} t^{1/2} + \frac{K_m t}{2a}\right] \qquad (3.4)$$

Thus the growth rate decreases as the solid/melt interface progresses towards the center of the casting (McLean, 1983).

As said before, the engineering materials are alloys, and then they have a range of melting temperatures.

Figure 3-6 shows portions of idealized phase diagrams where increasing solute concentration leads to either decreased (Fig. 2a) or increased (Fig. 2b) melting temperatures. In both cases the addition of solute gives rise to a finite melting range. The liquidus and solidus boundaries are represented by straight lines of slopes m_L and m_S respectively and it is convenient to relate the liquidus and solidus concentrations at a given temperature (i.e. C_L, C_S respectively) by a partition coefficient k:

$$k = \frac{C_S}{C_L} = \frac{1 - m_S^{-1}(T' - T_L)}{1 - m_L^{-1}(T' - T_L)} \qquad (3.5)$$

Where T' is the melting temperature of the pure solvent, and T_S, T_L are the solidus and liquidus temperatures of an arbitrary alloy. With this partition coefficient the composition at the beginning and at the end of solidification can be related with the starting composition of the alloy (Figure 3-7). Then, the first solid have a composition kC_0, the rejecting solute enrich the liquid, and then the last solid have a composition C_0/k. (McLean, 1983)

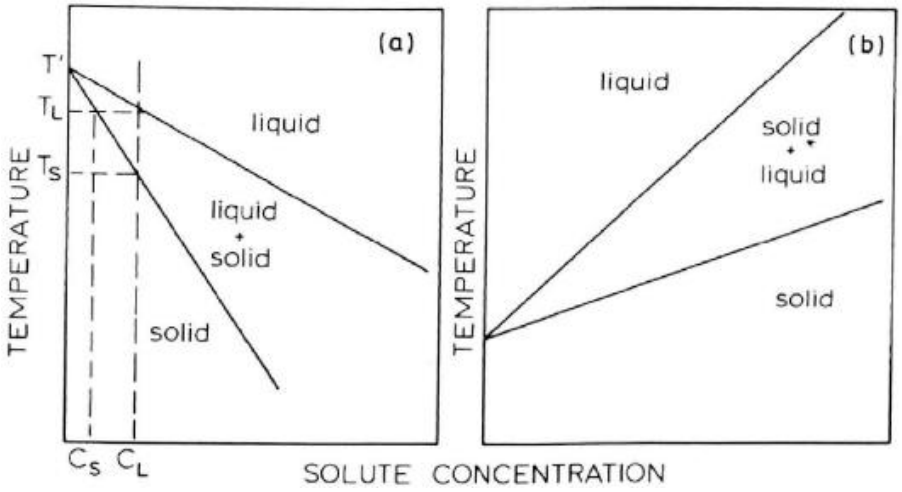

Figure 3-6: Schematic diagrams of simple binary phase diagrams showing (a) decreasing and (b) increasing melting temperatures with increasing solute concentration (McLean, 1983)

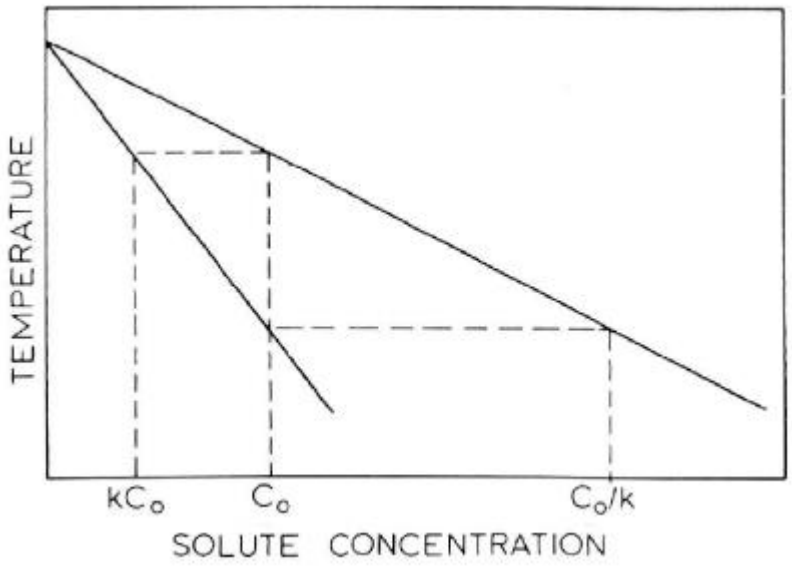

Figure 3-7: Equilibrium solidification (McLean, 1983)

As said before, the solidification begin with columnar, that can have planar, cellular (Figure 3-9) or dendritic solid/liquid interface, while in equiaxed growth the interface is unstable and lead to a dendritic solidification (Figure 3-8).

Dendritic solidification is a tree-like structure of crystal, and can form on one-component as well as multi-component material. Initially, the first solid formed have spherical shape. During the solidification the surface of the sphere becomes unstable and the solid begin to express a preferred growth direction, due for example to anisotropy in solid/liquid surface energy. The dendrite is the most important growth form.

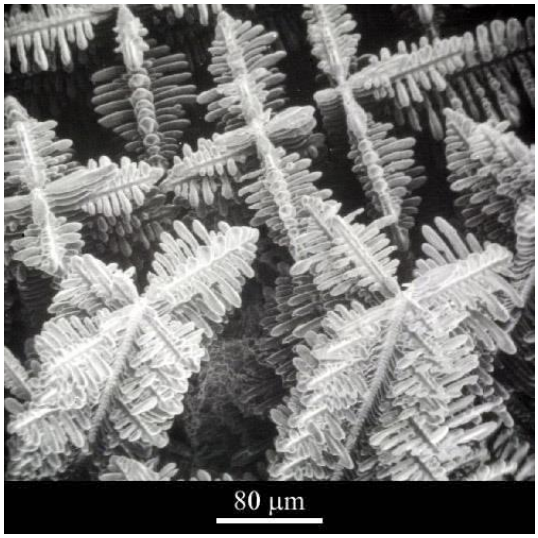

Figure 3-8: A typical dendrite growth (Cambridge)

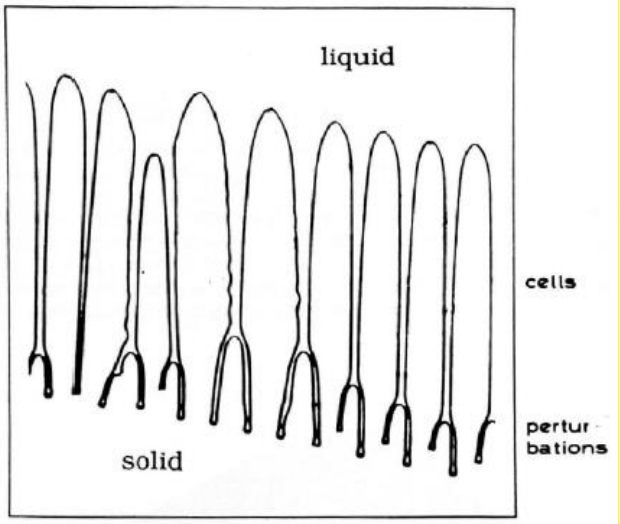

Figure 3-9: Breakdown of a Plane Solid/Liquid Interface to Give Cells (W. Kurz, 1992)

The cellular growth occurs when there is a breakdown of the planar solid/liquid interface. Perturbations are amplified until a marked difference in growth of the tips and depressions of the perturbed interface has occurred. As the tip can also reject solute in the lateral direction, it will tend to grow more rapidly than a depression, which tends to accumulate the excess solute rejected by the tips. Therefore, the form of perturbation is no longer sinusoidal, but adopts the form of cells.

3.1.1 Eutectic growth

As seen before, for each alloy there is a certain composition where only one solidification temperature exists, not a range (Figure 3-10). This temperature is the minimum melting temperature of this alloy, called eutectic temperature. The phase diagram was used in the same manner as explained in chapter 3.1. In a non-eutectic alloy, the formations of the two phases occur during the solidification temperature range, then with a certain period of time. During this time, with the phase diagram it is possible to anticipate the composition and the percentage quantity of the two phases. With a eutectic material, this is not possible. From liquid, the melt become solid in a (ideally) infinitesimal time. Then, the two (or more) phases in a eutectic material growth simultaneously. Due to their excellent casting behavior, which is often similar to that of a pure metal, and the advantageous composite properties which are exhibited when solid, casting alloys are often of near eutectic composition.

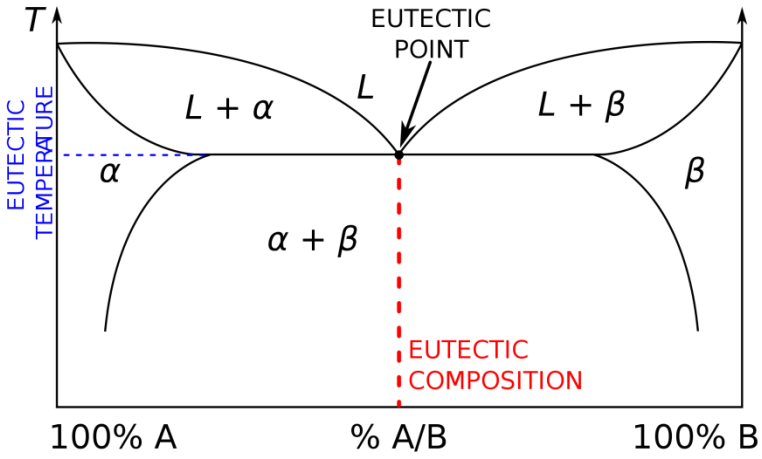

Figure 3-10: Eutectic composition in phase diagram

Due to the fact that they are composed of more than one phase, eutectics can exhibit a wide variety of geometrical arrangements.

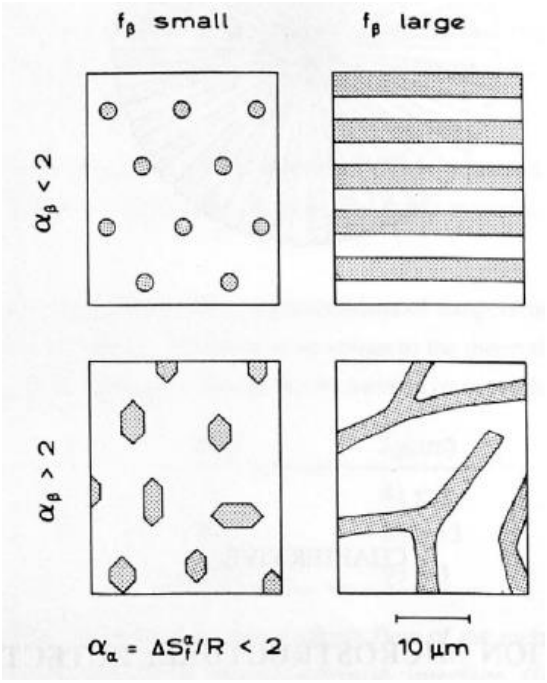

Figure 3-11: Types of binary eutectic morphology, in left picture the transversal and in the right the longitudinal intersections of the discretionally solidified microstructure (W. Kurz, 1992)

These geometrical shapes can be regular or irregular, fibrous or lamellar. In Figure 3-11 these eutectic morphologies are shown. In the upper part of the figure, the eutectic structure is regular. This happens when both the phases have low entropy of fusion. When the low volume fraction phase has high entropy of fusion, the structure is irregular, shown in the lower parts of the figure. The two images on the left in Figure 3-11 have a fibrous structure. This occurs when a small volume fraction of one phase is present. Conversely, with higher volume fraction is present, the preferred growth is the lamellae (right images).

We can suppose that when the volume fraction of one phase is between zero and 0.28, the eutectic will probably be fibrous, if it is between 0.28 and 0.50, the eutectic will tend to be lamellar.

In order to determine the growth behavior of the two eutectic phases, the simplest morphology for the solid/liquid interface will be assumed, i.e. that which exists during the

growth of a regular, lamellar eutectic. For this case, the problem can be treated in two dimensions. In Figure 3-12 the alloy is imagined to be growing in a crucible which is being moved vertically downwards at the rate *V'*. In a steady state thermal environment, this is equivalent to moving the solid/liquid interface at a rate *V=V'*. The alloy of eutectic composition is growing with its essentially isothermal interface at a temperature $T^*=T_e-\Delta T$ below the equilibrium eutectic temperature. It can be seen from the phase diagram that the two solid phases are of very different composition, while the melt composition, C_e, is intermediate in value. Obviously in the steady state, the mean composition of the solid must be equal to the composition of the melt. This makes it clear that eutectic growth is largely a question of diffusive mass transport. (W. Kurz, 1992)

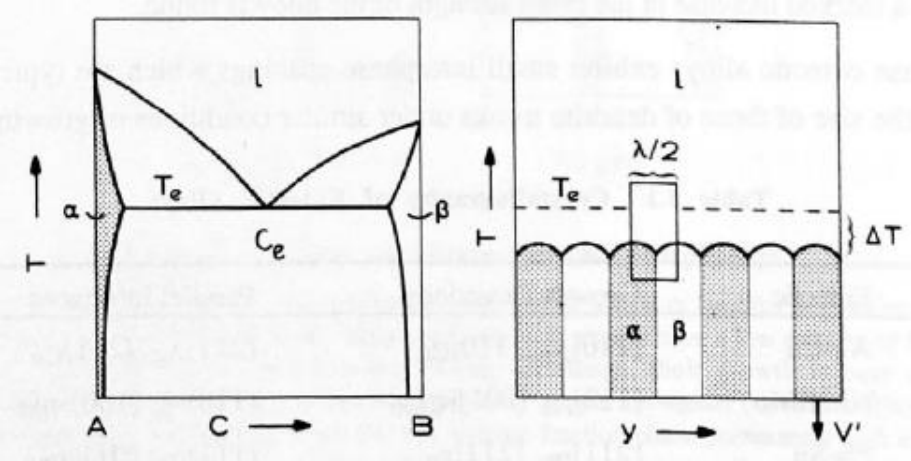

Figure 3-12: Eutectic phase diagram and regular lamellae growth, (W. Kurz, 1992)

During growth, the solid phases reject solute into the liquid. Thus, the α-phase will reject B-atoms into the melt, while the β-phase will reject A-atoms. The solute which is rejected by one phase is needed for the growth of the other. Therefore, lateral diffusion along the solid/liquid interface, at right-angles to the lamellae, will become dominant and lead to a decrease in the solute build-up ahead of both phases. A periodic diffusion field will be established. Because the maximum concentration differences at the interface (compared to the eutectic composition) are much smaller than in the case of single-phase growth, the temperature of the growing interface will be close to the equilibrium eutectic temperature. The diffusion field causes the λ-value of the structure to be minimized, and this leads to more rapid growth (Figure 3-13). (W. Kurz, 1992)

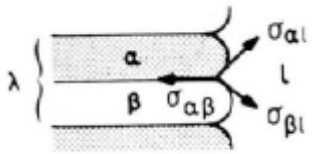

Figure 3-13: Effect of the diffusion at solid/liquid interface, (W. Kurz, 1992)

Then, during the solidification the paths of the B component rejected from the A component was shown in Figure 3-14 (a). Because of this reason the concentration in the liquid is not constant, but varies as in Figure 3-14 (b). We can find this concentration variation only in the liquid at the solid/liquid interface, but decays over one interphase spacing in the growth direction. The equilibrium between an attractive force arising from the diffusion field and a repulsive force between the three-phase junctions arising from capillarity effects at small λ determines the eutectic spacing. (W. Kurz, 1992)

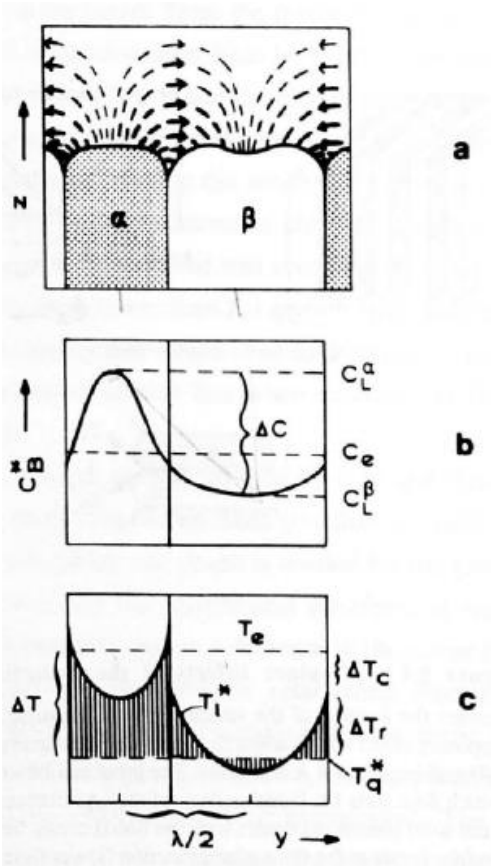

Figure 3-14: Eutectic interface concentration and temperature, (W. Kurz, 1992)

The growing interface can be regarded as being in a state of local thermodynamic equilibrium. This means that the measurable temperature, T_q^*, of the interface which is constant along the solid/liquid interface (over λ/2) corresponds to equilibrium at all points of the interface. Figure 3-14 (c) is a function of the local concentration and curvature. The sum of the solute (ΔT_c) and the curvature (ΔT_r) undercooling must be equal to the interface undercooling ΔT. A negative curvature, as shown here at the center of the β lamella, is required when the solute undercooling, ΔT_c, is higher than ΔT. The discontinuity in the solute undercooling is only an equilibrium temperature discontinuity and not a real temperature discontinuity. (W. Kurz, 1992)

Then, the corresponding liquidus temperature varies from values greater than T_e for certain regions of the α-phase, to values below the actual interface temperature, T_q^* for the central region of the β-phase. The difference has to be compensated by the local curvature in order to maintain the local equilibrium at the interface. Thus, since T_q^* is constant due to the high thermal conductivity and small dimensions of the phases, a negative curvature (depression) may appear at the center of a lamella in order to compensate for a high local solute-controlled interface undercooling

which is often associated with a large spacing, λ. The curvature of α/l (or β/l) interface, which is necessary in order to match the angles at the three phase junction, changes the equilibrium temperature by an amount, ΔT_r, which is a function of y. (W. Kurz, 1992)

In binary eutectic can be two types of morphological instability: single phase or two phase (Figure 3-15).

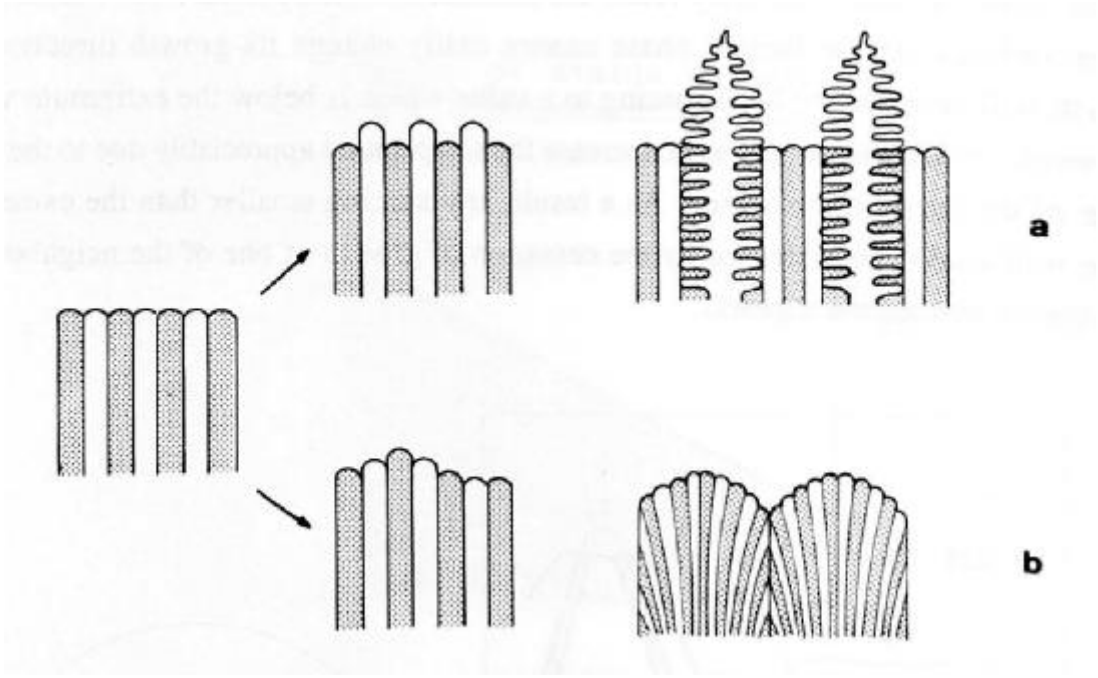

Figure 3-15: Type of eutectic interface instability, (W. Kurz, 1992)

The normally planar solid/liquid interface can become unstable and then lose their planar shape. In Figure 3-15 there are two different types of instability, instability of one phase (a) or instability of both phases (b). The instability of one phase arises when one phase to grows ahead of the other phase. This can happen if the alloy has an off-eutectic chemical composition. In this case, there is a small solidification temperature interval that permits to this phase to solidify earlier than the other. Considering that this phase grows earlier, the structure can be dendritic. The reason for the latter effect is that, due to the long-range boundary layer built up ahead of the solid/liquid interface in this case, one phase becomes heavily constitutionally undercooled. This can be deduced from the fact that, in an off-eutectic composition, the alloy liquidus is always higher than the eutectic temperature: the corresponding primary phase will be more highly undercooled and tend to grow faster than the eutectic (see Figure 3-16).

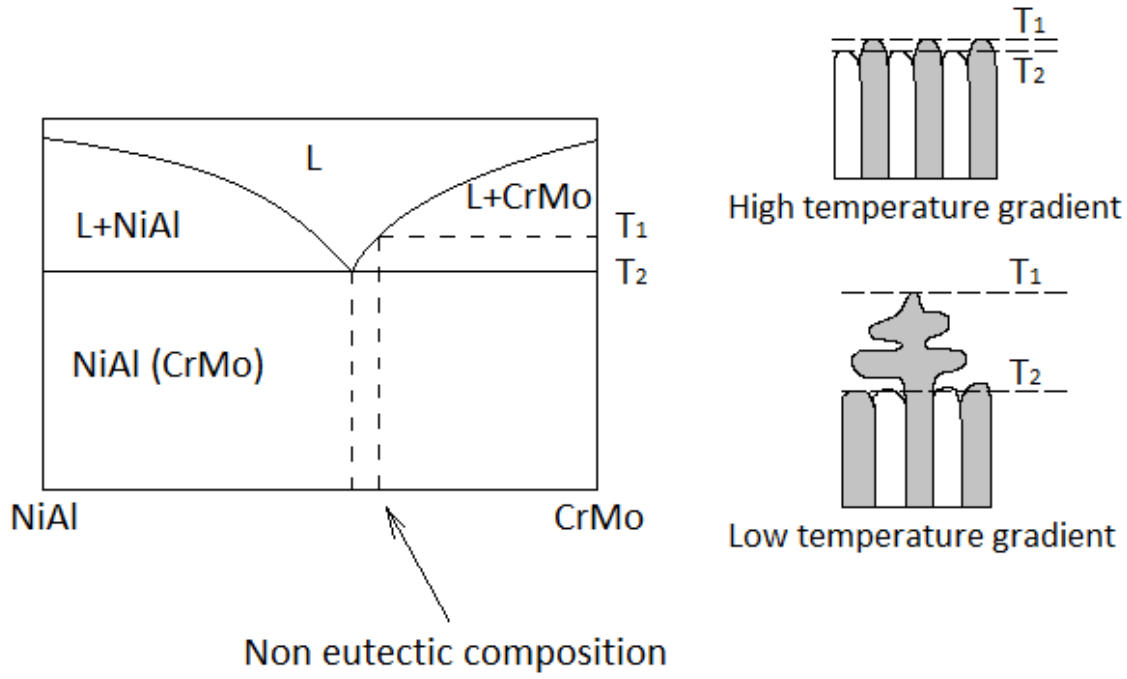

Figure 3-16: Effect of non-eutectic composition and temperature gradient

In the case of instability of both phases, a third element (impurity) may destabilize the morphology of the solid/liquid interface that can lead to an appearance of two phase eutectic cells, or even eutectic dendrite.

3.1.2 Directional solidification

Until now it has been described the behavior of a non-eutectic and eutectic alloy during a conventional solidification. It is seen in chapter 3.1 that, for components that have to work at high temperature and high longitudinal stress, the main problem of the conventional casting is the presence of the grain boundaries that lowered the creep strength of the material. With a directional solidification it is possible to remove the grain boundary longitudinal to the direction of the force, increasing the creep strength (Figure 3-17), or it is possible to create a mono-crystalline material without grain boundaries.

Figure 3-17: Elongated grains in a directional solidification of a turbine blade.

The directional solidification is a controlled process where the solidification starts in a precise point of the mold, and continues in a predefined direction under controlled parameters. The simplest method to obtain a directional solidification is with using a mold with good thermal conductivity at one end, and good insulation elsewhere. For example, the complete mold can be realized in ceramic material, but the base of the mold can be made with a cooled copper plate. The solidification then starts from the cooled copper plate, because of the high thermal gradient and consequently the high undercooling in the alloy near this plate. This method has some limits. The solidification is completely predetermined by the size and geometry of the component, by the thermal properties of the alloy, the properties of the mould and the cooling plate and by the initial temperature of the alloy. Consequently, there is no control in the various parts of the mold; this approach cannot be used to control the microstructure.

A better method to do a directional simulation is with moving furnace or ingot. The casting is removing at a controlled withdrawal velocity from the furnace maintained at full power (or vice versa).

The main purpose of the directional solidification is to control the grain morphology, in order to have aligned grain in the growth direction, but this process influences several other microstructural characteristics. For example, also the dendrites are similarly aligned, and with a eutectic alloy also the lamellae. Less obviously, but perhaps also of importance in relation to the mechanical behavior of the material, there is lower porosity than in the conventionally cast material and there are significant differences in the nature and distribution of the precipitated phases.

The microstructures obtained on solidifying complex alloys depend in a complicated manner on how the heat extracted from the solidifying material is distributed between normal heat flow mechanisms, such as radiation or conduction, and the latent heat L_f created on freezing. Directional solidification provides a particularly potent means of

controlling the heat flow characteristics and the associated microstructures in order to optimize particular properties. (McLean, 1983)

Kraft (Kraft, 1960) proposed to use the directional solidification in material that during solidification create two or more phases (like eutectic), in order to create a new class of material named in-situ composite. The goal to obtain is to create a brittle, but strong, fiber in the direction of the force, in order to improve the strength of the material in that direction. By definition, composite is material made from two or more constituent that, when combined, produce a material with better characteristic compared to the constituent. The main advantages to create in situ composite is that the final material is ready in a single stage, without the creation of the two material separately and then mixing it together. The main disadvantage is that the two constituent materials cannot be chosen for optimize the characteristic of the composite, but the choice are restricted to the appropriate eutectic material that have two phases with interesting characteristic and with high volume fraction of the two phases.

With directional solidification the casting is usually removed at a predetermined withdrawal rate V_w, normally constant, relative to the heating source, which maintains part of the charge molten, to some cooler zone below the alloy melting point. Consequently a temperature gradient is imposed along the solidifying material. Assuming that the solidifying interface is planar and advancing at a rate V_I, the heat balance there equates the heat of fusion to the differences in thermal conductivity of the solid and liquid alloy.

$$K_S G_S - K_L G_L = \rho_S L_f V_I \tag{3.6}$$

Where the subscripts S and L refer to the solid and liquid alloy respectively and K_i is the thermal conductivity, G_i is the temperature gradient and ρ_i is the density ($i = S$ *or* L) and L_f is the latent heat of fusion. This shows that V_I depends on the difference between $K_S G_S$ and $K_L G_L$ and that V_I, G_S and G_L are not independent variables. We can consider various extremes in the solidification behavior that will depend on the practical details of heat input and removal:

- If G_L and G_S can be fixed, then V_I is completely determined by eqn (3.6) and, consequently, is independent of the withdrawal rate V_w· However, this is physically unlikely.

- For a given macroscopic temperature gradient (determined by the furnace/casting arrangement) the maximum freezing rate V_I attainable without undercooling of the melt, i.e. V_I^{max}, occurs as $G_L \rightarrow 0$ and V_I^{max} increases with increasing G_S.
- For $V_I < V_I^{max}$, the values of G_S and G_L will adjust to satisfy eqn (3.6) and also will be compatible with the macroscopic temperature gradient imposed by the geometry of the furnace.

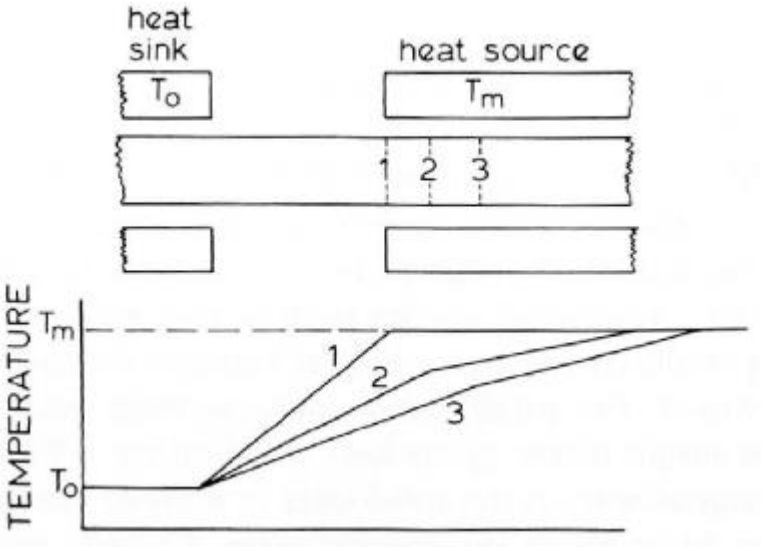

Figure 3-18: Schematic temperature profiles for different solidification rates: 1) $V_I = V_I^{max}$; 2) and 3) indicate decreasing V_I, (McLean, 1983)

Although it cannot be assumed that the rate of mould withdrawal V_w is identical to the velocity of the alloy melt/interface V_I, the major differences will be transient effects at the beginning and end of solidification; for most of the solidification length where the temperatures on either side of the solid/liquid interface attain steady state profiles, $V_I = Vw$. However, the position of the solid/liquid interface will vary, as indicated in Figure 3-18, giving values of G_L and G_S that depend on V_w. (McLean, 1983)

As seen before, the composition of the first solid that forms is kC_0, and then the solute concentration in the solid proceed toward C_0. In the solid, then, there is a concentration gradient. When heat flow and diffusion occur in the same single dimension and the solid/liquid interface is planar the solute concentration in the solid increases from kC_0 to C_0 over a characteristic distance x_c ((W.A. Tiller, 1953), (V.G. Smith, 1955)):

$$x_c = \frac{D_L}{kV_I} \tag{3.5}$$

A typical value of this x_c can be 0.5 mm; after this initial transient when the solute concentration in the solid approaches C_0 a steady state configuration is achieved. The concentration profile in the liquid decays from the equilibrium value C_0/k at the interface ($x = 0$) to C_0 at $x = \infty$ as indicated in Figure 3-19, (a).

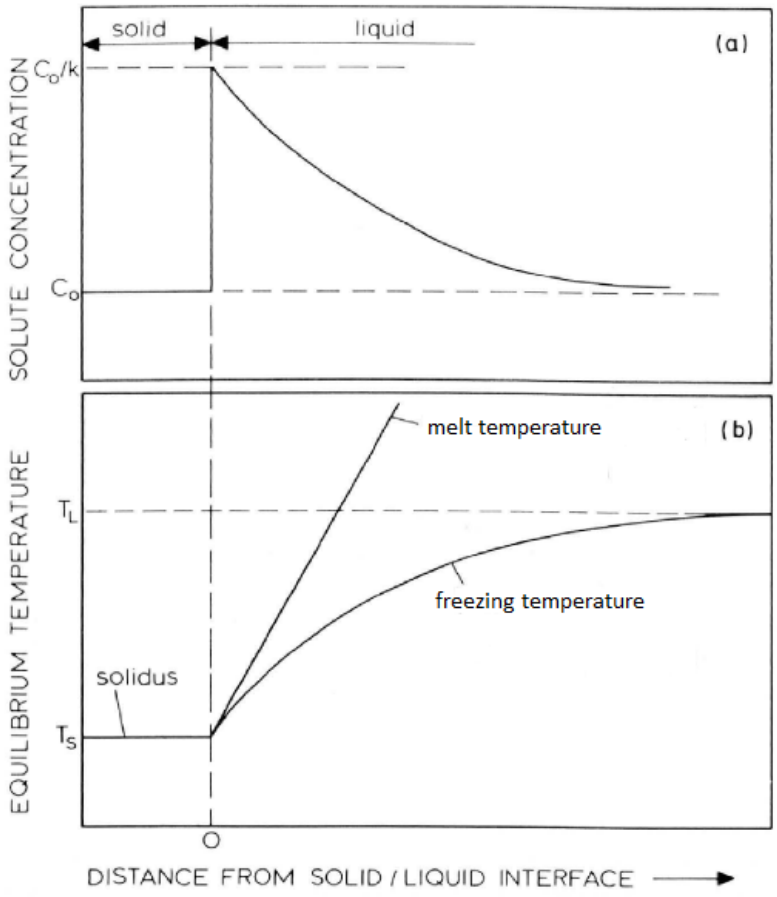

Figure 3-19: (a) Steady state concentration profile in the melt ahead of the solidifying interface. (b) Equilibrium liquidus temperatures associated with the varying composition ahead of the solidifying interface, (McLean, 1983)

The steady state solute distribution in the liquid must satisfy the Laplace diffusion equation:

$$D_L \frac{d^2 C_L}{dx^2} + V_I \frac{dC_L}{dx} = 0 \tag{3.8}$$

The first term represents the diffusion flux and the second the contribution from the moving boundary. Equation (3.6) must be solved with the boundary conditions:

$$C_L = \frac{C_0}{k} \; at \; x = 0$$
$$C_L = C_0 \; at \; x = \infty \tag{3.9}$$

And the flux continuity condition:

$$-D_L \frac{dC_L}{dx}\Big|_{x=0} = V_I C_0 (1-k) \tag{3.10}$$

The solution, first given by (W.A. Tiller, 1953), is:

$$C_L = C_0 \left[1 + \frac{1-k}{k} exp\left(-\frac{V_I x}{D_L}\right)\right] \tag{3.11}$$

As a consequence of this solute segregation in the liquid there is a local variation in the liquidus temperature ahead of the solidifying interface, shown schematically in Figure 3-19 b and defined by:

$$m_L(C_L - C_0) = T_L - T_S = m_L \frac{C_0(1-k)}{k} exp\left(-\frac{V_I x}{D_L}\right) \tag{3.12}$$

The gradient in liquidus temperature dT_L/dx at the solid/liquid interface is given by the expression:

$$\frac{dT_L}{dx}\Big|_{x=0} = -m_L \frac{C_0 V_I (1-k)}{D_L k} = -\frac{V_I \Delta T}{D_L} \tag{3.13}$$

Where ΔT is the melting range at the composition C_0. If the actual temperature gradient in the liquid G_L is less than dT_L/dx given by eqn (3.13) then the melt temperature locally falls below the freezing temperatures of some compositions and nucleation of solid can occur in the liquid ahead of the solidifying interface (Figure 3-20). This leads to the condition given first by (W.A. Tiller, 1953) for the stability of a planar solidifying interface (McLean, 1983):

$$\frac{G_L}{V_I} \geq \frac{\Delta T}{D_L} \tag{3.14}$$

Plane front solidification occurs when the solute diffusional flux through the liquid normal to the solidifying interface is sufficiently large to supply enough latent heat of fusion to satisfy the heat flow condition (eqn 3.6). When heat flow is more rapid than that supplied by normal diffusion, for example at high rates of solidification, then radial components of flux supplement the longitudinal contribution to give the additional solidification required to satisfy the heat conservation condition. This leads to the formation of cells and dendrites. As the experimental value of G_L/V_I increasingly deviates from the critical value of eqn (3.14), a progression of microstructural forms, shown schematically in Figure 3-21, has been observed on many materials.

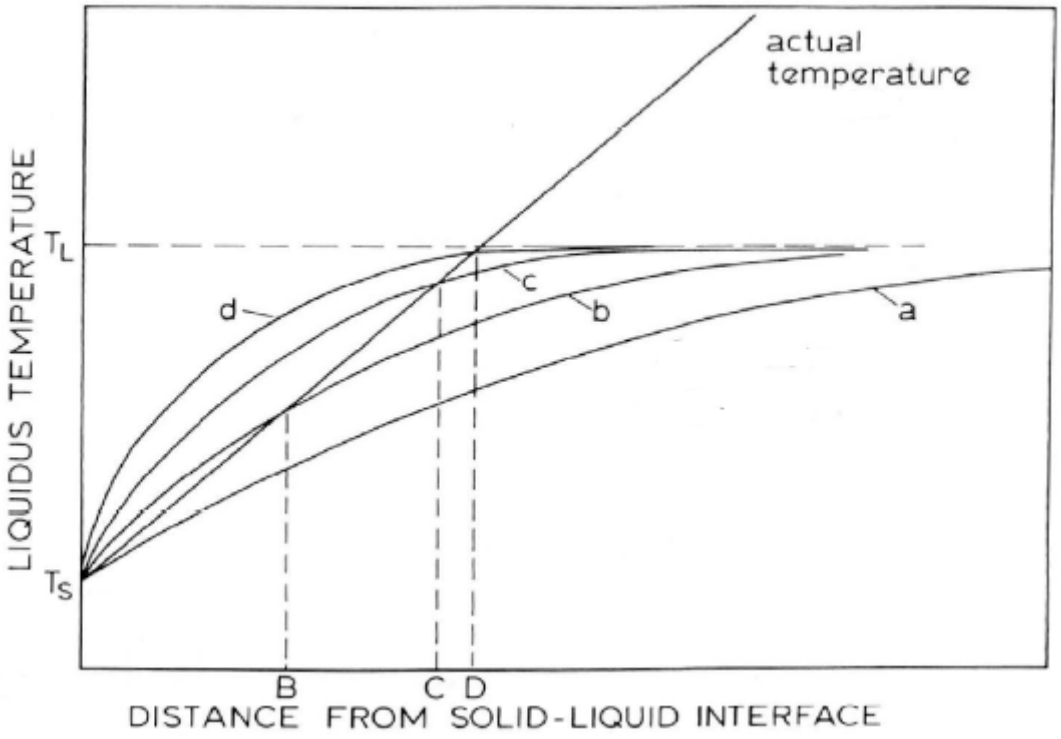

Figure 3-20: Change in liquidus temperature profile ahead of the solidifying interface with change in V_I velocity. Actual temperature is the temperature if the melt, while the curves from *a* to *d* is the freezing temperature of the alloy. V_I increases from *a* to *d*. In cases b, c and d constitutional supercooling occurs at distance B, C and D, (McLean, 1983)

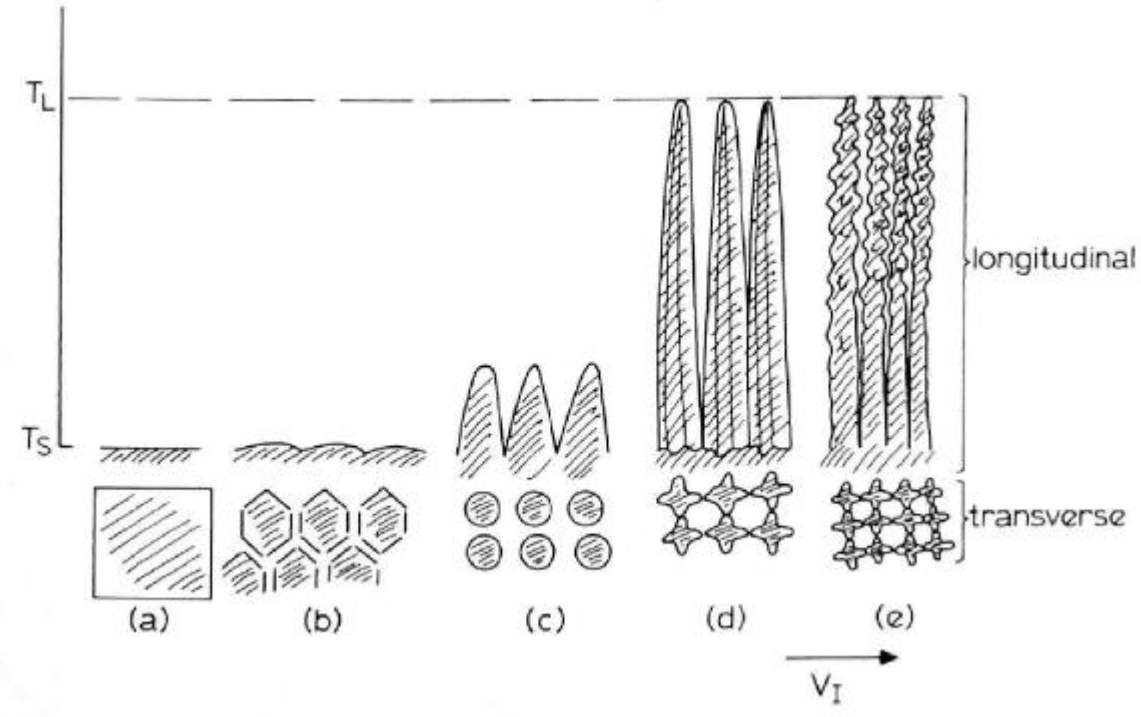

Figure 3-21: Schematic illustration of the changing shape of the solidifying front with increasing V_I for a constant G_L as the range of constitutional supercooling extends to the equilibrium melting range of the alloy, (McLean, 1983)

The categorization of these morphologies is somewhat arbitrary and here we adopt the scheme described by (M.C., 1974):

a) Plane front;
b) Cellular, with cylindrical cells parallel to the direction of heat flow;
c) Cellular with near cylindrical cells parallel to the crystallographic direction of easy growth. Normally the heat flow and the easy growth directions are only slightly misoriented;
d) Cellular/dendritic with flanged cells, having sections shaped like maltese crosses, parallel to the crystallographic direction;
e) Dendritic where the flanges of the cellular/dendritic structure have broken down further to form secondary, and higher order, arms;
f) Equiaxed with no obvious directionality.

Although as yet there are no rigorous theories describing the evolution of these solidification morphologies some qualitative observations can be made. There is clearly a progressive increase in the ratio of surface area to volume for the cells with increasing V_I and G_L. This is necessary to generate by radial diffusion the greater latent heat of solidification required to balance the greater heat losses at high V_I and G_L. The factors leading to the transitions between the various solidification morphologies are quite similar and it is probably possible to identify a different critical value of G_L/V_I for each transition, although a theoretical expression is only available for the plane front to cellular transition (eqn 3.14). (McLean, 1983)

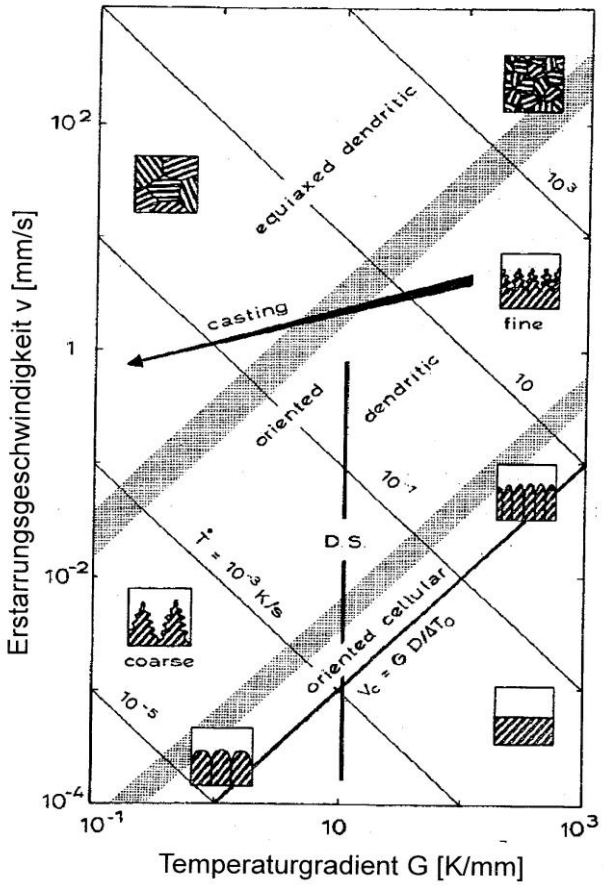

Figure 3-22: Morphologies of directionally solidified superalloys.

Figure 3-22 indicates the type of microstructures possible to obtain with various values of G_L and V_I. From this diagram it's clear that at a certain value of solidification rate V_I, a higher value of G_L is needed to obtain a plane front of solidification.

The previous equation was made with the assumption of only diffusion between the solid/liquid interfaces. But there is a temperature gradient and then an inevitable variation of density that can lead to a convective flow and then mixing of the fluid. Under normal circumstances, convection has relatively little effect on the general solidification characteristics in super alloys and then will not be treated.

It has seen that the main parameter of the directional solidification is the temperature gradient in the liquid G_L and the withdrawal velocity V_I. The development in directional solidification is directed to:

- Suppression of variation in G_L in order to maintain a consistent microstructure;
- Increasing G_L in order to obtain faster V_I that permits to have finer microstructure, and also to reduce the single-phase instability in case of near-eutectic alloy;

- Independent control of G_L and V_I to maintain the microstructure in complex shape parts and to improve the economies of operation.

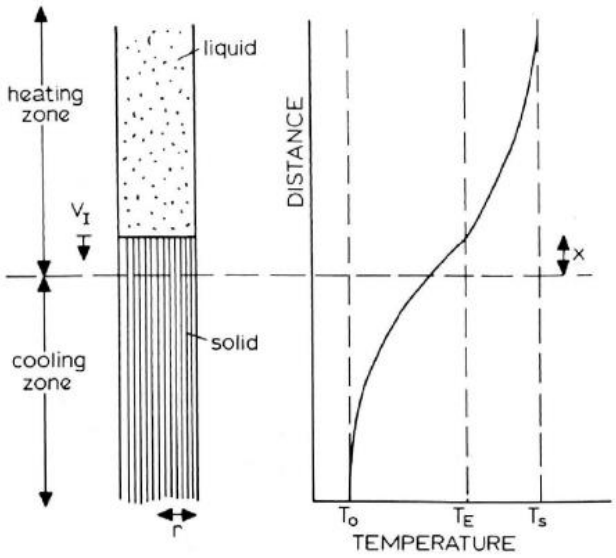

Figure 3-23: Directional solidification of a rod and steady state temperature profile, (McLean, 1983)

In Figure 3-23 it is shown a schematic representation of a directional solidification and temperature profile. Heat is dissipated by a combination of conduction along the ingot and radiation from the mold surface to the cooler outside. It is essential to reduce the radiant heat loss from the heating chamber to the cooled chamber of the furnace in order to maximize the temperature gradient.

With directional solidification, it is possible to create a single crystal parts. In a common directional solidification, when the solidification starts the initial crystal are randomly orientated. Those crystal then growths in one direction and with overgrowth mechanism tends to eliminate the other crystal (Figure 3-24).

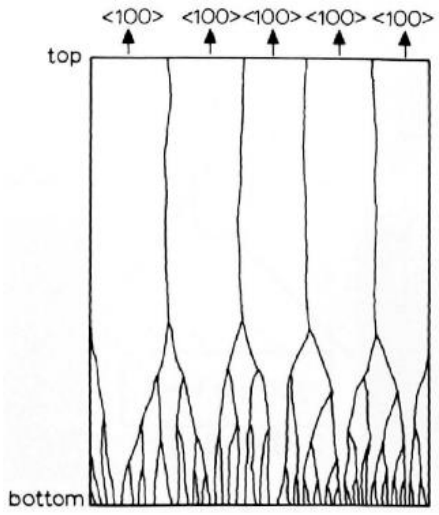

Figure 3-24: Variation of the grain structure along the direction of solidification, (McLean, 1983)

There is an initial transient regions in which the density of elongated grains increases. After that the steady state in the grain section was reached, in order to have a single crystal parts only one of these grains have to continue his growth, and the other can stop. For this purpose was inserted a constriction in the mold, to select only one grain that continue to growth.

3.2 Ni Al Alloy

The demand for new structural materials to replace superalloys in advanced jet engines and other high performance aerospace applications has been one of the strongest driving forces behind the development of intermetallic, ceramic and composite materials. These efforts have been necessitated primarily by the need for greater engine operating efficiencies. However, this goal can only be met by materials that possess a balanced range of properties. Intermetallic compound NiAl possesses high melting point, low density, high Young's modulus and excellent oxidation resistance at elevated temperature. Additionally, the thermal conductivity of NiAl is four to eight times greater than that of Ni-based superalloys (R.D. Noebe, 1993). However, its shortcomings, such as low ductility, poor damage tolerance and inadequate elevated temperature strength, hinder its industrial use. Based on micromechanisms obtained through fracture mechanics study, ductile-phase-toughened intermetallic composites have been developed as a way to improve the fracture toughness. A subset of this class of materials is insitu eutectic composites. NiAl offers a number of distinct advantages over conventional superalloys including:

- Significantly higher melting point: Stoichiometric NiAl has a congruent melting temperature of 1638 °C, which is nearly 300 °C higher than the melting temperature of conventional Ni-based superalloys. Nonstoichiometric compositions possess a reduced melting temperature (Figure 3-25), but still maintain an advantage over current airfoil materials (Daniel B. Miracle, 1995).
- Density which is about two-thirds that of a typical superalloy (Taylor R.E., 1986): The density of nonstoichiometric NiAl ranges from 5.35 g/cm^3 at the Al-rich boundary of the NiAl phase field to 6.50 g/cm^3 at the Ni-rich boundary. The decreased density results in lower selfinduced stresses in rotating turbine airfoils, and the turbine disks may be downsized to reflect the lower operating stresses imposed by the reduced mass of the blades. As an added performance benefit, lower weight blades and disks result in lower inertial mass for rotating parts, providing better engine acceleration (Daniel B. Miracle, 1995).
- Specific modulus which is about 35 percent greater than the stiffest superalloys (Harmorche M.R., 1987), (Tressler R.E., 1991): A high elastic modulus is often considered to be beneficial in aerospace applications, since service loads produce smaller elastic deflections. In addition, a higher modulus of elasticity influences the frequency of harmonic vibrations, and a higher modulus increases the natural frequency of vibrations, thereby possibly avoiding vibrational modes at the highest rotational speeds. However, thermally induced stresses are directly proportional to the elastic modulus, and so larger thermal stresses are produced in a material with a higher modulus for a given thermal gradient. Since thermal fatigue is one of the primary modes of failure in a turbine airfoil, a lower modulus is desirable to improve the thermal fatigue resistance (Daniel B. Miracle, 1995).
- A three- to eight-fold advantage in thermal conductivity (Harmorche M.R., 1987), (Tressler R.E., 1991) (Figure 3-26): Thermal conductivity influences the design and application of airfoil materials in two ways. First, more efficient airfoil cooling is achieved with the rapid heat transfer afforded by high thermal conductivity, providing either a lower metal temperature or a reduction in the amount of cooling air required. Higher thermal conductivity also produces lower thermal gradients. This reduces the magnitude of thermally induced stresses, since thermal stresses are directly proportional to the thermal gradients (Daniel B. Miracle, 1995).
- Cyclic oxidation resistance that is superior to any existing high temperature alloy (Lowell C.E., 1990), (Doychack J., 1989), (C.A., 1988): High-temperature

structural components of advanced aerospace systems typically require service in an oxidizing environment, and this is especially true for turbine airfoils. Resistance to hot salt corrosion and sulfidation is also required. Environmental attack leads to degradation of mechanical properties, and compromises the structural integrity of turbine airfoils, especially in areas with thin cross-sections. NiAl forms the basis of a family of high-temperature, oxidation-resistant and corrosion-resistant alloys which have been used as coatings on Ni-based and Co-based super alloys in gas-turbine engines over the past 30 years (Daniel B. Miracle, 1995).

- Coefficient of thermal expansion: The coefficient of thermal expansion (CTE) is important for structural applications since thermal stresses depend directly on the magnitude of the CTE. The CTE of NiAl is comparable to that typical for Ni-based super alloys, and is $15.1 \times 10^{-6}\,K^{-1}$ from 820 °C to 1560 °C for stoichiometric NiAl (Wachtell, 1952). Deviations from stoichiometry and minor alloying additions have little influence on the CTE (Daniel B. Miracle, 1995).

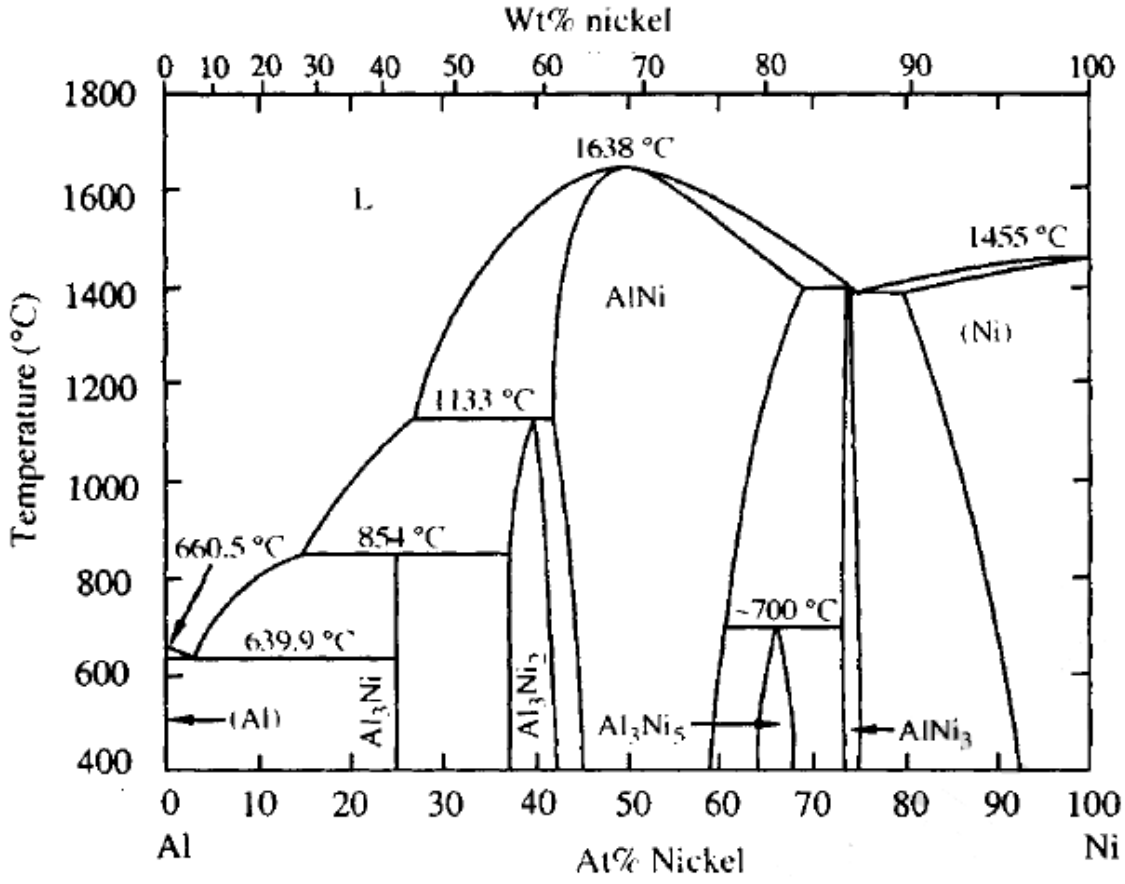

Figure 3-25: The binary Ni-Al phase diagram from Nash, Singleton, and Murray (1991)

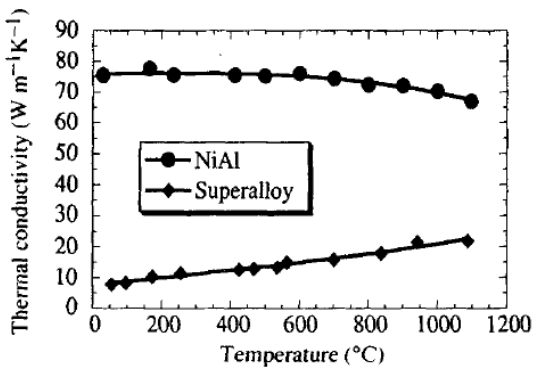

Figure 3-26: The thermal conductivity of NiAl single crystals as a function of temperature. Data for a typical Ni-based superalloy are provided for comparison (Darolia, 1991)

The immediate benefits that would be derived from using NiAl in engine applications would include reduced cooling requirements, reduced weight, and higher operating temperatures. Together these benefits would lead to increased engine thermodynamic efficiency and an increased thrust-to-weight ratio. The weight savings alone would be significant. For example, design studies have shown that the replacement of superalloy turbine blades with NiAl could lead to a 40 percent reduction in the weight of the rotor system (blade and disk) (R., 1991). (Ronald D. Noebe, 1992)

3.2.1 Ni Al 28Cr 6Mo

Binary NiAl alloy possesses low ductility and fracture toughness at ambient temperatures as well as inadequate strength and creep resistance at elevated temperature, which limit its application in the aviation industry. In order to enhance the elevated-temperature creep strength and room-temperature fracture toughness of NiAl alloy, relevant researches have been proceeded for many years, and some strengthening and toughening methods were proposed, such as alloying, second-phase strengthening and single crystal preparation (Zhao Shang).

With the development of technique of directional solidification, people combined second-phase strengthening with directional solidification by adding refractory metals like Cr, Mo, V, Ta, and paid more attention to directionally solidified eutectic in-situ composites. Walter and Cline (Walter J.L., 1970) investigated directionally solidified NiAl-Cr alloy, it consisted of fibrous Cr strengthening phase and NiAl matrix. In contrast to binary NiAl alloy, the toughness and strength of NiAl-Cr alloy were enhanced markedly. What's more, Cline et al. (Cline H.E. W. J., 1970), (Cline H.E. W. J., 1971) found that substitution of Cr with Mo led to a change of microstructure from Cr fibers to Cr(Mo) lamellae when the Mo content exceeded 0.6%(at.%) (Zhao Shang). In terms of fracture resistance, a lamellae structure is more desirable than a fibrous structure since the crack front doesn't have access to the brittle matrix.

The eutectic NiAl-Cr(Mo) was obtained with the percentage of element reported below:

$$Ni - 33Al - (34 - x)Cr - xMo, with\ 0 \leq x \leq 6$$

Cline et al. (Cline H.E. W. J., 1971) had analyzed the microstructure of an eutectic NiAl-Cr(Mo) directionally solidified alloy at different percentage of second phase element, with a three-dimensional scanning electron microscopy. They had found that with low molybdenum alloy (0.6%) there is a formation of faceted Cr(Mo) rods and plates, compared to a ternary alloy NiAl-Cr that shown a non-faceted rods. Increasing the percentage of molybdenum, the plates become longer, and with 6% of molybdenum (the alloy used for this experiment) the structure becomes cellular (Figure 3-27 and Figure 3-28).

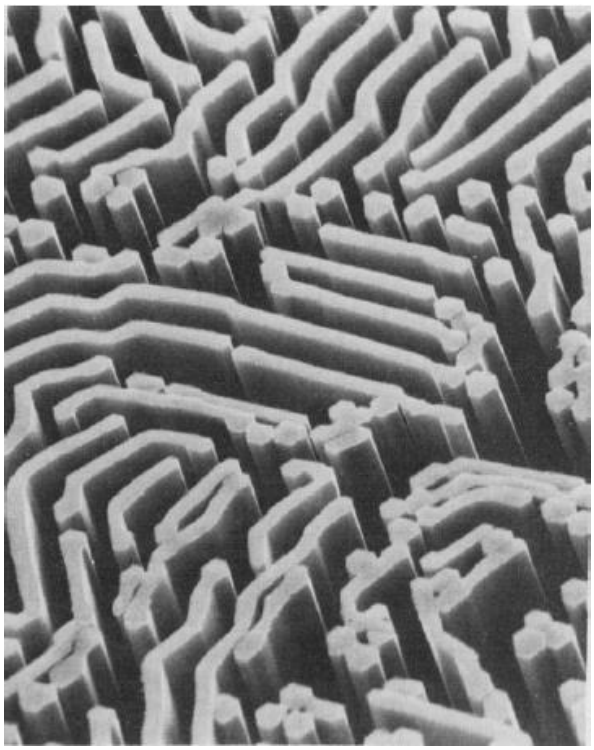

Figure 3-27: NiAl-Cr(0.6Mo) at 2780X, (Cline H.E. W. J., 1971)

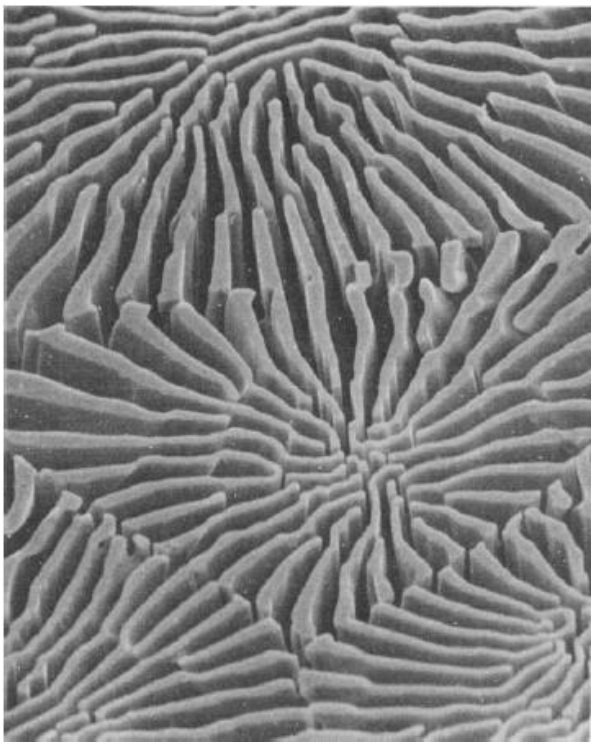

Figure 3-28: NiAl-Cr(6Mo) at 990X, (Cline H.E. W. J., 1971)

3.3 Investment casting

Investment casting, also called lost-wax casting, is a manufacturing process in which a wax model, with the same shape (or near) of the final product, was covered with a refractory ceramic material. When this ceramic coverage was dried and strengthened, the wax was removed, and the melt was poured into this ceramic shell mold. When the metal solidifies, the ceramic shell mold was removed mechanically. Generally, this process was used for

small casting, but there are some applications, especially in aerospace field, where big part was produced with this technique.

The first operation is to produce the master pattern physically (made by wax, wood, steel or other materials) or as a 3D CAD model. Then, a permanent mold with a cavity that reproduces the shape of the master pattern was produced. This mold can be produced by machining with a manual tool (like lathe or milling machine), with a CNC machine starting from a CAD parts, or with cast directly from the master pattern. This is constructed in two or more parts, with insert if necessary, to permits the extraction of the expendable patterns. When this part is ready the wax was poured into the mold just realized to obtain the wax pattern, that have the same shape of the master pattern. Natural and synthetic waxes were used, with various additives in order to achieve minimum shrinkage and close reproducibility of the pattern. Usually, the parts realized with investment casting process have a complicate shape, for this reason more simple wax pattern was produced and then assembled in a more complicated shape. This final shape is comprehensive also of the sprue for melting the liquid metal. Now, this pattern assembly was coated with the ceramic mold. The ceramic mold, called investment, was produced by three steps: coating, stuccoing and hardening. The first step involves dipping the wax pattern in slurry with refractory ceramic particles to produce a uniform surface. The second step involves the coverage of this layer of slurry with ceramic sand. Now, the coating is allowed to harden, by waiting for a variable time depending on which type of slurry was used. These three steps were repeated many times, until the desired thickness of the investment was reach. The investment is then allowed to completely dry, and successively the wax pattern can be removed by placing the investment in an autoclave or furnace to melt out or vaporize the wax. The mold was successively heat at temperature around 1000 °C to remove any residual wax and sinter the mold. Usually specials heating conditions are required to avoid shell cracking. The mold is ready for the cast. It is preheated and then placed in the oven. The liquid metal can be poured simply by gravity, with air pressure, tilt casting, vacuum cast or with centrifugal technique, depending on which process is required for the desired final results. When the metal was solidified, the shell mold can be removed mechanically or chemically.

The major feature of the process is the design freedom of the parts produced, afforded to the capacity of intricate shaping. It is also possible to design a single complex component instead of more simple parts, eliminating assembly operation. Most of the finished details include holes, slots and fins can be formed with the original casting. This is helpful in the

case where the casting material is very hard or brittle and doing successively these parts can be problematic.

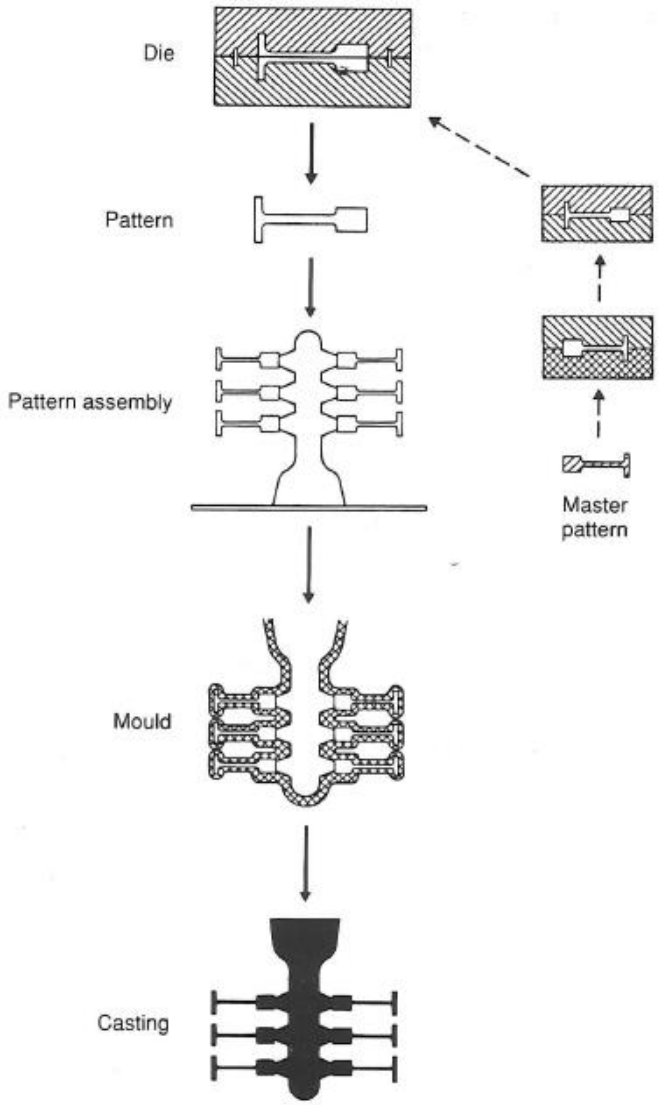

Figure 3-29: Schematization of the process described above, (Peter R. Beeley, 1995)

Advantages of investment casting:

- Certain unmachinable parts can be cast to preplanned shape.
- Excellent surface finish
- High dimensional accuracy
- Extremely intricate parts are castable
- Almost any metal can be cast
- No flash or parting lines

Disadvantages:

- This process is expensive, is usually limited to small casting, and presents some difficulties where cores are involved.
- Investment castings require very long production-cycle times versus other casting processes.
- This process is practically infeasible for high-volume manufacturing, due to its high cost and long cycle times.

3.4 Simulation

During this work FEM (Finite Element Method) software was used. This is a numerical technique that gives an approximate solution of problems by dividing space into parts thus delivering a discretization of space where numerical calculations can be performed upon in order to solve problems, where an analytical solution cannot be obtained. All of these parts are called finite elements.

A finite element analysis consists in three steps:

1. Pre-processing: in this first part a model becomes realized, in which the geometry is divided into more simple parts, connected at discrete points called nodes. This process is named discretization of the model and the mesh is created. Also the material properties are assigned in this first part. In every node there is some boundary condition, like loads or constrains.
2. Analysis: the problem is solved temporally and spatially using numerical methods.
3. Post-processing: in this part of the process the solution gets visualized using graphical displays. Further results can be obtained by using criterion functions or subsequent simulations.

At first the geometry needs to be modeled, in two or three dimensions. Not only the geometry of the e.g. casting parts needs to be modeled, but also the ambient elements if this is important for the model. For example, in a mechanic model where the strength of the parts has to be investigated, only the model of these parts was needed. In a fluid dynamics problem, conversely, not only the shape but also the work fluid is important to the model, in order to study the interaction between them. Again, if there is thermal interaction between two mechanic parts separated by some fluid, this fluid need to be modeled.

When the model is ready, its discretization with the creation of mesh is needed. A mesh is a collection of vertices, edges and faces that define a shape of the geometry modeled before. During the meshing the entire geometry was divided into more polygons that could be triangle, quadrilateral or polygon with more than four sides. One of these polygon is the simplest part of the problem where the solution was calculated, and the interaction between all these parts give the solution of the entire problem with a resolution equal to the dimension of the mesh. The dimension of the elements of the mesh is an important parameter to set. The smaller these parts are, the more accurate is the solution while also resulting in longer calculation times needed to converge. The dimension of the mesh needs to be chosen accurately, by assigning bigger mesh polygons at the less important parts of the geometry, and smaller polygon at the critical point of the geometry where the accuracy of the solution is important in order to improve the calculation time of the simulation and its accuracy. An example of a mesh used in this work is shown in Figure 4-22, Figure 4-23 and Figure 4-24. In this case, the temperature gradient in the melt and in the shell mold is very important and thus was modeled with small mesh elements. The temperature gradient in the furnace wall, conversely, was not important and so the mesh polygons were chosen to be bigger in these parts.

The next step is to set the boundary conditions. These conditions depend on which type of simulation is needed. Here was set the temperature of the parts, speed of possible fluid interacting with some shape, force or constrains etc. In addition to the boundary conditions, the properties of the used materials (which comprise also a fluid or liquid material present in the simulation) and physical models also need to be set. In fact, in certain situations some simplifications can be used, and then some physical models can be removed in order to obtain a solution less correct but faster to calculate, or can be added if a high accuracy of the solution is needed and the convergence velocity is not important.

When all the parts are set correctly, the solution can be run and then, if it converges, the results can be analyzed.

Usually, FEM software is very expensive, but the main advantages are that many simulations can be conducted in order to optimize the parts before its creations. This means that the improvements can be conducted without the creation of the physical model, with a faster design time and less costs for the company.

4 Experimental

The experimental part is divided into two separated parts. The first part is the physical experiment, which involves the production of the shell molds, the melting of the alloy and subsequently the analysis of the specimen. The second part is simulations with the software Star CCM+.

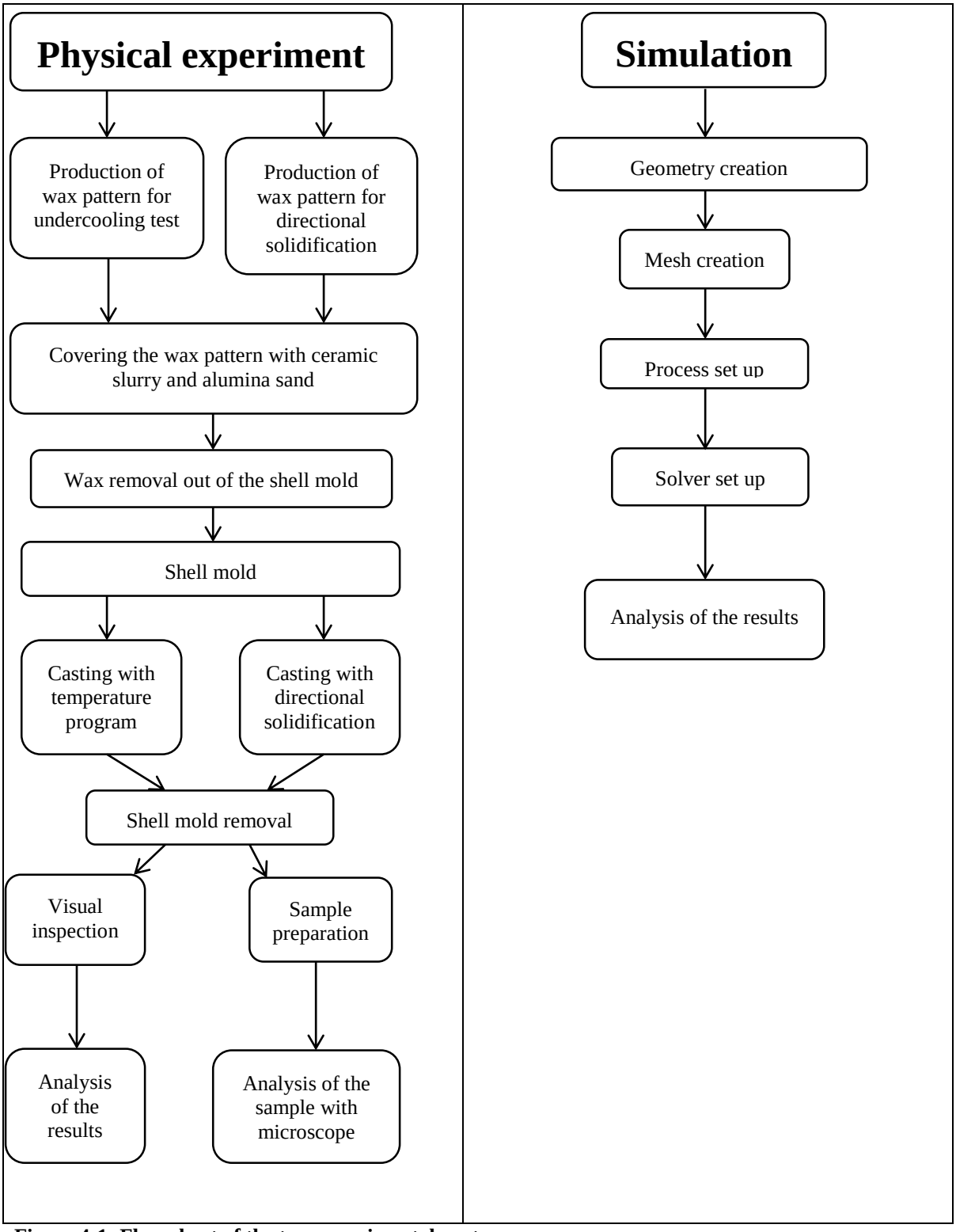

Figure 4-1: Flow chart of the two experimental parts

The two required shell molds mentioned in Figure 4-1 are needed to realize two different types of experiment. In the first experiment there is a 10 mm spherical specimen with a thermocouple in the middle of the sphere, and it was used to measure the critical undercoolability and the melting range of three different materials (NiAl 28Cr 6Mo, NiAl 9Mo and NiAl 34Cr), and the second experiment has a cross shape to study the lamellae growth behavior in a directional solidification with change of section.

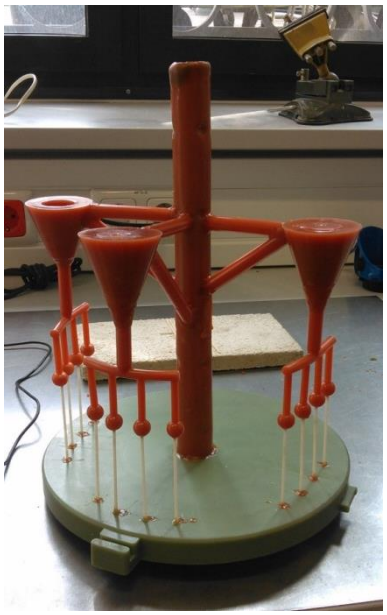

Figure 4-2: Wax shape to measure the undercoolability properties of three different alloy

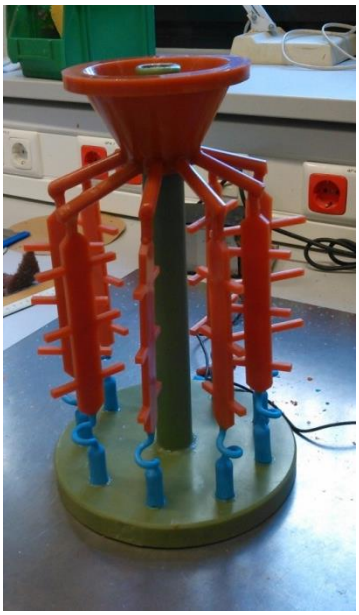

Figure 4-3: Wax shape to study the directional solidification behavior

Figure 4-4: Standard parts

4.1 Physical experiment

The physical experiment's goal is to obtain the undercoolability properties of the used alloy and to analyze the directional growth of the lamellae during the directional solidification in a cross shape specimen. The investment casting process of the two shell mold is the same for both, and thus will be described only once.

Wax pattern manufacturing and wax cluster assembling

At the beginning, the complete shape of the cavity of the shell mold was modeled with wax. Each part (like the specimen, sprue, runners, plate, grain selector etc…) was made singularly, and then all these parts were assembled using wax soldering. Some of these parts, like the runners, the plate or the central column, are standard elements (Figure 4-4), because they also are used for other parts in the institute and were realized in (relatively) high quantity with the industrial scaled wax injection machine (Figure 4-5, on the left).

Connected to these standard elements there are the specimens, that usually are manufactured only when it is needed by using the manual wax injection machine (Figure 4-5, on the right).

Figure 4-5: On the left, the wax injection machine used to prepare the standard parts, on the right the manual wax injection machine used for the parts needed in small quantity

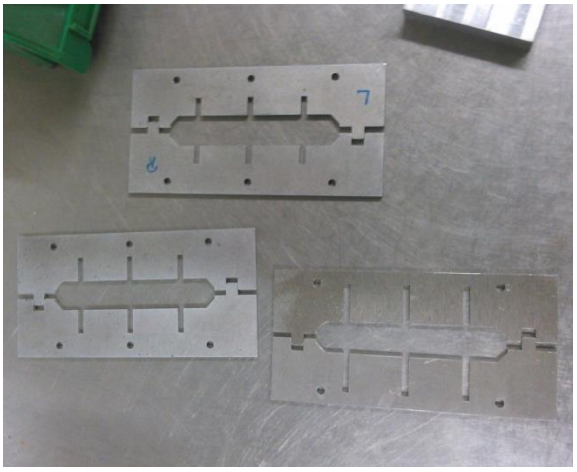

Figure 4-6: Cavity shape of the permanent shell mold to realize the wax specimen

These two machines use two different types of wax that are maintained at a constant temperature of 65 °C for the industrial scaled machine, and 69 °C for the manual machine. During this thesis work, the directional solidification experiment was conducted for specimens with different arm lengths of 30, 20 and 15 mm. In one shell mold there are three specimens for each arm lengths (Figure 4-3). The aluminum die to make the wax model was formed by three parts, the cavity shape of the specimen that can be changed (Figure 4-6), and two coverage parts. The cavity shapes were then changed to realize all the shapes of the specimens with the different arm lengths.

For making the spherical specimen there is a similar aluminum die and the same manual machine was used. After the preparation of the required wax shell specimen, these parts are soldered together with the other standard parts, to create the wax cluster (Figure 4-2, Figure 4-3 and Figure 4-4). At this point, the wax cluster for directional solidification is ready.

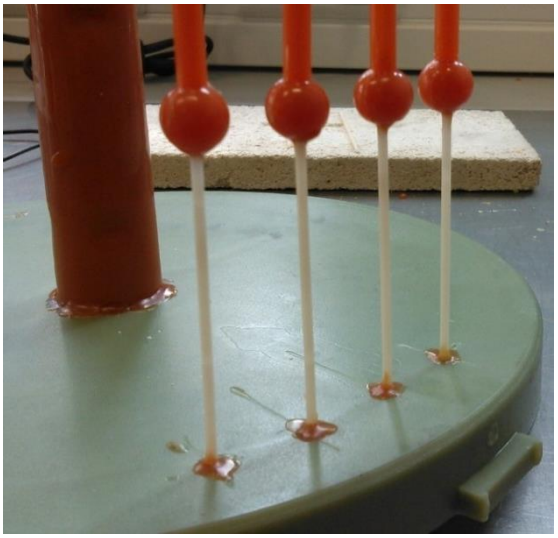

Figure 4-7: Ceramic tubes for thermocouple positioning

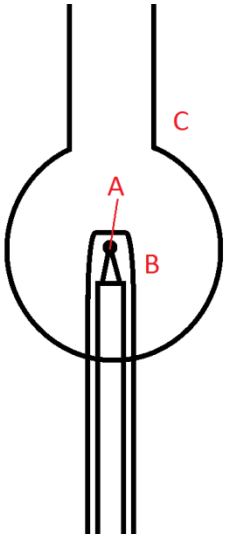

Figure 4-8: Thermocouple position

Thermocouple preparation and attachment

In the shell mold used to measure the undercooling of the alloy there are some thermocouples to measure the temperature of the alloy during the melting and solidification process, placed in the middle of the spheres. Type B thermocouples were used (Pt 6Rh / Pt 30Rh), because this type of thermocouple can operate at high temperatures of up to 1800 °C.

The wires were fused together with a hydrogen flame at approximately 2500 °C. The wires and one of the thermocouples are visible in Figure 4-9.

Figure 4-9: In the top, the Thermocouple, in the bottom the two different rhodium percentage wire

These thermocouples must be protected from the molten alloy, by placing it in a ceramic tube closed at one end. In Figure 4-8 the scheme of the thermocouple position placed in the mold is shown, with the connection between the two platinum-rhodium wire (A), the protection ceramic tube (B) and the cavity for the molten alloy (C). After the placement of these ceramic tubes, the wax cluster for undercoolability test also is ready, and both these wax parts can be covered with slurry to produce the ceramic shell mold.

Shell mold production

For this model, two types of slurries were used; the first three layers with SiO_2 free slurry for this type of alloy, named NH, and the other nine layers with SiO_2 containing slurry, named AK. The wax cluster was dipped into the slurry once the correct value of viscosity was adjusted and after the previous coat had dried. To measure this viscosity level a Zahn viscosity cup #4 was used, which is a stainless steel cup with a drilled hole at the bottom. The cup was completely filled with the liquid and the time needed to drain the cup through the hole, called "efflux time", was measured. Appropriate efflux times, for this application have to be between 8 and 12 seconds. If the measured time does not correspond with this range, the viscosity has to be adjusted. When the viscosity was too high (time under 8 seconds), distilled water was added to the slurry. Conversely, if the viscosity is too low (time over 12 seconds) some time has to pass in order to provide the time needed for the evaporation of some water this increasing the slurry's viscosity again. A picture of this process and a table with the measured times was reported in Figure 4-10 and Table 4-1.

Figure 4-10: Viscosity measurement

Table 4-1: Measured efflux time for each layer of slurry

SLURRY	t_m	SAND	SAND SIZE
NH	11,8	Al_2O_3	Fine
NH	11,1	Al_2O_3	Fine
NH	11,2	Al_2O_3	Medium
AK	9,1	Al_2O_3	Coarse
AK	9,6	Al_2O_3	Coarse
AK	9,3	Al_2O_3	Coarse
AK	9,2	Al_2O_3	Coarse
AK	9,6	Al_2O_3	Coarse
AK	9,7	Al_2O_3	Coarse
AK	9,7	Al_2O_3	Coarse
AK	9,9	Al_2O_3	Coarse
AK	10,2	Al_2O_3	Coarse
SEAL	SEAL	SEAL	SEAL

Using the efflux time it is possible to calculate the kinematic viscosity of the slurry. For the Zahn viscosity cup #4, the equation is:

$$v = 14{,}8(t - 5) \tag{4.1}$$

Where *t* is the efflux time and *v* the kinematic viscosity in centistokes. Then, the average of the viscosity for NH slurry is 94 ± 4,6 centistokes, while the medium value of viscosity of AK slurry is 68 ± 5 centistokes. After the coverage of the wax cluster with the correct slurry, it was covered with alumina sand with different grain sizes. The first two layers were covered with fine grain sized alumina (0,12 – 0,25 mm), the third with medium grain sized alumina (0,25 – 0,50 mm) and the other nine layers with coarse grain sized alumina (0,50 – 1 mm) (see Table 4-1). For this operation, the correctly grain sized alumina sand was put in a sieve moved by electrical vibration, and then the wax cluster covered with slurry was moved behind this sieve. In this manner the alumina sand can cover the cluster uniformly. After the coverage of the wax cluster with the slurry and the alumina sand, wait for the drying of this coating is necessary, before put a new layer. This waiting time is at least one day for the NH slurry, and three hour for AK slurry. The last layer, called seal, is only AK slurry and it is used for fixating the sand on the shell surface. For this reason, the viscosity of this layer is not important and thus was not measured.

Wax removal and sintering

When the two shell molds are completely dried, the wax can be removed in an boil autoclave, and then the shell mold can be burned for strengthening it. The process in the autoclave is completed after applying 160 °C and 6 bar for ten seconds, followed by 2 minutes of holding time for dewaxing and then the shell molds were sintered in a firing furnace up to 1250 °C.

The last step is to close the hollow of the central column, to avoid the filling of this part with melted material. For this operation, this cavity was filled with alumina wool, with AK slurry and alumina sand at the bottom and top of the shell mold.

Casting set-up and casting

The melting operation was conducted in a vertical industrial scaled Bridgman furnace made by ALD Vacuum technologies GmbH thus being a furnace composed by two chambers. The one on the top is the hot chamber, that contains two graphite heaters, and the one in the bottom is the cooling chamber. Between the two zones a graphite baffle provides thermal insulation. The shell mold was put on a water cooled copper plate, which can be moved between the two chambers. A scheme of this furnace can be shown in Figure 4-24.

The preparation of the furnace consists of the positioning of the shell mold on the copper plate and the connecting all thermocouples with extension wire for the data acquisition.

The thermal insulation of the extension wire is made with alumina wool, in order to minimize the heat between the heaters and the thermocouples that may give a wrong value of temperature (Figure 4-11).

Figure 4-11: Thermocouple connection at the furnace software, before of the isolation of the wire

Once this was achieved the furnace is ready for the melting procedure and the material can be tested. Three different materials were tested: NiAl 28Cr 6Mo, NiAl 9Mo and NiAl 34Cr. For each material there are four spherical chambers with respectively four thermocouples (one of these chambers is shown in Figure 4-8). This first melting procedure consists of melting and cooling/solidifying the materials with a program temperature. The temperature was elevated to 1620 °C, maintained for ten minute, and then reduced to 1300 °C. The heating and cooling rate of the resistant heater were 20 K/min. This heating/cooling procedure was repeated four times, to verify the measured temperature values statically (Figure 4-12). All the process was completed in the Bridgman furnace mentioned above, but only in the hot chamber, without movement of the shell mold between the two chambers.

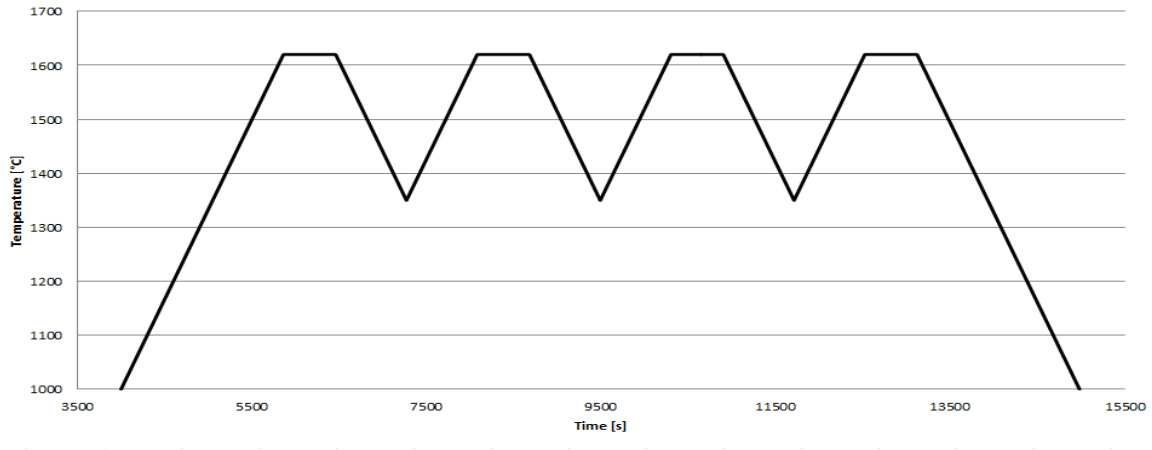

Figure 4-12: Temperature program in the vacuum furnace

When this test ended, the second shell mold for the directional solidification test was positioned in the furnace. The eutectic alloy for this casting is NiAl-28CR-6Mo, and the directional solidification was conducted at a withdrawal velocity of 3 mm/min from hot to cold chamber, with a heaters temperature of 1620°C. When this operation was concluded, the ceramic shell mold was removed (Figure 4-13, Figure 4-14 and Figure 4-15) and the specimen analyzed. The alloy used in this test at ambient temperature is very brittle and the different coefficient of expansion lead to cracks in the casting parts during cool-down.

Post processing

The first attempt to remove the shell mold from the specimen was by sandblasting. But this method take a lot of time and after the arms of the first specimen was freed, were all broke. This is probably due to the different expansion coefficient between the alloy and the shell mold after the solidification. Then, the successive specimen was freed from the shell mold with vise. Most of the specimens were broken during the removal of shell mold, but it is still possible to analyze it.

Figure 4-13: Shell mold with solidified material after the test

Figure 4-14: Removal of one specimen from the shell mold

Figure 4-15: Mechanically removal of the shell mold from the specimen

Figure 4-16: Cutting of the specimen

Figure 4-17: Specimen cut to analyze it

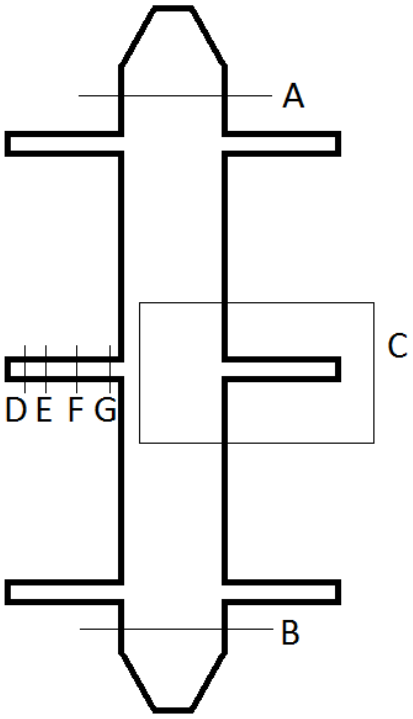

Figure 4-18: Specimen cut to take the sample

Specimen preparation and analysis

After the removal of the shell mold, the specimens were cut to the correct dimensions for analysis under a microscope and then were put in a phenolic thermoset polymer. This polymer is a powder and was hardened at 180 °C and 140 bar for 8 minute, and then was maintained at this pressure and cooled for 6:30 minute. Eleven samples was realized, nine of the side section of the specimen (C in Figure 4-18 and the sample in the right in Figure 4-19), one of the transversal section (compared to the direction of solidification) of the specimen that contain two cut, one in the top and one in the bottom (A and B in Figure 4-18, picture in the center in Figure 4-19) and one at different area in one arm (D, E, F and G in Figure 4-18, picture on the left in Figure 4-19). The samples were grinded and polished in order to analyze it on microscope. This grinding/polishing operation was conducted with the same parameter for each sample, in order to ensure the same results. A metallographic grinding machine was used, an ATM Saphir 550. For grinding, a force of 25 N with a rotational speed of 150 1/min and a time cycle of 2,5 minute was used. Applying these parameters different types of sandpaper, from coarse (grit 80) to fine (grit 2500), were used. After each cycle the new sandpaper was replaced with a new one. When the grinding is done the samples were polished. The same machine was used, with a suspension of diamond powder in water. In the first step a 9 μm grain sized diamond powder was used, in the second step 3 μm grain sized and in the last step 0,25 μm grain sized powder. At this point the specimens are ready for microscopic analysis. In the first analysis that was performed the surface of the nine longitudinal section samples is not regular and there are a lot of cracks. It is thus difficult to perform an analysis. All these samples then were put in a vibratory polishing machine for three hours. Afterwards the last step of polishing with 0,25 μm diamond grain sized was repeated to remove the remaining impurities from the surface. Now, the sample was ready for the analysis.

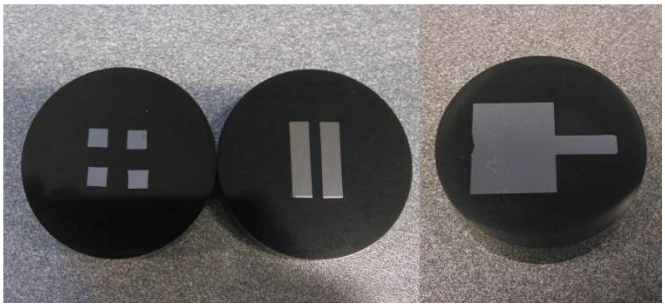

Figure 4-19: From left to right: cross section of arm, cross section of specimen at the top and bottom, side section of specimen

The first analysis was conducted with an optical microscope, a type of microscope which uses visible light and a system of lenses to magnify images of small samples. The image from an optical microscope can be captured by normal light-sensitive cameras to generate a micrograph.

In a second time was used also the Scanning Electron Microscope (SEM), to analyze only one of the samples. Two types of detection mode were used; detection of secondary electrons emitted by atoms excited by the electron beam (SE2) and detection of backscattered electrons (BSD). Then the samples were analyzed with the EDX technique (Energy-dispersive X-ray spectroscopy) to understand which phases appear dark and light (NiAl or CrMo) in order to know if the alloy is hyper or hypo eutectic.

4.2 Simulation

Figure 4-20: Shell mold

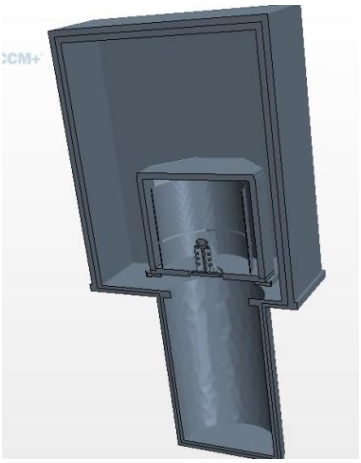

Figure 4-21: Bridgman furnace

In order to simulate the directional solidification STAR-CCM+ software with a Star CAST user interface was used. STAR-CCM+ (Computational Continuum Mechanics) is a finite element program that can simulate various types of physical situations, like heat transfer, solid stresses, combustion or casting processes. This program has been developed since 2004, by using computational fluid dynamics algorithms extracted from the old STAR-CD code. The first release included the world's first commercially available polyhedral meshing algorithm, which is more accurate for fluid-flow problems than a hexahedral or tetrahedral mesh. For the simulation, the program needs a valid 3D geometry that either can be modeled directly in STAR-CCM+ with 3D-CAD, a feature-based parametric modeler within STAR-CCM+ that allows to build geometries from scratch, or can be imported from other software via standardized formats. The geometry import possibility will not be detailed here, because during this work the geometry was created directly using 3D-CAD incorporated in the software. The geometry that has been created with 3D-CAD is stored as 3D-CAD models, which can then be converted to geometry parts for integration with the meshing and simulation process. The program works like most of the other types of 3D CAD programs. Models are created by carrying out a series of operations like sketching, extruding and cutting. In general, the processes begin with the creation of 2D sketches. For an accurate simulation of the entire process, not only the geometry of the casting itself needs to be modeled but also the Bridgman furnace (Figure 4-20, Figure 4-21).

When the 3D model is ready, the mesh must be created. A mesh is the discretized representation of the computational domain, which the physics solver uses to provide a numerical solution. For improving the speed of the simulation, the Bridgman oven is modeled with sparser mesh than the shell mold mesh. With the simulation of the entire oven and the entire shell mold, the resulting mesh is too extensive and the simulation requires very long calculation times. For this reason, only one ninth of the geometry will

be modeled, with the correct boundaries at the interfaces (Figure 4-22 and Figure 4-23). The oven, with vacuum and the shell mold were modeled separately and saved as two different volume meshes and finally reimported into one project. This operation is necessary because the moving part (cooled plate, shell mold and melt) must not have interfaces with the static part (vacuum).

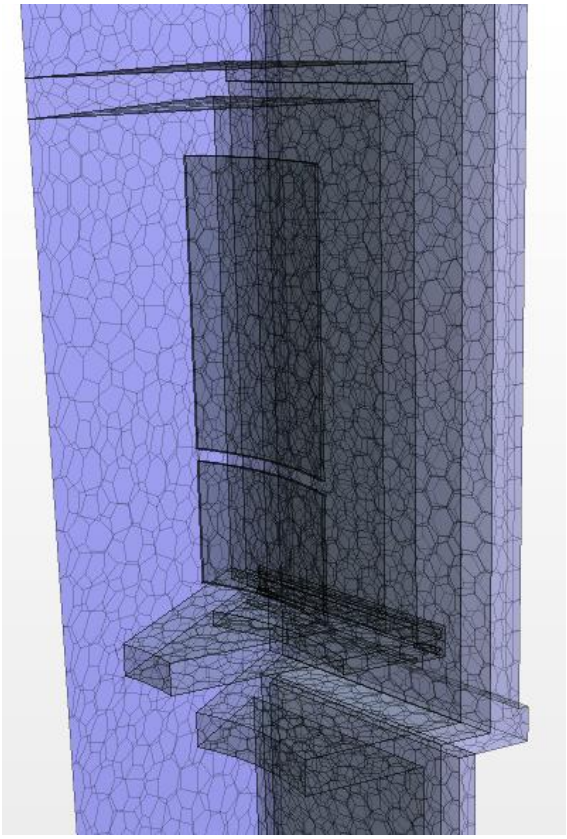

Figure 4-22: Mesh of the ninth part of the oven

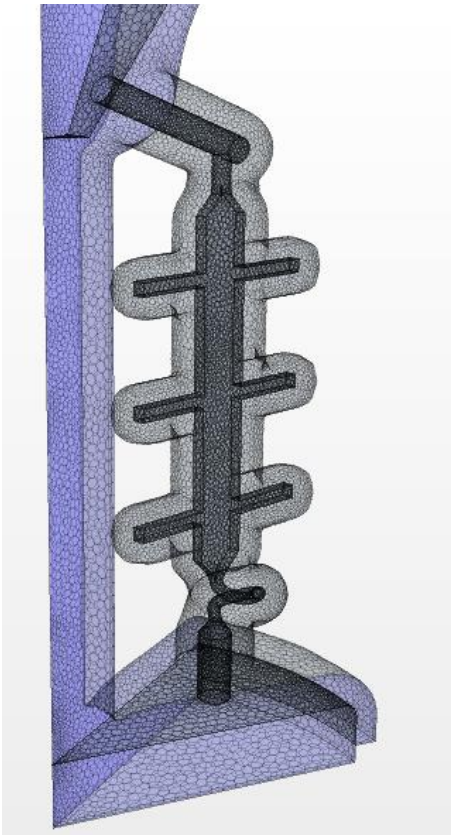

Figure 4-23: Mesh of the ninth part of the shell mold with melt and cooled plate

The next step is to set-up the initial condition, boundaries and so on. The user interface Star Cast was used at first, in order to simply set-up the most important things of the simulation, and then a more accurate setting was completed in the original Star-CCM+ user interfaces. Then the type of solidification, the temperature of the melt and the direction of gravity were applied. Next the material used was inserted from the Star Cast interface. SIGRATHERM (a registered material for high temperature insulation) was used for both baffle and isolation, graphite for the heater, copper for the cooled plate, a Nickel-based superalloy for the melt (modified manually with the desired characteristics in a second time), iron for the external wall of the oven and the vacuum was modelled as a solid with very low value of specific heat, thermal conductivity and density. The exact material used

for the shell mold is in the Star-Cast material database, as well as the copper plate, iron and SIGRATHERM. Some properties were variable with the temperature, as example was reported in Figure 4-25 the specific heat capacity and the thermal conductivity of the ceramic shell mold.

Table 4-2: properties of materials

	Specific heat [J/Kg-K]	Thermal conductivity [W/m-K]	Density [Kg/m^3]
SIGRATHERM®	140	0,1	
Graphite	700	24	
Vacuum	1,0E-04	1,0E-05	1,0E-05
NiAl-28Cr-6Mo	640	76	

Initially, the vacuum was set as solid, the graphite as SIGRATHERM and the used alloy as normal Nickel-based superalloy. The characteristics of these materials then were changed for a second time from the original interface of Star-CCM+. In fact, from the continuum manager, it is possible to change the physics characteristics of the materials. The characteristics then were set as shown in Table 4-2, and for the alloy the temperatures of solidus and liquidus also were applied.

As the alloy is a eutectic composition, these two values must be equal, but the alloy really used for the test is not perfect eutectic with the exact composition being unknown. As solidus and liquidus temperatures the temperature found through the undercooling test were used. These are not the correct solidus and liquidus temperatures, but the real values probably are very similar.

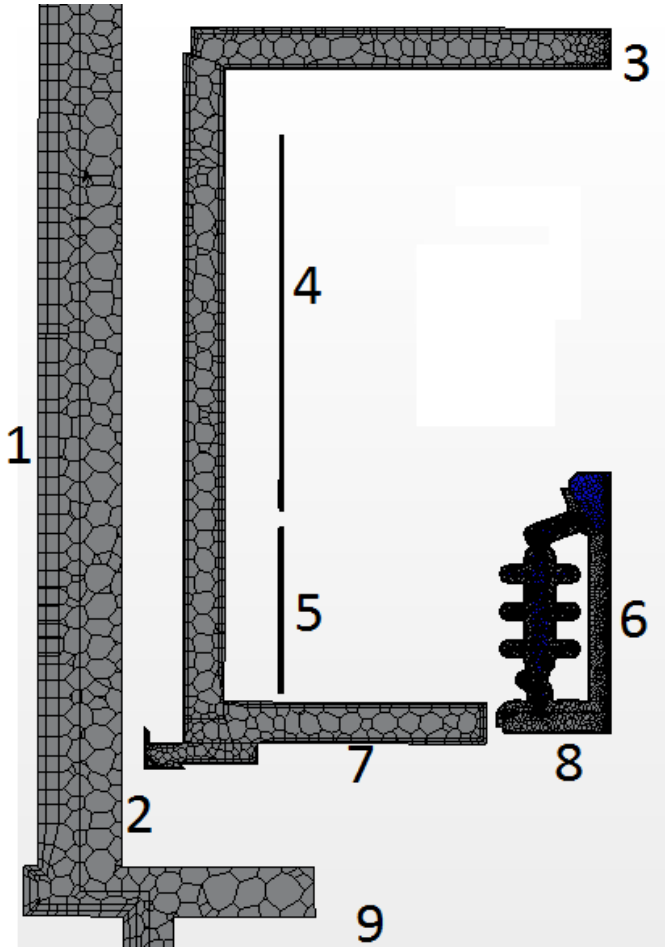

Figure 4-24: Parts of the furnace.

1. **External wall of the furnace**
2. **Internal wall of the furnace**
3. **Isolation**
4. **Heater 1**
5. **Heater 2**
6. **Shell mold**
7. **Baffle**
8. **Copper plate**
9. **Cooling chamber**

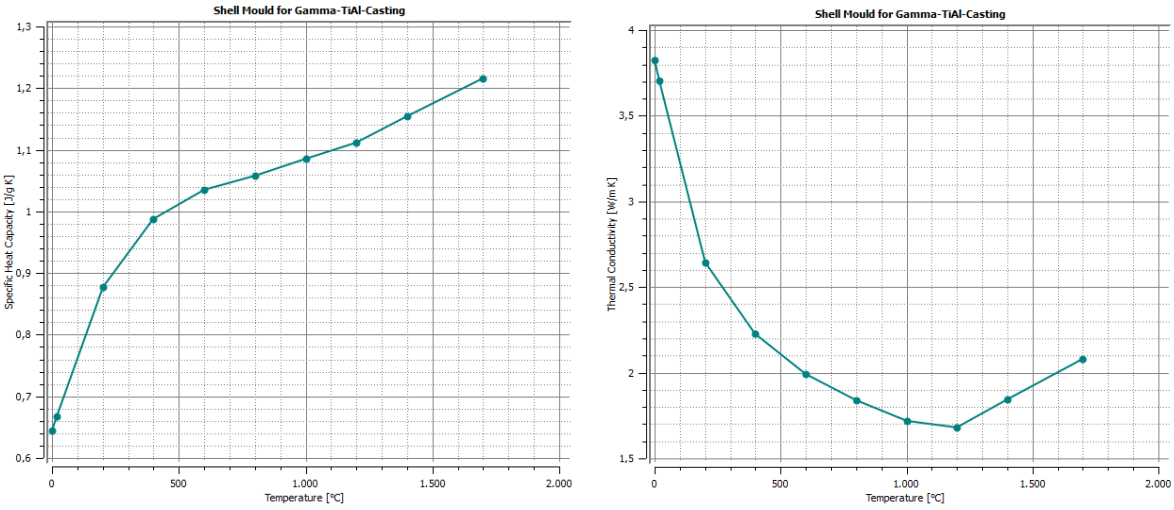

Figure 4-25: Properties of the ceramic shell mold. In the left picture, the specific heat capacity, in the right pictures the thermal conductivity (Temperatures in x-axis [°C], in the y-axis there are specific heat capacity [J/gK] in left picture, Thermal conductivity [W/mK] in right picture).

After the setup of the materials, the initial conditions were set, again using the Star-Cast user interface. A completely filled mold was chosen as initial case as simulating the

pouring process turned out as heavily time-consuming while giving no noticeable advantages for the solidification simulation being the main focus of this thesis. The melt region thus received an initial temperature of 1620 °C. The temperature of the heater, the shell mold and of the heating chamber walls were set to the same temperature (1620 °C), while the vacuum, the external wall of the furnace and the cooled copper plate were set to 20 °C.

As for the boundaries set-up, the heater, the copper plate and the wall of the cooling chamber were set to a fixed temperature of 1620 °C for the heater and 20 °C for the other two parts. The internal wall of the heating chamber was implemented as a solid wall boundary with emissivity of 0.6, the same boundary was applied to for the shell mold surface, but with an emissivity of just 0.5, from the data give by Access company.

Table 4-3: Temperature-variable heat transfer coefficient for the fluid/solid interface

Temperature(C)	Heat Transfer Coefficient(W/m...
0	100
500	100
1430	500
1460	5000
2000	5000

Regarding the interface properties, the fluid/solid interface (melt/shell mold and melt/copper plate) has a temperature dependent heat transfer coefficient (Table 4-3). A solid/solid interface of 500 W/m^{2}K was set between the shell mold and the copper plate, and of 100 W/m^{2}K for the other solid interfaces.

For the physical model, only a flow stop solid fraction of 0.9 was set, founded as a probable value from data of other similar alloy. The last setup is the solvers. Stopping criteria of maximum 30, minimum 5 inner iteration were set, and an asymptotic energy criterion was chosen. The chosen time step is time variable, reported in Table 4-4.

Table 4-4: Time variable time steps

Time	Time Steps
0	0.001
0.1	0.01
1	0.1
10	1

Now it must be taken into account that the geometry is a ninth part of the real geometry, with rotational symmetry. A rotational axis was then set in the region manager, under physic values label, and the entire external boundary (the symmetry wall) was set as periodic internal interface. Under the interface label, it is possible to check the rotational angle that must be 40 degree, if not the rotational axis is not set correctly and must be changed.

The simulation is ready and can start, but with this set-up there are some instability problems. It had been solved by switching off the pure thermal model and freeze flow solver, and the dynamic viscosity was set to a very high value of 1000 Pa-s. In this situations, without the freeze flow model but with the high value of viscosity, the behavior of the model is the same, but avoided a bug of the program's present version that doesn't let the solution converge. The heater geometry was also removed, the shape was modeled only as a hole in the vacuum with a constant temperature boundary. In fact the temperature field in the heater is not important, only the heat that they give to the system is important. With its removal, the system loses some not important mesh elements and surfaces, while providing an improvement of the simulation times needed.

5 Results and discussion

During the previous chapter the entire set-up of the physical and simulated experiment was presented. During this chapter the results of these experiment will be discussed.

5.1 Physical experiment

5.1.1 Undercooling

At first, the undercoolability properties of the alloy were examined. Three different materials were tested, NiAl-9Mo, NiAl-28Cr-6Mo and NiAl-34Cr. Unfortunately, during this test only NiAl-34Cr was melted completely and thus reached the spherical chamber with the thermocouple (Figure 4-8). The other two materials don't have melted and thus don't reach the spherical chamber. The data of these materials is thus not available. The thermal property of the NiAl-34Cr alloy however is very similar to the thermal properties of the NiAl-28Cr-6Mo alloy used during the directional solidification tests, and so it is possible to use this data instead. In fact, solidus and liquidus temperature are the same, specific heat and thermal conductivity are very similar, and the undercoolability behavior probably is different, but the difference is not too big.

Figure 5-1: melted alloy after the test

Moreover, in the material that was melted correctly, one of the four thermocouples had measured a temperature very different from the other three. Simply, the data of this thermocouple was considered wrong and was not taking into account, to don't affect the final results with a wrong value.

In order to get feedback if the alloy was melted correctly, the shell mold was mechanically removed from the melted material. In Figure 5-1 it is possible to check the shape of the melted material. The specimen was broken during the removal of the shell mold, but it is possible to visually analyze it. The spherical chambers were correctly filled with the

material. The hole in the middle is the location of the thermocouple measurement, and there is no other hole, cavity or porosity. Then during this experiment a correct melt-thermocouple contact was present. These results are shown in Figure 5-2.

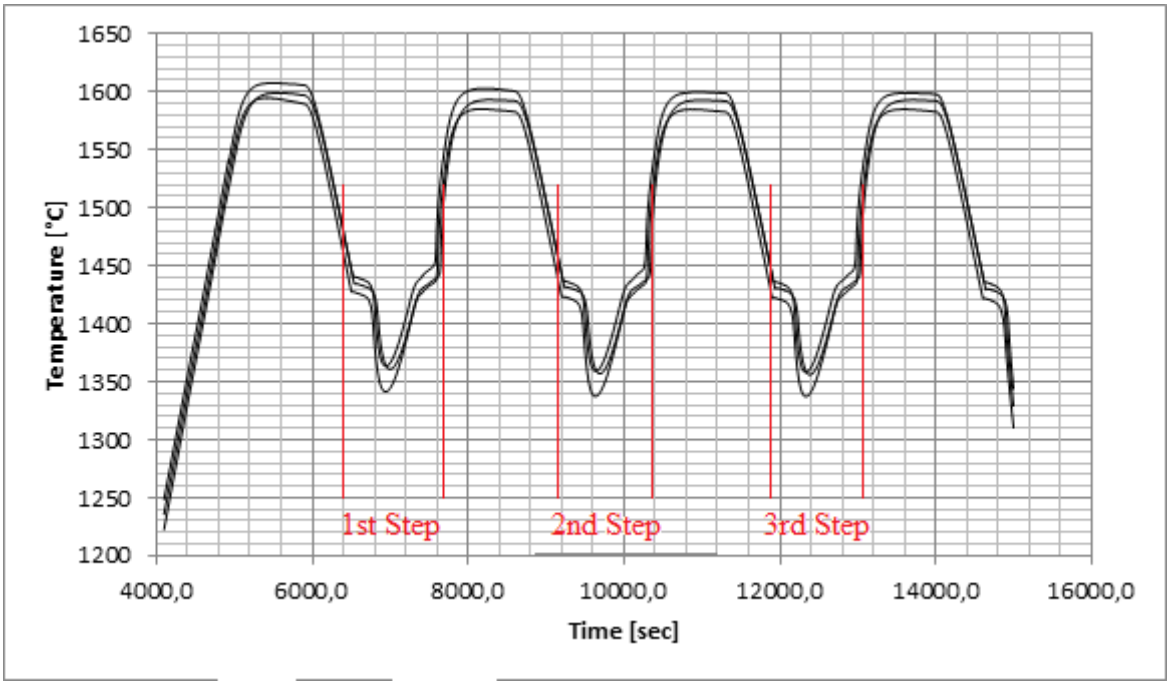

Figure 5-2: Temperature value during the undercoolability test

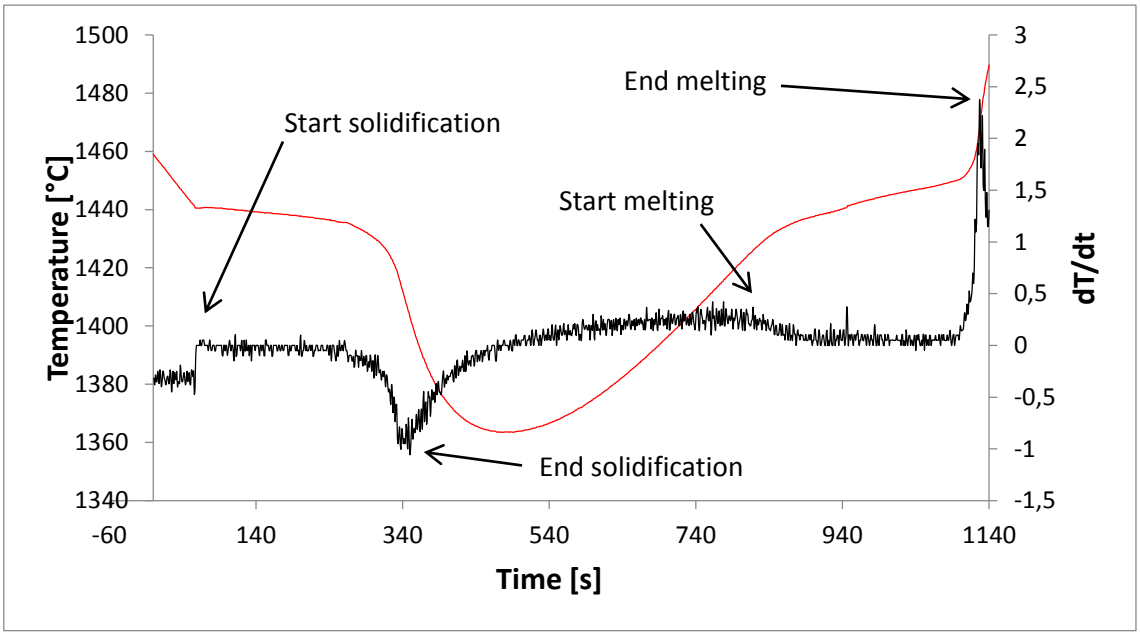

Figure 5-3: Curve of melting and solidification (red) and curve dT/dt (black)

As shown in Figure 5-2, the test is composed of three steps, for each step and for each thermocouple the graph of melting and solidification was recorded, and the derivative curve dT/dt was calculated. An example of one melting/solidification curve with the corresponding derivative curve is shown in Figure 5-3.

In this curve, by following the red line from left to right, the material starts liquid and in the first change of temperature the solidification starts. By looking the first peak of the derivative curve this first temperature of interest can be found which corresponds to the nucleation and thus can be named T_N. Then there is a second peak during a period with strong temperature decrease. After this peak the material is totally solidified. Then the heating up starts, by following the derivative curve in correspondence of the first change of slope there is a change of temperature curve slope that means that the alloy start to melted. Again, by following the derivative curve there is a high peak of that curve that mean a strong change of the temperature curve slope. At this point the alloy is melted. These two temperatures were called solid and liquid temperature T_S and T_L. These two values are different from the solid and liquid temperature, because in this case the system is not in equilibrium, but probably the real value is not far off. For each step and for each thermocouple these temperature values were taken.

The temperature melting interval equation is shown in equations 5.1.

$$\Delta T_{MI} = T_L - T_S \tag{5.1}$$

The critical undercooling values are calculated with the equation 5.2:

$$\Delta T_U = T_L - T_N \tag{5.2}$$

The experimental values of T_N, T_L, T_S founded during the test are listed in Table 5-1.

For the undercoolability properties of this material was then found an average value of 23.9 ± 4.4 °C. For comparison, the binary alloy Ni2Re, Ni4Re and Ni9Re have an average undercoolability value of respectively 44 ± 7.4 °C, 23 ± 4.7 °C and 29 ± 10.6 °C, while the cmsx-6 nickel-based superalloy have an average undercoolability value of 117.9 ± 5.1 °C. (Bogner Samuel, 2015)

Table 5-1: Experimental liquid and solid temperature

	T_N [°C]	T_L [°C]	T_S [°C]	ΔT_{MI} [°C]	ΔT_U [°C]
Thermocouple 1:					
Step 1	1427	1453	1420	33	26
Step 2	1423	1455	1423	32	32
Step 3	1422	1446	1420	26	24
Thermocouple 2:					
Step 1	1434	1452	1426	26	18
Step 2	1431	1450	1428	22	19
Step 3	1430	1449	1427	22	19
Thermocouple 3:					
Step 1	1441	1464	1434	30	23
Step 2	1437	1464	1431	33	27
Step 3	1436	1463	1431	32	27

Compared to the other alloy, the NiAl 28Cr 6Mo have a quite low critical undercoolability. Due to the curvature of the liquidus isotherm line during the solidification, the area with change of section could be highly undercooled. When a critical value of undercooling is reached, some solid can nucleate in the ceramic shell mold wall. For this reason, alloy with high value of critical undercoolability can avoid stray grains in platform zone.

5.1.2 Directional solidification

In this experiment a NiAl-28Cr-6Mo alloy was used. The goal is to understand, for improve in a later time, the directional growth of the lamellae. The first sample that was analyzed is the arm (sample 1). It was take one arm, and was cut transversally respect of the arm axis in four parts to analyze the microstructure at different length (Figure 4-18, parts D, E, F and G).

From Figure 5-4 to Figure 5-7 there is a picture of the cross section (cut transversal respect of the arm axis) of the longest arm (30 mm), and the microstructure was analyzed in two different parts of the arm, in the center and near the edge. In these figures, only the sample

cut D and G was taking, because the structure is almost the same in all the length of the arm, then it's enough to look only at the beginning and at the end of the arm.

The analyzed structure looks like a cross section of cellular growth. This means that the solidification is probably directional, but along the arm, in orthogonal direction compared to the withdrawal velocity direction. In the structure, moreover, there is no only eutectic lamellae structure, but there is also some darker zone without lamellae. Probably, these parts are the dendritic arm of one of the two phases that growth above the other (single phase instability, seen in Eutectic growth chapter). This means that the alloy used for this experiment is not perfectly eutectic.

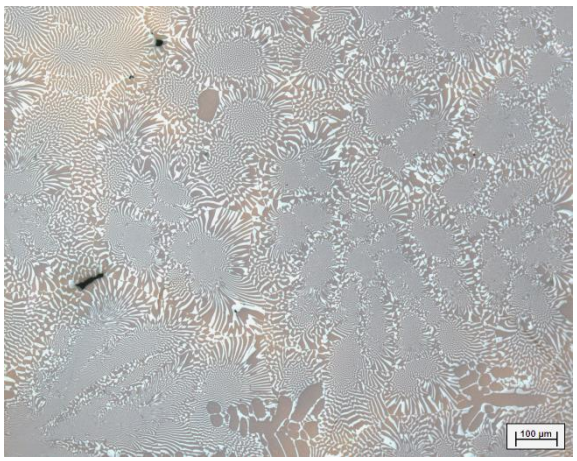

Figure 5-4: 100X, end of the arm, center (scale legend 100 µm)

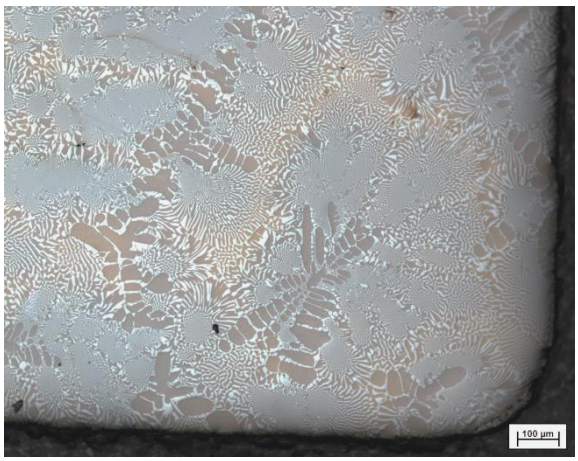

Figure 5-5: 100X, end of the arm, edge (scale legend 100 µm)

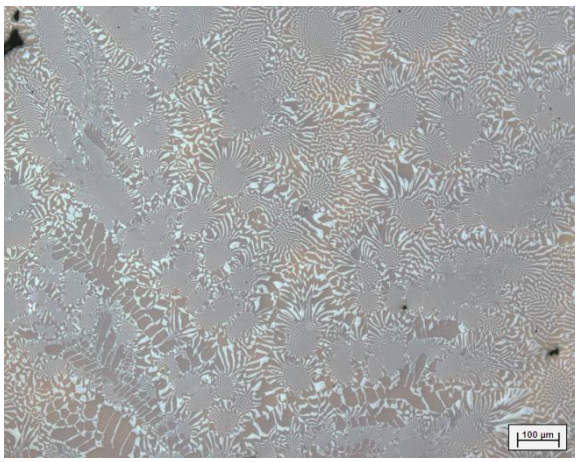

Figure 5-6: 100X, base of the arm, center (scale legend 100 µm)

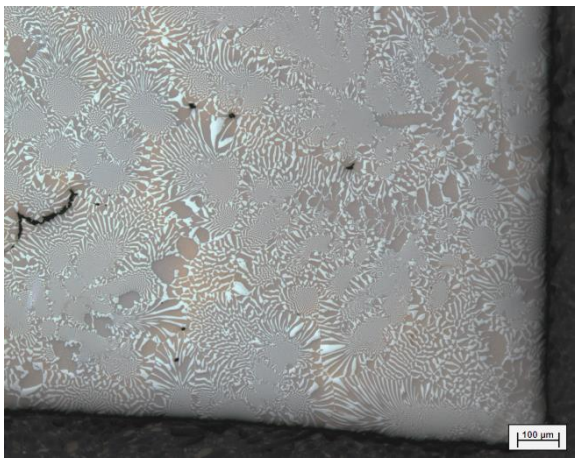

Figure 5-7: 100X, base of the arm, edge (scale legend 100 µm)

The second sample investigated is the cross section at bottom and top of the specimen (from Figure 5-8 to Figure 5-11). As with the sample 1, also in this case a picture in two parts

was take, in the center of the specimen and near the edge (Figure 5-12). The first interesting things to analyze is that the structure at the bottom (start of directional solidification) near the edge is different that the structure at the top (end of directional solidification) of the samples. In fact, at the bottom the structure is more or less the same along all the cross section, but in the top the structure in the edge is different, very similar to the structure of the sample 1. The explanation for this fact is that at the bottom of the specimen the thermal gradient is very high, due to the proximity to the chill plate, and then the single phase instability (explained in Solidification) does not happen. At the top, the thermal gradient is lower than the thermal gradient at the bottom, and because of the curvature of the solid/liquid interface, near the edge is lower than in the center.

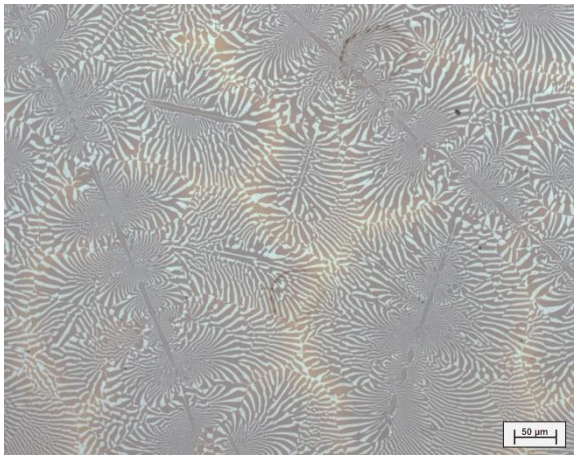

Figure 5-8: 200X, bottom, center (scale legend 50 µm)

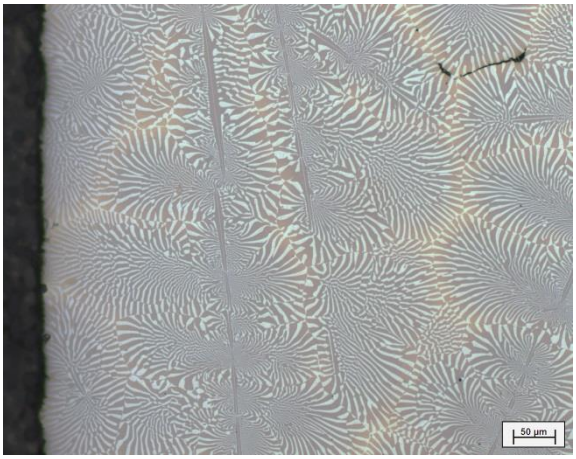

Figure 5-9: 200X, bottom, edge (scale legend 50 µm)

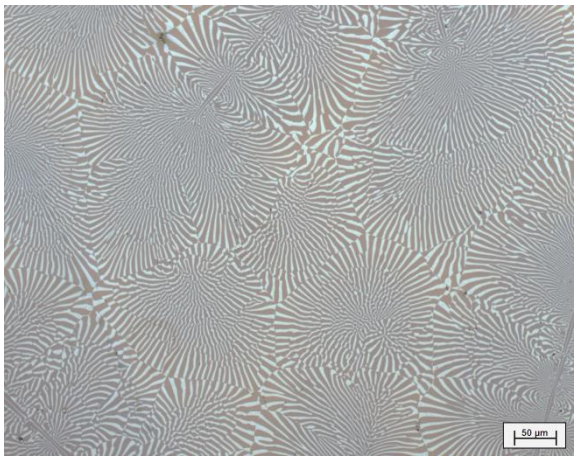

Figure 5-10: 200X, top, center (scale legend 50 µm)

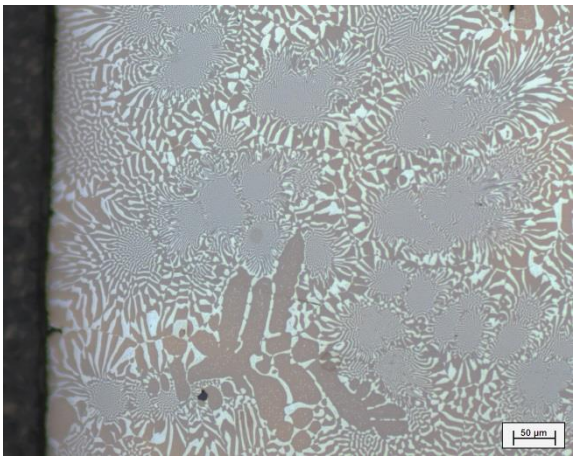

Figure 5-11: 200X, top, edge (scale legend 50 µm)

In this case the structure is not really regular, but the main problem is probably due to the low thermal gradient. It is clear that the solidification is directional, with a cellular

solid/liquid interface. In order to have perfectly aligned lamellae planar solidification morphology is needed, instead of cellular. Again, to solve this problem the thermal gradient need to be increased or the growth rate has to be decreased, as shown in Figure 3-22.

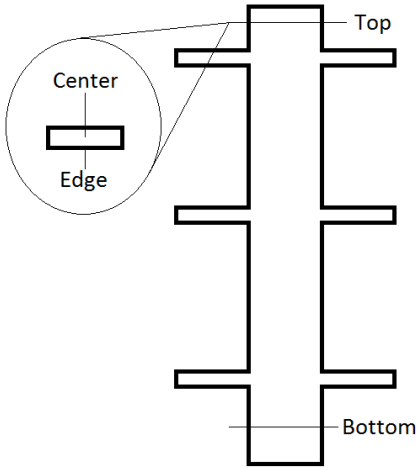

Figure 5-12: Point where the microscope picture was take

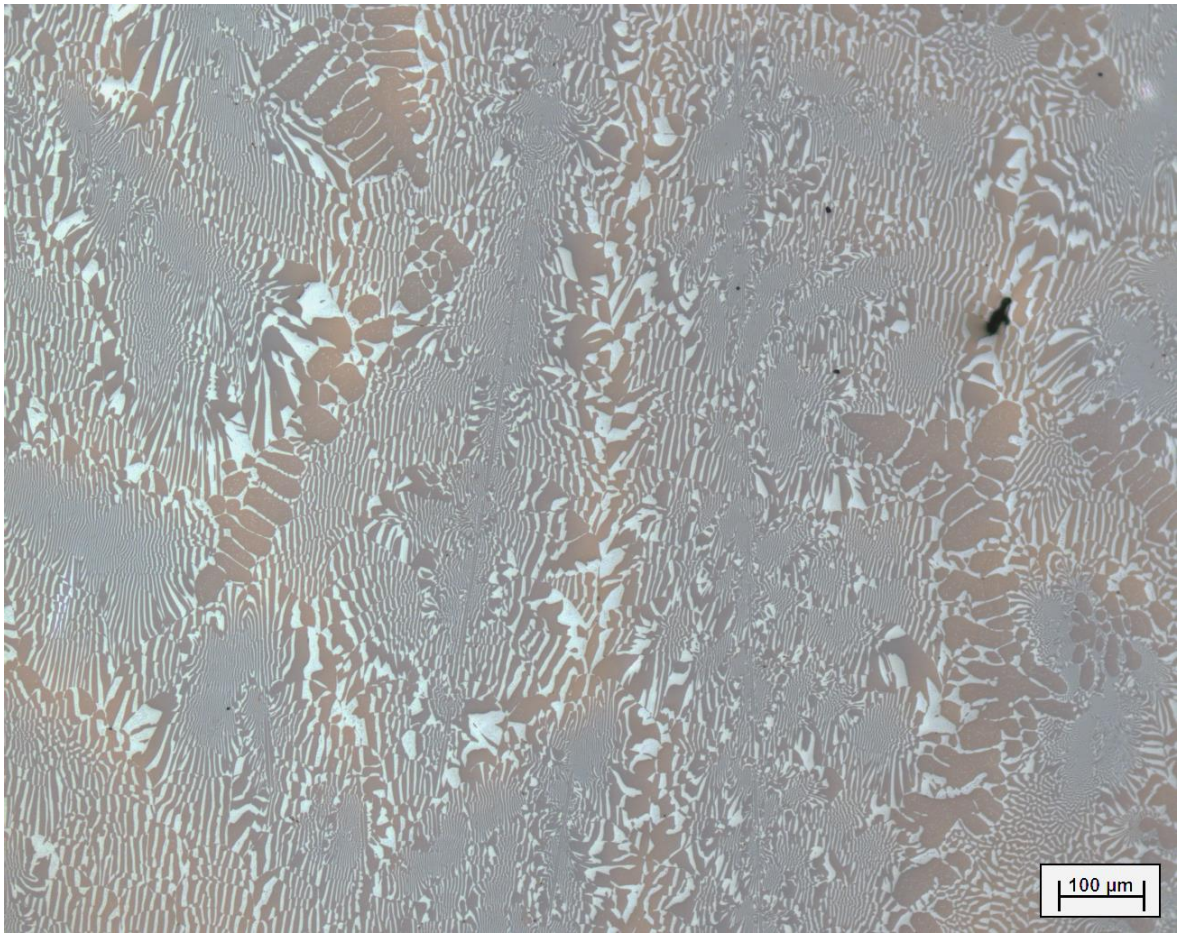

Figure 5-13: 100X, directional solidification in the center of the body

In Figure 5-13 the growth direction is from bottom to top, and was taken in the middle of the central body. It is possible to see an aligned growth of the lamellae that is all in one direction but the structure is not regular. There are some lamellae not aligned and there are a lot of dendrite arms of NiAl phase. The structure is almost disoriented because the picture was taken in the side of specimen that is the part near the edge (as in Figure 5-11), where there is the lower thermal gradient and then the most disorientated structure. The structure is obviously 3D but in these picture just look an intersection of a more complicated structure, for this reason a cellular structure viewed in the side can look disoriented.

Again, in Figure 5-14 there are some picture take in the side of the sample at 200X. Also in this sample, in the center of the body (picture in top right position in Figure 5-14) it is possible to see the direction of solidification, but in the other two parts (the other two picture in Figure 5-14) the structure looks isotropic. In the arm and in the connection between the arm and the body, then, the solidification is not directional.

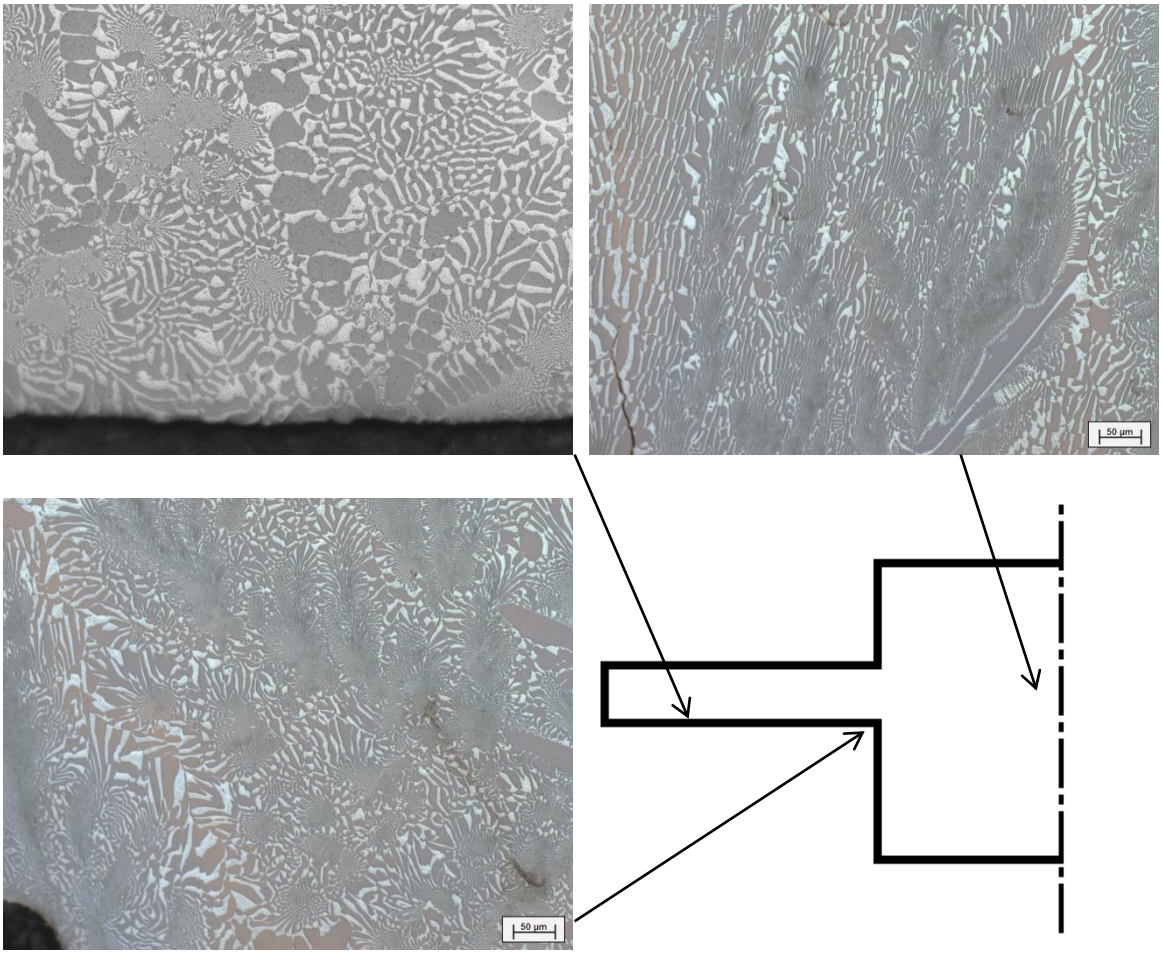

Figure 5-14: 200X, metallography of one sample, all these picture are taken in the side. In all these three picture the scale in bottom right position is 50 µm

Only the cross section at bottom and top samples was analyzed with SEM. The goal is to obtain a better view of the sample at high magnification and to identify the chemical composition of phases. In fact, from the picture taken by the optical microscope it can be seen not only a lamellae structure, but also a dendritic arm; the alloy is then not perfect eutectic as explained above. With SEM analysis it is possible to identify NiAl phases and CrMo phases, and then with EDX analysis the exact atomic percentage of element can be known.

As example, one picture was recorded at the bottom section at 1000X of magnification, with BSD detector (Figure 5-15).

Figure 5-15: Bottom section at 1000X magnification

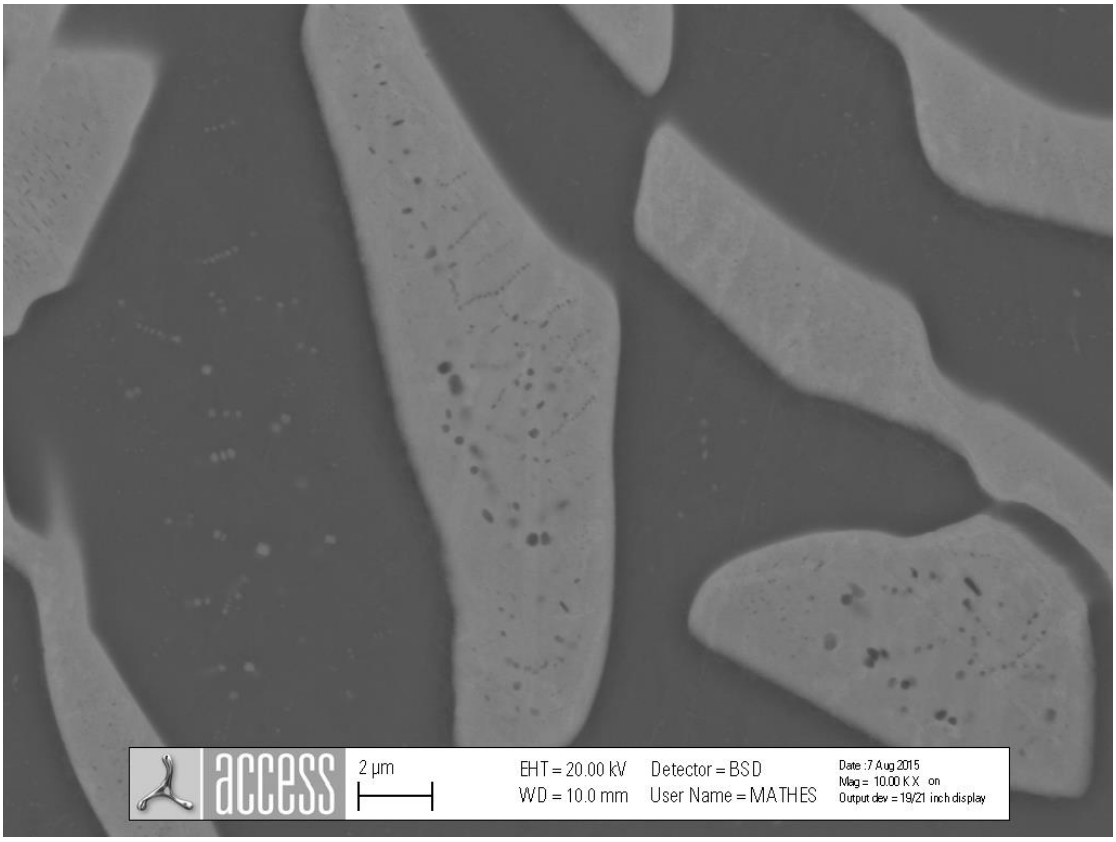

Figure 5-16: Top section at 10000X magnification

The color of the phases is the same. The dark phase in SEM corresponds with the dark phase in optical microscope, and the same for the light phase, as it is possible to see compared the Figure 5-15 with Figure 5-8. In some light zone there are few dark dots, and conversely there are some light dots in the dark zone. This particular is more visible at a high magnification level (Figure 5-16) where these dots can be distinguished exactly. As it is seen in the phase diagram (like Figure 3-1) the solubility of each phase goes down with the temperature. If the lamellae are too thick the diffusion paths are too long to reach the other phase. Therefore, after solidification there will be precipitations of the other phase for thick lamellae. Near the boundary between the two phases there aren't these dots. A possible explanation is that when the temperature decreases, this small content of the second phase is reduced by diffusion. If the lamellae are big, the diffusion don't happen in the center because of the too big distance that don't permits diffusion. Then, this small concentration of the second phase becomes precipitate.

Table 5-2: EDX Analysis 1 (at%)

Spectrum	Ni	Al	Cr	Mo
1	3,49	8,20	64,36	23,95
2	3,37	8,24	63,94	23,47
3	45,31	50,29	4,40	
4	46,17	50,52	3,31	
5	3,48	7,93	64,21	23,46
6	3,81	8,11	65,76	21,46
7	45,62	49,82	4,56	
8	7,26	12,03	60,08	20,63

Table 5-3: EDX Analysis 2 (at%)

Spectrum	Ni	Al	Cr	Mo
1	7,93	12,28	60,67	19,13
2	4,51	8,59	66,85	20,06
3	45,61	48,73	5,65	
4	46,24	49,27	4,49	
5	11,06	12,36	58,18	18,40

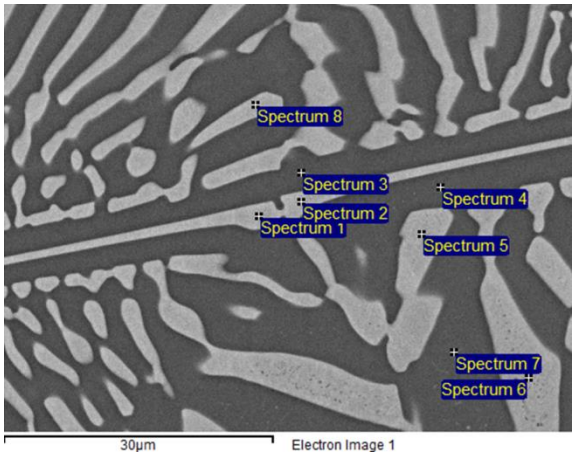

Figure 5-17: Sample for EDX Analysis 1

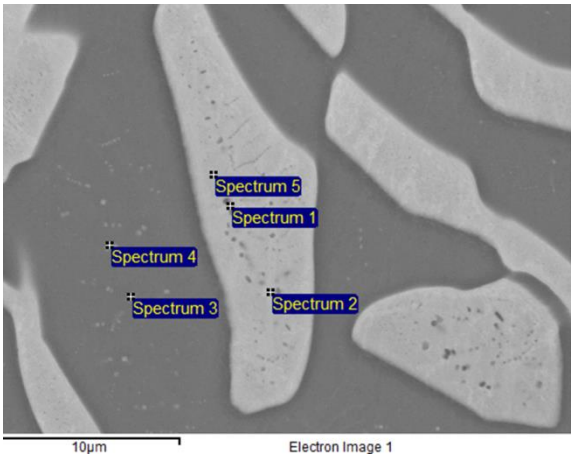

Figure 5-18: Sample for EDX Analysis 2

From the EDX analysis it was clear that the dark zone is NiAl phase while the light zone is CrMo phase. The number in the table is the atomic percentage of the elements in these zones. From these data, the average value of the elements of the two phases is reported in Table 5-4.

Table 5-4: Atomic and weight percentage of elements

	Ni	Al	Cr	Mo	
NiAl	45,79	49,73	4,48		at%
	63,05	31,48	5,47		wt%
CrMo	5,61	9,72	63	21,67	at%
	5,53	4,41	55,10	34,96	wt%

In the previous picture taken with optical microscope, it is clear that is the dark zone that growth in dendritic shape, i.e. the dendritic arms is NiAl. This means that this alloy is hypoeutectic.

5.2 Simulation

During the simulation of the solidification, the temperature and the solid volume fraction were analyzed. The goal is to understand the behavior of the material during the solidification and looking at the position and shape of the front of solidification in order to improve the process. At first, a simulation with the same parameters of the physical experiment was done. A melt and heater temperature of 1620 °C (the maximum temperature possible to reach with the used oven), a cooling plate temperature of 20 °C, and a withdrawal velocity of 3 mm/min were used. After the first simulation and according to its results, other configurations for temperature and withdrawal velocity will be tested aiming at an optimized process.

Simulation 1

During this simulation the same parameter of the physical experiment was used. In Figure 5-19 the solid volume fraction is shown, where 0 is liquid and 1 is solid, and the areas between 0 and 1 is the mushy zone. Looking on this area, the shape of the solidification front is shown.

In the central body the front of solidification is quite planar, but the problem is in the arm section. In these parts the solidification in fact is almost directional, but from the left to the right, or in other terms orthogonal to the desired solidification direction. This is due to the presence of the heater on the right and the central column of the shell mold on the left, that lead to a shadow effect which lowered the temperature on the left, with a temperature gradient from left to right. Moreover, the mushy zone (the region between solidus and liquidus line) is bigger than the height of the arm, and this fact leads to a non-directional growth in the arm. This last aspect is easier to understand with an analysis of the temperature gradient provided in Figure 5-20.

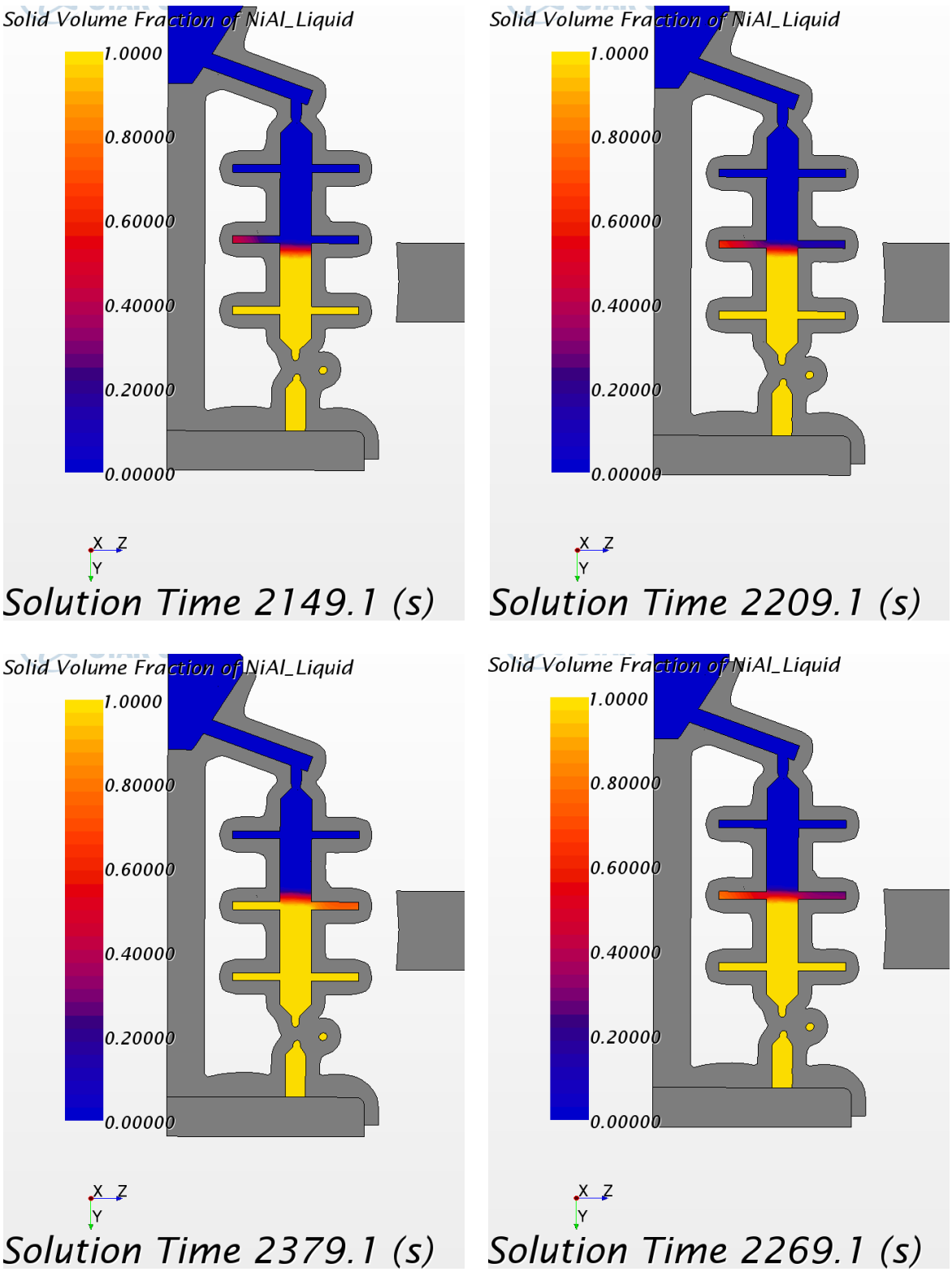

Figure 5-19: Evolution of the front of solidification over time, from top left picture in clockwise direction, at 3 mm/min of withdrawal velocity and 1620 °C of maximum temperature

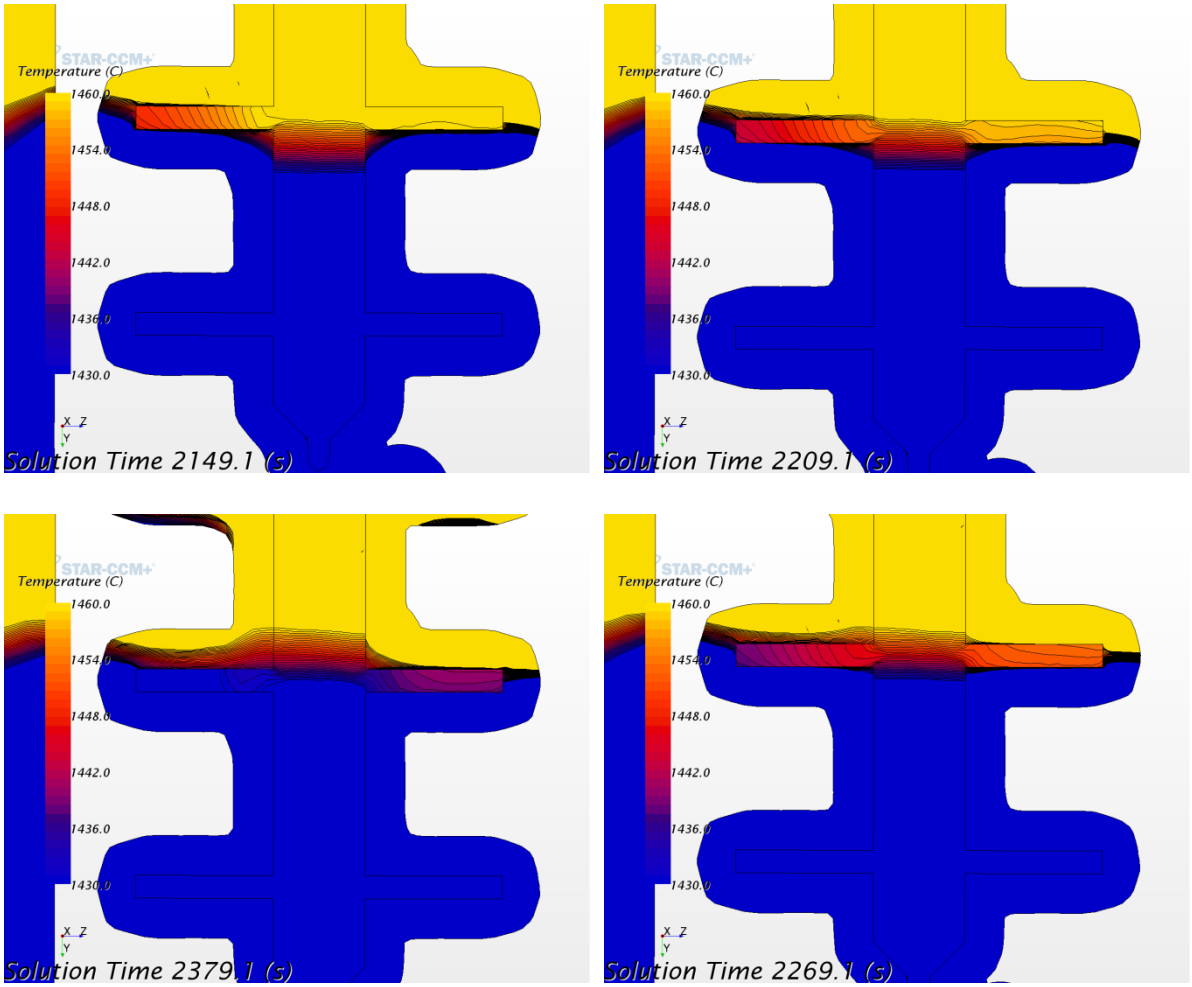

Figure 5-20: Temperature evolution over time in the mushy zone, from top left picture in clockwise direction

In Figure 5-20 there is the same part of Figure 5-19, but with different zoom and the isotherm lines were shown. In this case were shown only the lines between solidus and liquidus temperature, in order to understand the behavior of the temperature in the mushy zone. From these pictures, the behavior of the solidification can be understand, by following the shape of the solid and liquid line at respectively 1430 °C and 1460 °C. While in the left arm the solidification starts from left and proceed rightward, in the right arm the isotherm line at the beginning of solidification are horizontal, then the solidification begin with the desired shape, but in the end proceed from left to right as in the left arm. An explanation for this fact is the presence of a gradient of temperature from left to right, due to the presence of the heater on the right, and the central column of the shell mold on the left that lead to a shadow effect which lowers the temperature.

In the specimen there are three couples of arms i.e. three parts where there is a change of shape. It is interesting to observe that the fronts of solidification in the middle and in the top couple of arms are the same while it is different for the lower couple of arms.

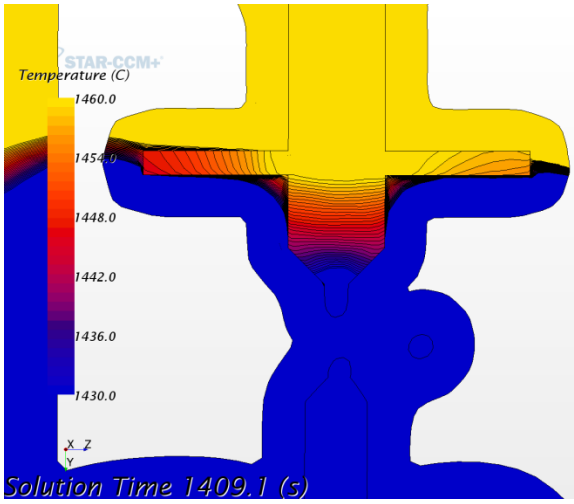

Figure 5-21: Temperature behavior in the mushy zone in the first couple of arm

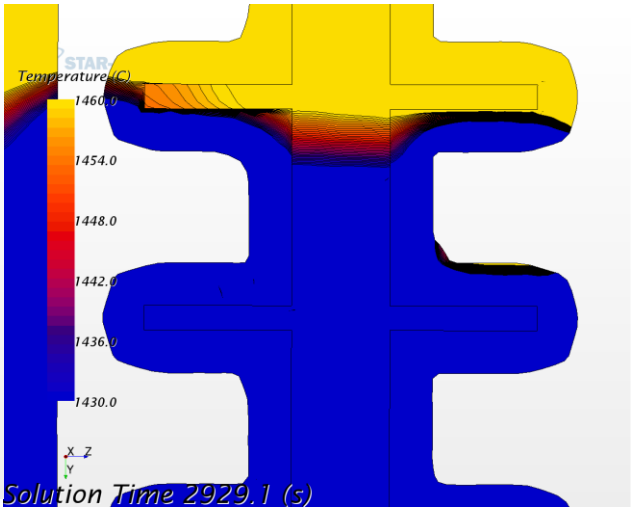

Figure 5-22: Temperature behavior in the mushy zone in the last couple of arm

This fact is shown in Figure 5-21 and Figure 5-22, where it clearly is visible that the mushy zone is bigger compared to the previous case, and has a visibly more curved shape of the solidification front. The probable explanation for this fact is that in this first part of solidification there is a lot of change in cross section (the first solidification chamber, the helix, the cone shape of the first part of specimen all altering the shape and cross section and thus destabilizing the solidification front) which is why a steady state i.e. a planar front couldn't be reached yet.

With this analysis of the solidification with the parameters used for the physical experiment, the main problem lies within the solidification inside the arm sections which needs to become more planar while also being oriented in accordance to the solidification of the central column. The desired structure is directional and at the same direction in all the parts of the specimen, without different solidification direction in the arms. Another goal is to reduce the distance between the solid and liquid line (i.e. reduce the thickness of mushy zone by increasing the temperature gradient inside the Bridgman furnace), in order to have a more regular structure. As explained before in chapter 3.1, with a higher temperature gradient the problem of one phase instability will be reduced.

Simulation 2

In this simulation the withdrawal velocity was lowered from 3 mm/min to 1 mm/min. During the analysis of the specimen it was seen that the structure is cellular. As shown in Figure 3-22, in order to obtain a planar front of solidification the withdrawal velocity has to be lower or the temperature gradient has to be higher. With modify of this value the microstructure cannot be analyzed using this software, but the macroscopic shape of the solidification front can. A higher temperature gradient is impossible to obtain with the used furnace, because it depends on the difference of the temperature of the two chambers and on the thickness of the insulation baffle, which is fixed for a certain furnace. As shown in the microstructure analysis the front of solidification that we have is cellular. With a lower withdrawal velocity it can become planar.

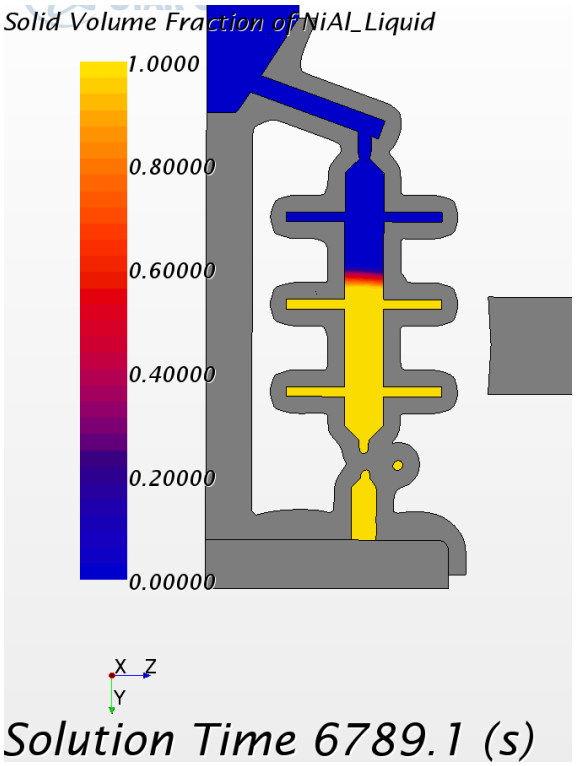

Figure 5-23: Position of front of solidification with 1 mm/min of withdrawal velocity

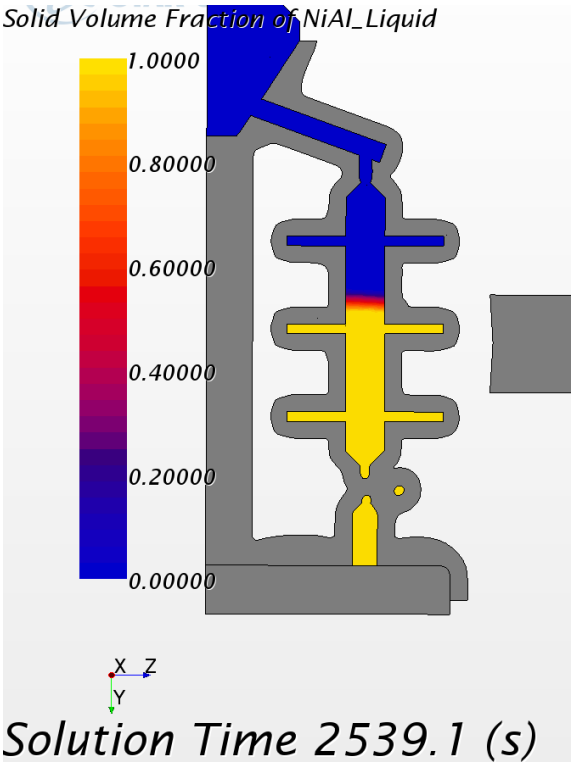

Figure 5-24: Position of front of solidification with 3 mm/min of withdrawal velocity

As shown in Figure 5-23 and Figure 5-24 (taken with the front of solidification positioned at the same height in the specimen), with a lower withdrawal velocity a new problem appears. The front of solidification, with a withdrawal velocity of 1 mm/min, is in higher position in respect to the baffle than for the case with 3 mm/min. This is because the NiAl 28Cr 6Mo have a higher thermal conductivity compared to the other Ni-based alloy. The difference is

not big, but there is also a more visible curvature of the solid/liquid surface for the slower case. Moreover, in the arms the behavior is exactly the same as in the previous case i.e. the solidification is orthogonal to the desired growth direction. This fact is explained in Figure 5-25, by following the isotherm line. The microscopic shape could be planar instead of cellular, but the macroscopic shape of the front of solidification is also more curved than before.

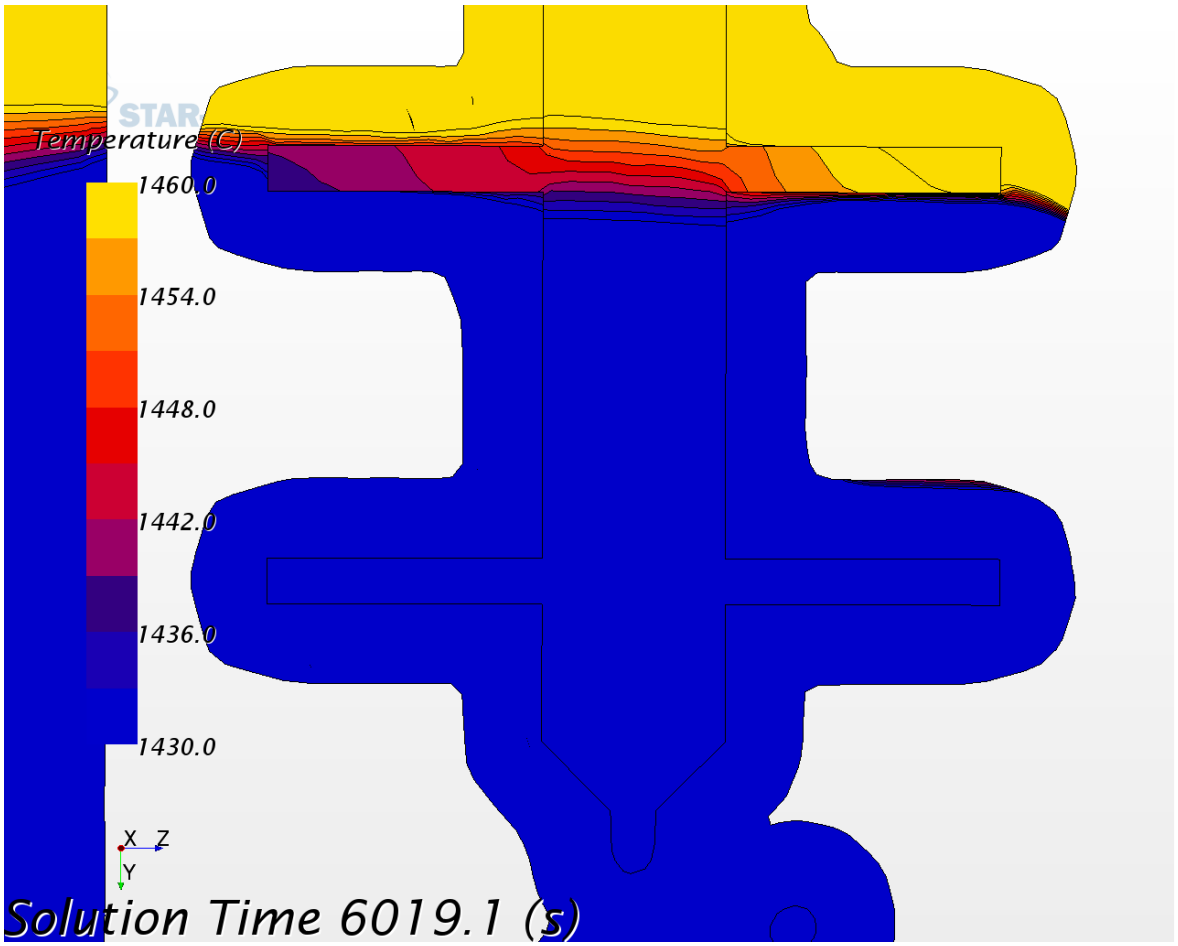

Figure 5-25: Solidification behavior at 1620 °C and 1 mm/min of withdrawal velocity

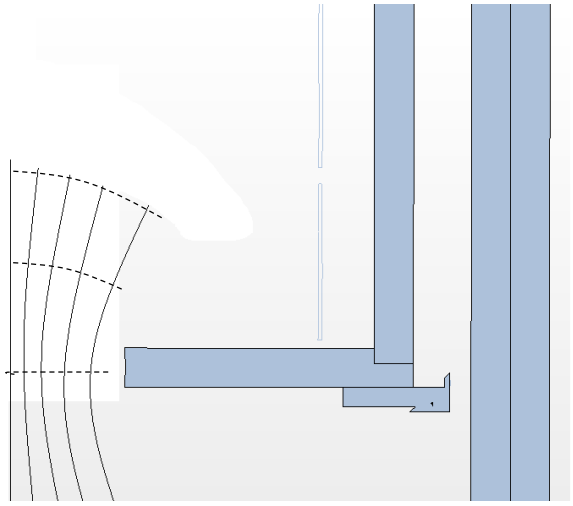

Figure 5-26: Temperature field between heating and cooling chamber, the curved line in the left are the temperature field between heated and cooled zone in the furnace.

As explained in Figure 5-26, there exists a temperature field between the two chambers of the Bridgman furnace, showed by the continuous line. The front of solidification shape is orthogonal to these lines, i.e. is the dashed line in figure and for this reason it has to be placed in the middle of the baffle between heated and cooled zone. As seen before, in the condition of the first test the front of solidification is placed in higher position compared to the middle of the baffle. The withdrawal velocity needs to be increased and not lowered, in order to obtain a front of solidification in lower position (and then a planar front of solidification). However, an increase of the withdrawal velocity is not recommended, because the microscopic shape of the front of solidification becomes worse (again, having a look to the Figure 3-22).

Simulation 3

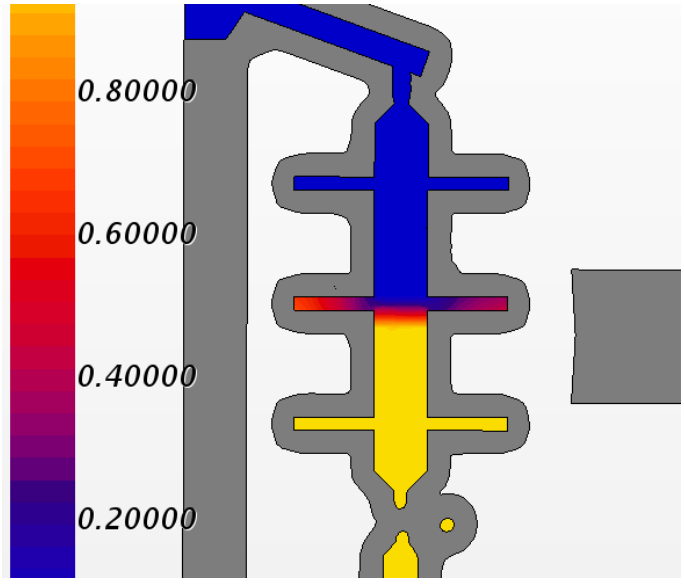

Figure 5-27: Front of solidification at 1620 °C and 5 mm/min of withdrawal velocity

A simulation with higher withdrawal velocity was done, only to verify if it is possible with this oven to reach a planar macroscopic front of solidification, but with this alloy the structure in this case most certainly won't be directional. Maybe it is possible to have a more regular structure with an exactly eutectic alloy, but an exact eutectic composition is very difficult to reach. The results of the solidification done with higher withdrawal velocity (cf. Figure 5-27) are not encouraging. A velocity of 5 mm/min has been chosen, but is not enough for place the solidification front in lower position, for this purpose the velocity must be higher. But also with this velocity, the solidification behavior

in the arm is worse than the previous case. Other simulation with the temperature of 1620 °C will not be made.

Simulation 4

A more practicable solution is using a higher temperature inside the heating chamber. The first attempt was made with 1700 °C in the heating chamber and 3 mm/min as withdrawal velocity. As shown in Figure 5-28, the front of solidification is in the desired position in the middle of the baffle, and Figure 5-29 shows that the thickness of the mushy zone is lower than before (because of the higher temperature gradient) and the front of solidification in the body is planar. A problem remains in the arm section: the behavior is certainly better compared to before, but the solidification in this area remains not directional. The temperature gradient needs to be increased more and the withdrawal velocity has to be lower to keep the front of solidification in the same position.

Simulation 5

This simulation was conducted with a heating chamber temperature of 1750 °C and a withdrawal velocity of 1.5 mm/min. Figure 5-30 and Figure 5-31 show the front of solidification in correspondence with the arms. With the given temperature and velocity settings, the front of solidification is positioned at the desired height and is planar. Also in the arm, the solidification happens in the desired direction, but is not perfectly planar. In the arm, moreover, the distance between two isotherm lines is higher than in the body, the temperature gradient, then, is lower. This means that probably, also if the solidification in the arm in this case is in the desired direction, the low temperature gradient give a misaligned structure.

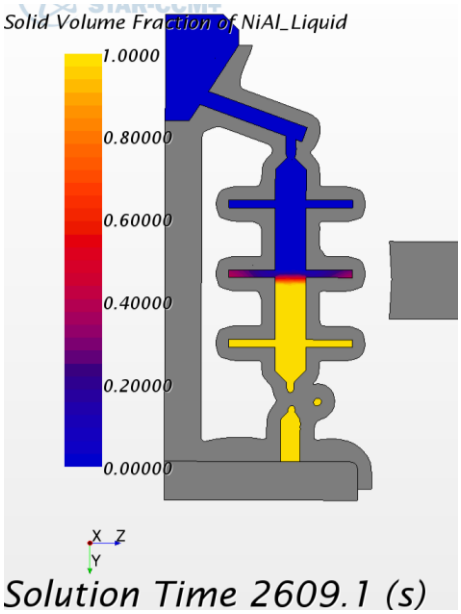

Figure 5-28: Position of the front of solidification, 1700 °C and 3 mm/min

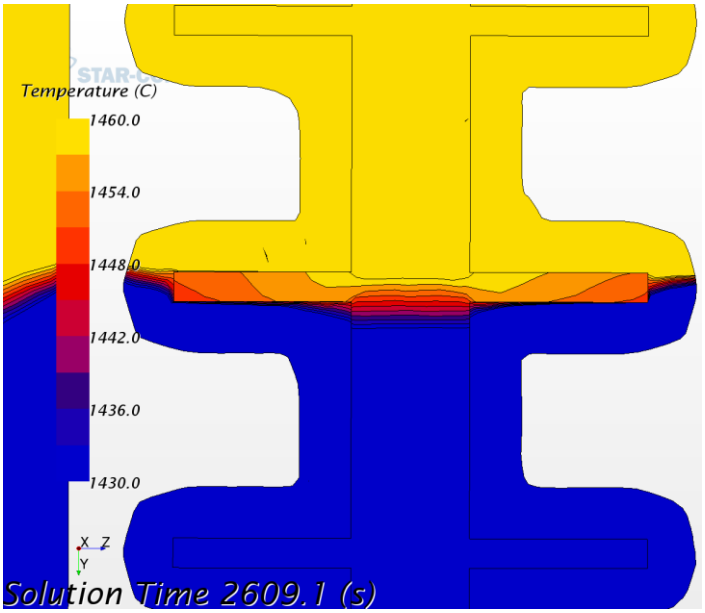

Figure 5-29: Temperature behavior with 1700 °C and 3 mm/min

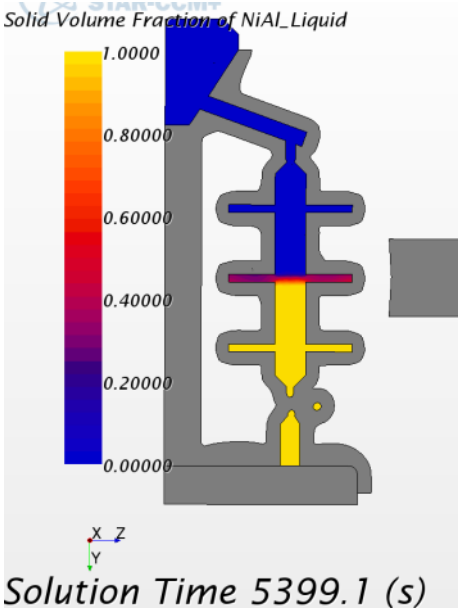

Figure 5-30: Position of the front of solidification, 1750 °C and 1.5 mm/min

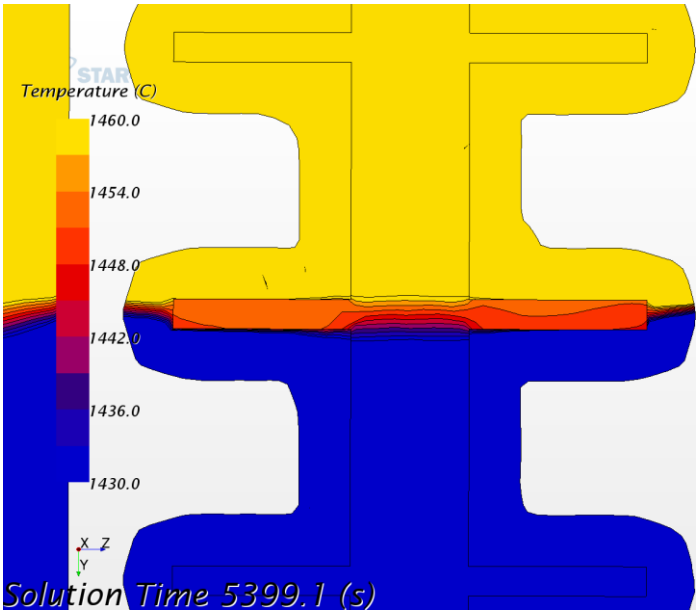

Figure 5-31: Temperature behavior with 1750 °C and 1.5 mm/min

After this simulation, it is seen that a planar front of solidification is possible to obtain with changing the parameters of the simulation in order to placing the front of solidification in the desired positions. With a fixed temperature gradient, the withdrawal velocity can be changed for this purpose. But also with a macroscopic planar front of solidification, the situation in the arm is not perfectly the same as in the central part of the specimen. Probably, the structure in these areas is not as desired. In order to also obtain the desired structure in the arm sections, the temperature gradient needs to be increased while the mushy zone has to be lowered.

Simulation 6

The next step is a temperature in the heating chamber of 2000 °C. A withdrawal velocity of 3 mm/min was chosen as first choice, in order to check how much the solidification front becomes lowered. In Figure 5-32 and Figure 5-33 this condition was shown.

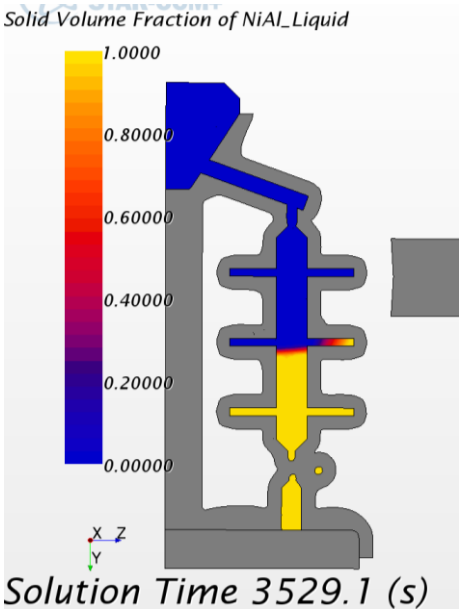

Figure 5-32: Position of the front of solidification, 2000 °C and 3 mm/min

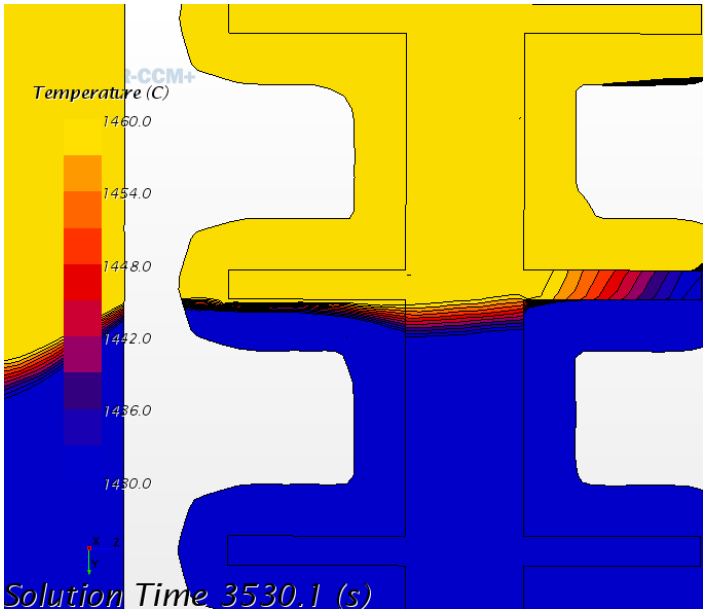

Figure 5-33: Temperature behavior at 2000 °C and 3 mm/min

The thickness of the mushy zone is smaller than in the previous case and the solidification front is at a very low position. Its curvature, moreover, is very distinct. This is not a practicable solution because the solidification front shape is curved, the lamellae will be not aligned. The withdrawal velocity needs to be lowered.

Simulation 7

A new test was then conducted, with the same temperature but with a low withdrawal velocity. In this case, a velocity of 0.3 mm/min was chosen. The result is not encouraging, the front of solidification is higher than before, but not so much while the withdrawal velocity is changed a lot. Probably, the temperature gradient is too high and a position of the solidification front in the middle of the baffle is not possible with this type of oven.

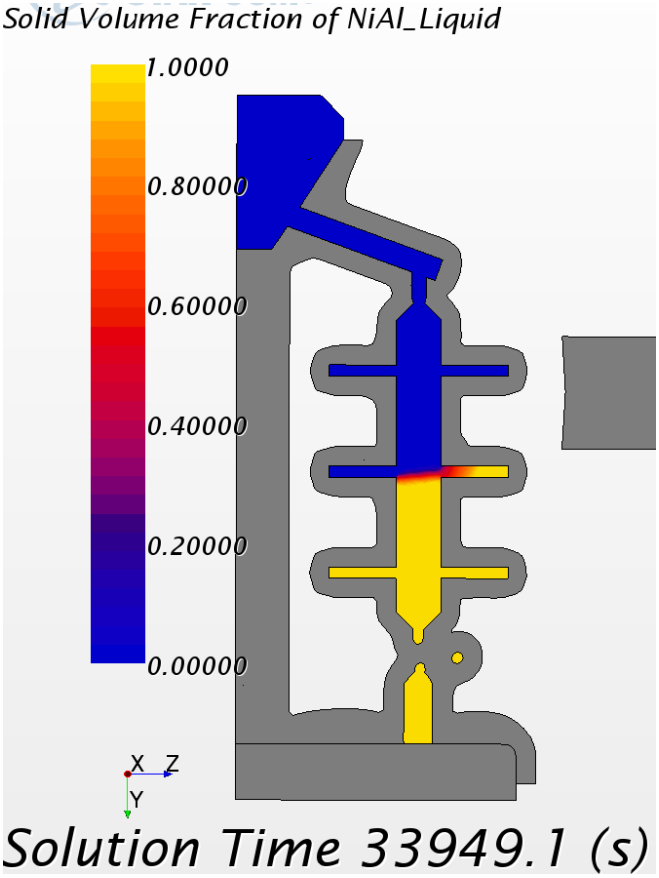

Figure 5-34: Solidification front at 2000 °C and 0.3 mm/min

6 Conclusion and outlook

Requirements

The goal of this work is to obtain an in-situ composite material with aligned lamellae. To obtain that, there are two conditions to satisfy: to obtain both macroscopic and microscopic planar solidification front.

The microscopic solidification front could be planar, cellular, dendritic or equiaxed. If it is not planar, the lamellae in the microscopic cross section grow in a non-linear manner. With a fixed material, the two changeable parameter in order to obtain a microscopic solidification front is the solidification rate and the temperature gradient.

The macroscopic solidification front is also important, because if it is curved lamellae grow curved instead of linear. In order to change this aspect, the position of the solidification front in respect of the baffle between heated and cooled furnace chamber have to be changed. For change this position, with a fixed material and furnace, the temperature gradient between the two chambers and the withdrawal velocity has to be changed.

Undercoolability test

With the first physical test the undercoolability properties of the material was tested. Was find an average undercoolability value of 23.9 ± 4.4 °C that is small compared to other superalloy. This means that during the solidification if there is small change of temperature in some areas (for example due to the curved macroscopic solidification front) this material can nucleate and thus create other grains with misaligned structure compared to the principal structure. Obtain a planar macroscopic solidification front with this material is for this reason more important than with other superalloy.

Directional solidification

The analysis of the structure during the directional solidification physical test showed a cellular microscopic solidification front in the body of the specimen, and again a cellular solidification front in the arm but in the orthogonal direction respect of the direction of the withdrawal velocity. With this test is possible to understand that a perfect macroscopic planar solidification front was not obtained, some changes of the process parameters is needed.

Simulation, outlook and possible developments

Also the simulation confirms that planar front of solidification was not reached. In the only configuration where the front of solidification is quite planar the structure probably will be not formed by perfectly aligned lamellae because of the low temperature gradient. In the simulation 7 a thinner mushy zone was reached, but with a bad shape of the solidification front. In this case the withdrawal velocity is very low, and this is not practicable for commercial use. The production time in fact became very high, and then the productivity will be very low. The temperature gradient could be incremented by using a different furnace, which would give the possibility to reach the desired position (in the middle of the baffle) of the solidification front through higher temperature gradients. This effect should be the focus of future investigations. Another focus for future improvement could be the study of that furnace that actually doesn't exist.

With the used oven, shape and alloy it is not possible to reach a perfectly directional solidification in the change of cross section zone. The real parts produced with directional solidification can be designed in order to optimize the structure. A first shape change can be made with using of filled corners instead of sharp edges. In the real parts the change of cross section needs to be lower, or more gradually, and for this purpose it will be interesting to produce a specimen with constant change of cross section, like a cone, to study the behavior of the solidification in this case. In fact a constant withdrawal velocity with a cone shape will lead to a non-constant position of the front of solidification.

Another problem is the material. Ideally, a eutectic alloy has not a range of solidification temperature, but only one solidification temperature called eutectic temperature. If the alloy is not perfectly eutectic, there is the problem of one phase instability discussed before, that will lead to a non-desired dendritic structure. The used material should be eutectic, but it is not, a better control of composition could give a better results but this is very hard to reach especially in an industrial process like this.

During this work an experiment and simulation with different thicknesses of the ceramic shell mold was not conducted, but this is an interesting change. A thinner shell mold can lead to a different shape of the front of solidification because of the lower thermal insulation of the shell mold. This is one of the possible changes that are simple to implement, because using a different thickness of the shell mold is a feasible change, as opposed to changing a furnace which is not feasible.

One of the major problems seen with the simulation is the difference between left and right arm, due to the shadow effect of the central column. The shape of the shell mold can be changed in order to avoid the shadow effect. This involves the use of only one central specimen instead of nine radial specimens. This modification of the shape could be a problem, because in industrial use the productivity will be lower. Moreover, for research purposes, with nine specimens there is a possibility to study nine different shapes with only one melting operation making the process faster. A shape without the central column could be produced, or better with a smaller central column. The shadow effect will be present, but lower than before.

Another problem seen on the simulation is that the front of solidification shape in the first couple of arms is different than the other two, and a possible explanation of this fact is that a steady state was not reached because of the change of cross section of the shape. Then, a specimen with longer initial parts could be produced, in order to also improve this initial part.

A different temperature gradient in the central body and in the arms was seen in the simulation. The arms have a very low temperature gradient, compared to that in the central body, and for this reason also if the front of solidification was planar, the structure probably is not directional as desired. A high temperature gradient in the arms was needed. Moreover, in the central body the solidification happens by growth of the crystal, but in the arms there is nucleation. A cooling of these parts could help.

With the used ceramic shell mold this is not possible, but is possible to use different type of shell mold. The purpose is to obtain a better cooling of the lower part of the arm and thus a cooling system for the lower part of the arm is needed. The high temperature in these parts must be taken into account which is why the use of a liquid metal cooling possibly is suitable for this task, and also in order to obtain a higher temperature gradient. This solution of course leads to a very complicated and expensive shell mold, but could be a possible solution to solve the problem of this process. Moreover, if it works properly a higher withdrawal velocity can be used and then the high cost of the process could be equilibrated with the higher productivity. Because of the probably high costs and time needed to realize that this solution first of all should be tested by running and optimizing a simulation of the process.

7 Bibliography

mtarr.co.uk. (1988). Retrieved from mtarr: http://www.mtarr.co.uk/

Bogner Samuel, I. E.-P. (2015). Investigation of the Undercoolability of Ni-Based Alloys Using High Temperature Thermal Analysis. *Metals*.

C.A., B. (1988). *Effect of 0.1 at % Zirconium on the cyclic oxidation resistance of β-NiAl* (Vol. 30). Oxidation of Metals.

Cambridge, U. o. (n.d.). Retrieved from doitpoms: http://www.doitpoms.ac.uk

Cline H.E., W. J. (1970). *The effect of alloy additions on the rod-plate transition in the eutectic NiAl-Cr.* MetTrans Journal.

Cline H.E., W. J. (1971). *Structures, faults and the rod-plate transition in eutectics.* MetTrans Journal.

Daniel B. Miracle, R. D. (1995). *NiAl and its alloys.*

Doychack J., S. J. (1989). *The oxidation of Ni-rich NiAl intermetallic.* Warrendale: The minerals, metals and materials society.

H.S. Carlslaw, J. J. (1959). *Conduction of heat in solids.* Oxford University press.

Harmorche M.R., W. A. (1987). *Temperature and composition dependence of young's modulus in polycrystalline B2 NiAl.* Journal of Testing and Evaluation.

Hillier. (1984). *Ph.D. Thesis.* Cambridge: University of Cambridge.

J.A. Burton, R. P. (1953). *21.* The Journal of Chemical Physics.

Kraft, R. (1960). *Patent No. US Patent 3129952.*

Lowell C.E., B. C. (1990). *Cyclic oxidation resistance of a reaction milled NiAl-AlN composite.* Pittsburgh: D.L.Anton.

M.C., F. (1974). *Solidification processing.* New York: McGraw Hill.

McLean. (1983). *Directionally solidified materials for high temperature service.* The metals society.

Northcott, L. (1938). *Inst. Met.*

Peter R. Beeley, R. F. (1995). *Investment casting.* London: The institute of materials.

R., D. (1991). *NiAl alloys for high-temperature structural applications* (Vol. 43). J. Met.

R.D. Noebe, R. B. (1993). *Int. Meter. Rev. 38.*

Ronald D. Noebe, R. R. (1992). *Review of the physical and mechanical properties and potential applications of the B2 compound NiAl.* Cleveland, Ohio: NASA.

Shank, F. V. (1970). *Mater. Sci. Eng.* (Vol. 6).

Taylor R.E., G. H. (1986). *Thermophysical properties of aluminides.* West Lafayette: Purdue University.

Tressler R.E., H. J. (1991). *Advanced high temperature composite materials for engine applications.* Pennsylvania: The Pennsylvania State University.

V.G. Smith, W. T. (1955). *33.* Canadian journal of physics.

W. Kurz, D. F. (1992). *Fundamentals of solidification.* Lausanne: Trans tech publications Ltd.

W.A. Tiller, K. J. (1953). *1.* Acta Metallurgica.

Walter J.L., C. H. (1970). *The effect of solidification rate on structure and high temperature strength of the eutectic NiAl-Cr.* MetTrans Journal.

Zhao Shang, J. S. (n.d.). *Effect of withdrawal rate on the microstructure of directionally solidified NiAl-Cr(Mo) hypereutectic alloy.* China: Northwestern Polytechnical University.

8 Compendio

8.1 Motivazione

La continua ricerca per incrementare la spinta e/o il rendimento delle moderne turbine a gas ha portato alla necessità di utilizzare materiali resistenti a temperature sempre più elevate. Infatti, l'efficienza delle turbine a gas è direttamente legata alla massima temperatura ottenibile, quindi un progresso nel campo dei materiali utilizzati significa un progresso nell'efficienza dei motori. Le pale di queste turbine sono sottoposte quindi a temperature elevate ed elevati stress dovuti alla forza centrifuga, è essenziale quindi che i materiali utilizzati abbiano una elevata resistenza al creep e alla fatica termica.

Entrambe queste proprietà sono legate alla presenza di bordi grano trasversali al carico applicato. Dalle prime turbine un rilevante miglioramento arrivò con la solidificazione unidirezionale, che creava dei grani allungati nella direzione del carico, eliminando quindi la presenza dei bordi grano trasversali. Un successivo miglioramento si ebbe con la creazione di un monocristallo, nel quale l'intera pala era formata da un unico cristallo, eliminando dal tutto i bordi grano. Quest'ultima soluzione è l'attuale stato dell'arte della tecnologia.

Sono attualmente utilizzate per questa applicazione leghe di nickel, scelte per la loro eccezionale combinazione tra resistenza alle alte temperature, durezza e resistenza all'ossidazione. Per migliorare ulteriormente la resistenza all'ossidazione e corrosione, aspetto importante per componenti che lavorano ad alta temperatura, sono stati sviluppati dei rivestimenti per le pale realizzati in leghe NiAl. Utilizzare questo materiale per produrre l'intera pala, e non solo il rivestimento, porterebbe ad una riduzione del peso per via della sua minore densità, e ad un aumento delle prestazioni e dei rendimenti, per via del suo elevato coefficiente di conduzione termica che porta ad un più efficace raffreddamento della pala e quindi alla possibilità di farla lavorare a temperature superiori. Lo svantaggio maggiore di questa soluzione è dovuto all'elevata fragilità a temperatura ambiente di questo materiale, che ne rende impossibile l'utilizzo.

Con l'utilizzo di una lega eutettica, abbinata alla solidificazione unidirezionale, è possibile creare un materiale composito in-situ, dove durante la solidificazione le due fasi si separano formando la matrice e le fibre o lamelle, disposte lungo la direzione della solidificazione. La creazione di un materiale composito di questo tipo può aumentare la tenacità del materiale, rendendo possibile il suo utilizzo per la realizzazione dell'intera pala e non solo come rivestimento.

8.2 Teoria e letteratura

In questo capitolo sarà discussa la parte teorica di tutti gli aspetti del lavoro fatto, a partire quindi dalla solidificazione, produzione dello stampo e simulazione via software.

8.2.1 Solidificazione

Per solidificazione s'intende il cambiamento di fase da solido a liquido. In molti materiali le temperature di solido e liquido sono diverse, dipende dagli alliganti presenti. Queste temperature possono essere trovate nel diagramma di fase, in altre parole un diagramma in cui sono presenti le fasi all'equilibrio per diverse percentuali di elementi e a diverse temperature (Figure 8-1).

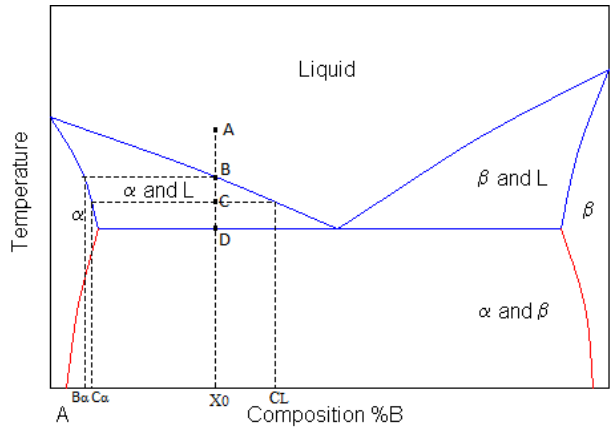

Figure 8-1: Diagramma di fase

Generalmente quindi esiste un range di temperature di solidificazione, eccetto che per le leghe definite eutettiche, in cui è presente una sola temperatura di solidificazione, dove il materiale passa direttamente da liquido a solido.

La solidificazione inizia da dei nuclei, in altre parole piccole particelle solide che poi crescono fino alla completa solidificazione di tutto il pezzo. La nucleazione, ovvero la creazione di questi nuclei, necessita di una certa energia. Questa energia è fornita termicamente, con un effetto di sotto-raffreddamento, in altre parole il materiale inizia a solidificare a una temperatura più bassa rispetto a quella di equilibrio. La solidificazione può quindi essere eterogenea, inizia cioè da siti di nucleazione esistenti come le pareti dello stampo, particelle presenti nel liquido o altri nuclei già esistenti, oppure omogenea, nel caso in cui non ci siano siti preferenziali di nucleazione. È chiaro che in un metallo liquido, durante la solidificazione non c'è un unico sito di nucleazione ma sono molti. Questi quindi crescono fino a unirsi tra loro, formando in questo modo i grani cristallini.

8.2.2 Solidificazione eutettica

Per ogni lega esiste una composizione in cui la temperatura di fusione è minima e non esiste un range di solidificazione. Per questo motivo, durante il raffreddamento della lega

questa diventa solida in un tempo idealmente infinitesimo. Le due fasi presenti crescono quindi contemporaneamente.

8.2.3 Solidificazione direzionale

La solidificazione direzionale è un processo controllato in cui la solidificazione inizia in un punto ben definito dello stampo e prosegue lungo una direzione predefinita. Il metodo più semplice per ottenere questo è l'utilizzo di uno stampo con un ottimo coefficiente di conduzione termica da un lato e un ottimo isolamento dall'altro. Questo sistema, d'altro canto, è anche quello che permette il minore controllo sulla solidificazione. Un metodo migliore si basa sullo stampo che si può muovere a velocità controllata tra due camere all'interno di un forno, una fredda e una calda.

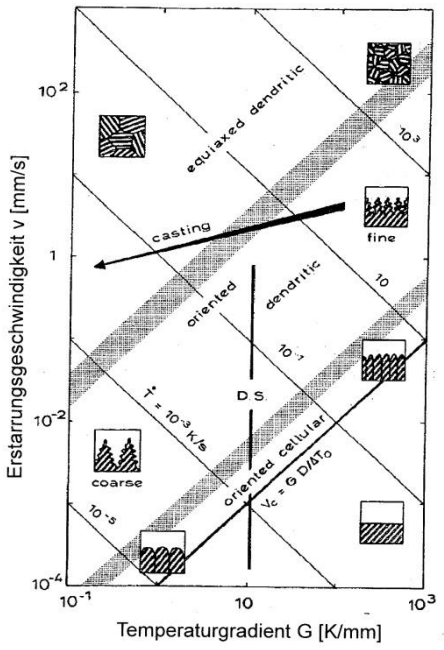

Figure 8-2: Interfacce solido/liquido ottenibili con diverse combinazioni tra gradiente di temperatura e velocità di ritiro dello stampo

Con questa tecnica si può controllare la direzione di crescita dei grani, ottimizzando determinate caratteristiche del componente. Utilizzando questa tecnica di solidificazione con un materiale eutettico, è possibile far crescere le due fasi nella direzione di solidificazione, creando un materiale composito, nel quale una delle due fasi forma la matrice, e l'altra fase forma le fibre. Il principale vantaggio nel creare un materiale composito con questa tecnica è che il pezzo è pronto in un singolo passaggio, senza creare i due materiali singolarmente e poi unirli. Lo svantaggio principale è dovuto alla non possibilità di scelta dei singoli materiali, non è possibile quindi ottimizzarli in base alle caratteristiche desiderate.

Durante la solidificazione direzionale, i parametri principali del processo sono il gradiente di temperatura tra le due camere e la velocità di ritiro dello stampo. Al variare di questi due parametri, varia l'interfaccia solido/liquido (Figure 8-2). Questa interfaccia può essere planare, cellulare, dendritica o equiassica. Quella desiderata per ottenere le lamelle della seconda fase perfettamente allineate è l'interfaccia planare. Le altre tipologie, infatti, comportano una deviazione dalla linearità delle lamelle.

8.2.4 Leghe nickel-alluminio

Le leghe NiAl presentano ottime qualità quali elevata temperatura di fusione, bassa densità, elevato modulo di Young ed eccellente resistenza all'ossidazione a temperature elevate. Inoltre, la conducibilità termica è da 4 a 8 volte superiore rispetto alle altre leghe di nickel. Presentano però una bassa duttilità e un'elevata fragilità a temperatura ambiente, fattori che ne limitano l'utilizzo industriale.

8.2.5 NiAl 28Cr 6Mo

In questa tesi sarà studiata la lega NiAl 28Cr 6Mo. Si tratta di una lega eutettica adatta alla creazione di un composito in-situ. Il materiale formato avrà una matrice in NiAl, con lamelle di CrMo. Dal punto di vista della fragilità, la struttura a lamelle è desiderata rispetto a quella a fibre, poiché una cricca presente nella matrice fragile troverà più difficoltà a superare una lamella per raggiungere il resto della matrice.

8.2.6 Investment casting

Chiamato anche processo a cera persa, è un processo industriale in cui dapprima viene realizzata la forma della cavità dello stampo in cera, questa è quindi rivestita da un materiale ceramico refrattario, che costituirà lo stampo vero e proprio, infine la cera viene sciolta e rimossa dallo stampo. Al termine di questo processo, lo stampo è posto in un'autoclave ad alta pressione e temperatura per un processo di sinterizzazione che serve a conferirgli resistenza.

8.2.7 Simulazione

Durante questo lavoro sarà condotta una simulazione tramite un software FEM (Finite Element Method), in altre parole una tecnica numerica che ottiene una soluzione approssimata di un problema dividendolo in molti piccoli sotto problemi. Un'analisi agli elementi finiti è divisa in tre steps:

1. Pre-processing: in questa prima fase è realizzato il modello, dal quale è creata la mesh, in altre parole è diviso in molte piccole parti connesse tra loro. Sono poi assegnate le proprietà dei materiali e le condizioni al contorno, in altre parole carichi e vincoli.
2. Analisi: il problema è risolto utilizzando metodi numerici.

3. Post-processing: nell'ultima fase i risultati sono visualizzati graficamente (con l'aiuto ad esempio di colori) o numericamente, in base al tipo di problema da risolvere.

8.3 Sperimentazione

La parte sperimentale è divisa in due parti, nella prima è fisicamente realizzato lo stampo e quindi i provini da analizzare poi in laboratorio, mentre nella seconda parte questo processo viene simulato con il software Star CCM+.

8.3.1 Sperimentazione fisica

In questa parte sono realizzati due stampi, uno con l'unico scopo di misurare le proprietà di sotto raffreddamento del materiale, mentre con l'altro sono creati i provini tramite solidificazione direzionale per poter poi essere analizzati. Entrambi gli stampi sono creati con la tecnica a cera persa.

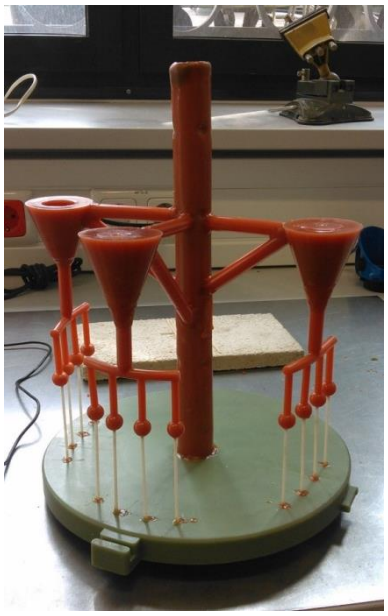

Figure 8-3: Forma in cera per la misurazione delle proprietà di sotto raffreddamento del materiale

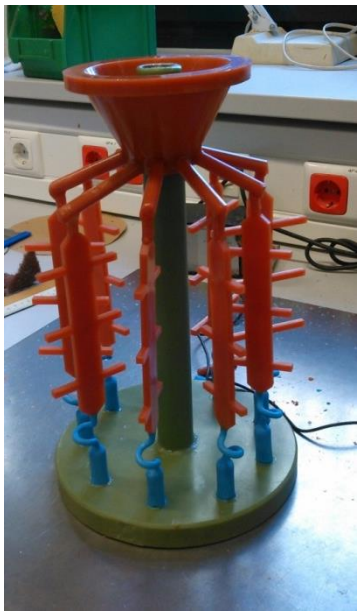

Figure 8-4: Forma in cera per la realizzazione dei provini tramite solidificazione direzionale

Creazione degli stampi

Le forme in cera sono assemblate da singoli componenti. Ogni componente viene realizzato tramite stampaggio ad iniezione, quindi sono saldati tra di loro fondendo la cera

tramite un saldatore apposito. La forma in Figure 8-3, formata da camere sferiche all'interno delle quali saranno poste le termocoppie per la misurazione della temperatura, protette dal tubo ceramico visibile in foto, è la cavità dello stampo per il test di sotto raffreddamento. Saranno utilizzate termocoppie di tipo B, scelte per la loro capacità di operare a temperature superiori ai 1800 °C. In Figure 8-4 invece si vede la forma della cavità per la creazione dei provini da analizzare, formati da un corpo centrale con dei bracci laterali. Questi bracci servono a valutare il comportamento della lega durante la solidificazione alla presenza di forti cambiamenti di sezione.

Queste cavità in cera saranno poi rivestite da diversi strati di ceramica refrattaria. Durante questo procedimento, la forma sarà rivestita da un collante e quindi da polvere di allumina, dopo l'asciugatura di questo primo strato si potrà procedere con la stesura del secondo e così via. Nel totale sono stati posti 12 strati. Per i primi tre, sarà realizzato un collante resistente alle alte temperature delle superleghe che non contiene SiO_2, mentre per gli altri sarà utilizzato un collante contenente SiO_2. La polvere di allumina utilizzata sarà di sezione crescente, fina per i primi due strati, media per il terzo e grossa per tutti quelli successivi. Serve della polvere sottile nei primi strati per ricalcare nel modo più fedele possibile la superficie della forma in cera. Quando questo stampo sarà pronto, sarà rimossa la cera in autoclave a 160 °C e 6 bar di pressione, successivamente lo stampo verrà sinterizzato a 1250 °C.

Set-up del forno

Per entrambi i test verrà utilizzato lo stesso forno, si tratta di una fornace Bridgman realizzata dalla ALD Vacuum technologies GmbH. La preparazione del forno consiste nel posizionamento dello stampo sul piatto in rame raffreddato ad acqua, e quindi per quanto riguarda il primo test tutte le termocoppie vanno collegate ai rispettivi cavi, per poter registrare le temperature in tempo reale. Sono poi rivestite da uno strato d'isolante, per evitare che i cavi si scaldino sfalsando la misurazione della temperatura. Nel test di sotto raffreddamento, il materiale è fuso portando il forno alla sua massima temperatura (1620 °C), quindi la temperatura è abbassata a 1300 °C per far avvenire la solidificazione, e questo è ripetuto ciclicamente per quattro volte. Alla fine di questo test, viene posizionato sul forno lo stampo per la realizzazione dei provini, anche in questo caso la temperatura viene portata a 1620 °C, il materiale fuso viene versato all'interno dello stampo e quindi lo stampo viene spostato tra la camera calda e quella fredda alla velocità di 3 mm/min.

Post-processing

Figure 8-5: Stampo ceramico con il materiale solidificato all'interno alla fine del processo

A questo punto, la ceramica deve essere rimossa per liberare i provini metalli. Nel primo stampo, questo serve per verificare che il materiale abbia fuso completamente e abbia riempito correttamente le camere in cui avveniva la misurazione della temperatura. La rimozione dello stampo è stata eseguita meccanicamente con l'utilizzo di una morsa da banco.

I provini liberati sono stati tagliati nelle sezioni d'interesse, immersi in una matrice polimerica di resina fenolica e quindi lucidati per essere analizzati al microscopio. Per tutte le analisi è stato utilizzato un microscopio ottico, mentre solo per un provino è stato utilizzato un microscopio elettronico a scansione con la tecnica EDX (Energy-dispersive X-ray spectroscopy) per analizzare la composizione delle due fasi che apparivano una nera, una bianca.

8.3.2 Simulazione

Al fine di simulare il processo di solidificazione è stato usato il software Star CCM+ attraverso l'interfaccia Star Cast sviluppata dall'azienda Access. La geometria è stata sviluppata direttamente all'interno di tale software, sfruttando il programma di modellazione 3D interno, e quindi trasformata in mesh. Data l'elevata quantità di tempo necessaria a completare una simulazione usando la geometria totale del pezzo, è stata modellata solo una parte (1/9) della geometria, sfruttando poi i vincoli di simmetria ciclica. Dopo la creazione della mesh, sono stati assegnati i materiali. Il materiale ceramico dello stampo, il piatto in rame, l'isolamento nella camera riscaldata e l'acciaio del forno erano già presenti nel database del programma, mentre il materiale da studiare (NiAl 28Cr 6Mo) e il vuoto presente all'interno del forno sono stati inseriti manualmente. Per il setup della superlega, sono stati usati i valori trovati durante la prova di sotto raffreddamento come temperature di liquido-solido, altri dati quali la conduttività termica sono stati presi da database online.

Successivamente sono state inserite le condizioni al contorno, ovvero le temperature iniziali, le temperature dei riscaldatori all'interno del forno e la velocità di ritiro dello stampo. La simulazione è quindi pronta per essere lanciata.

8.4 Risultati e discussione

In questo capitolo saranno discussi e commentati i risultati delle prove precedenti.

8.4.1 Sperimentazione fisica

Prova di sotto raffreddamento

La prova di sotto raffreddamento è stata la prima a essere eseguita. Durante questa prova sono stati testati tre materiali diversi: NiAl-9Mo, NiAl-28Cr-6Mo e NiAl-34Cr. Nonostante la temperatura del forno sia stata portata a 1620 °C, in altre parole oltre la temperatura di fusione, solo il NiAl-34Cr ha fuso ed è stato possibile quindi rilevarne i dati. Tuttavia le proprietà termiche di questo materiale sono molto simili a quelle del NiAl-28Cr-6Mo utilizzato anche per la seconda prova, la temperatura di fusione è la stessa, mentre le altre proprietà sono molto simili. Per il materiale che ha fuso, sono presenti i dati delle quattro termocoppie, ma una di queste ha rilevato temperature molto diverse dalle altre tre, per cui quel valore è stato considerato sbagliato e quindi non preso in considerazione.

Per ogni ciclo di solidificazione-fusione del materiale è stata calcolata la derivata dT/dt, attraverso la quale è possibile trovare i punti in cui il materiale inizia e finisce la fusione e la solidificazione (Figure 8-6).

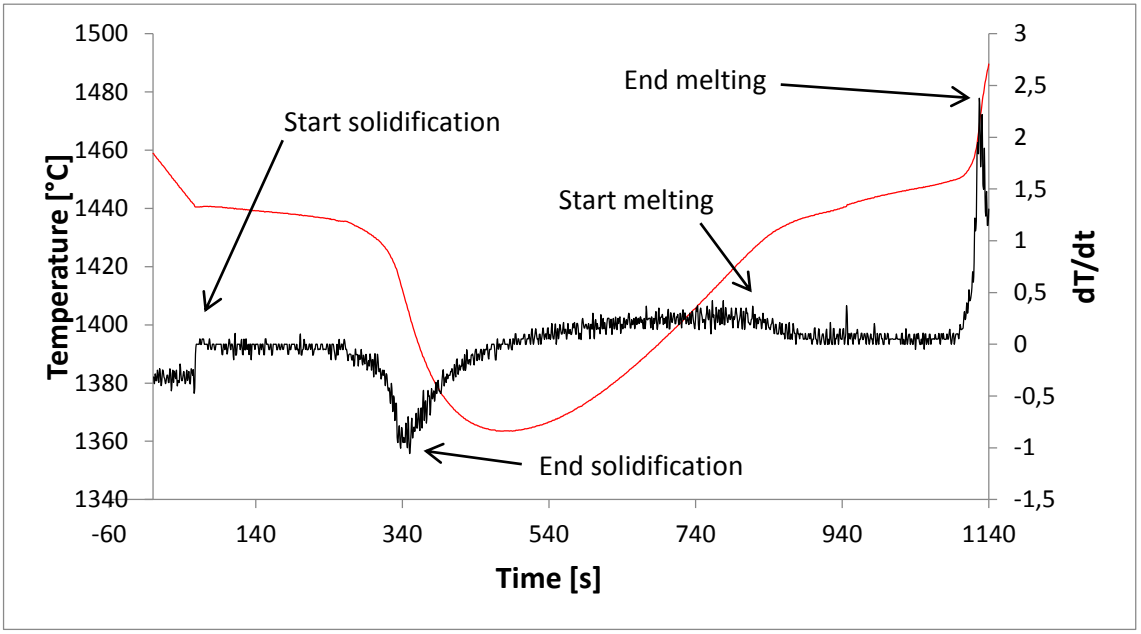

Figure 8-6: Curva temperatura-tempo (linea rossa) e sua derivata (linea nera) durante un ciclo di fusione-solidificazione del materiale

In corrispondenza del primo picco della derivata si ha la temperatura di nucleazione T_N, seguita dalla temperatura di fine solidificazione. Il materiale è fuso nuovamente, trovando le due temperature di solido (corrispondente con l'inizio della fusione) e di liquido (materiale totalmente liquido). Queste temperature saranno diverse da quelle del diagramma di stato, perché in questo caso non si ha l'equilibrio del sistema. La differenza tra la temperatura di liquido e quella di nucleazione da come risultato il valore di sotto raffreddamento cercato. Calcolando la media tra tutti i dati ricavati da questa prova, il materiale studiato ha un ΔT di sotto raffreddamento pari a 23.9 ± 4.4 °C. Si tratta di un valore piuttosto contenuto, se paragonato ad altre superleghe a base di nickel, questo significa che questa lega ha più probabilità di nucleare in punti diversi della struttura e quindi il raggiungimento di un'interfaccia solido-liquido perfettamente planare è ancora più importante che in altre leghe.

Solidificazione direzionale

Il provino realizzato mediante solidificazione direzionale è stato tagliato nei punti mostrati in Figure 8-7, ciascuno di questi pezzi tagliati è stato poi analizzato al microscopio. I tagli A e B servono a valutare il tipo di fronte di solidificazione, quello C va ad analizzare la forma delle lamelle nella parte laterale del provino, mentre i tagli D, E, F e G servono ad analizzare l'evoluzione della solidificazione nei bracci.

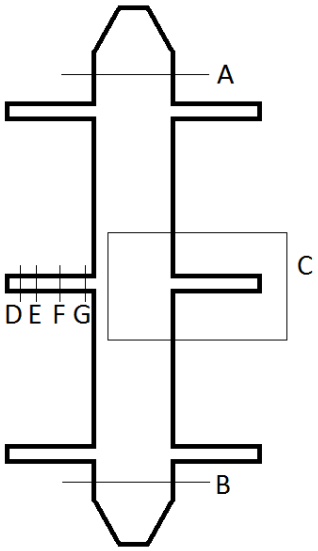

Dai provini A e B si vedono chiaramente le celle, quindi si può dire con certezza che il fronte di solidificazione è di tipo cellulare. Analizzando il provino C si vede che la solidificazione è di tipo direzionale nella parte centrale del corpo, ma nella zona del braccio la struttura appare disordinata. Analizzando meglio il braccio con i provini D, E, F e G, si nota una struttura cellulare del tutto simile a quella già vista nei provini A e B. Da quest'analisi si evince che la solidificazione nei bracci avviene in direzione ortogonale alla direzione di crescita desiderata, e il fronte di solidificazione è di tipo cellulare.

Figure 8-7: Zone in cui è stato tagliato il provino per l'analisi al microscopio

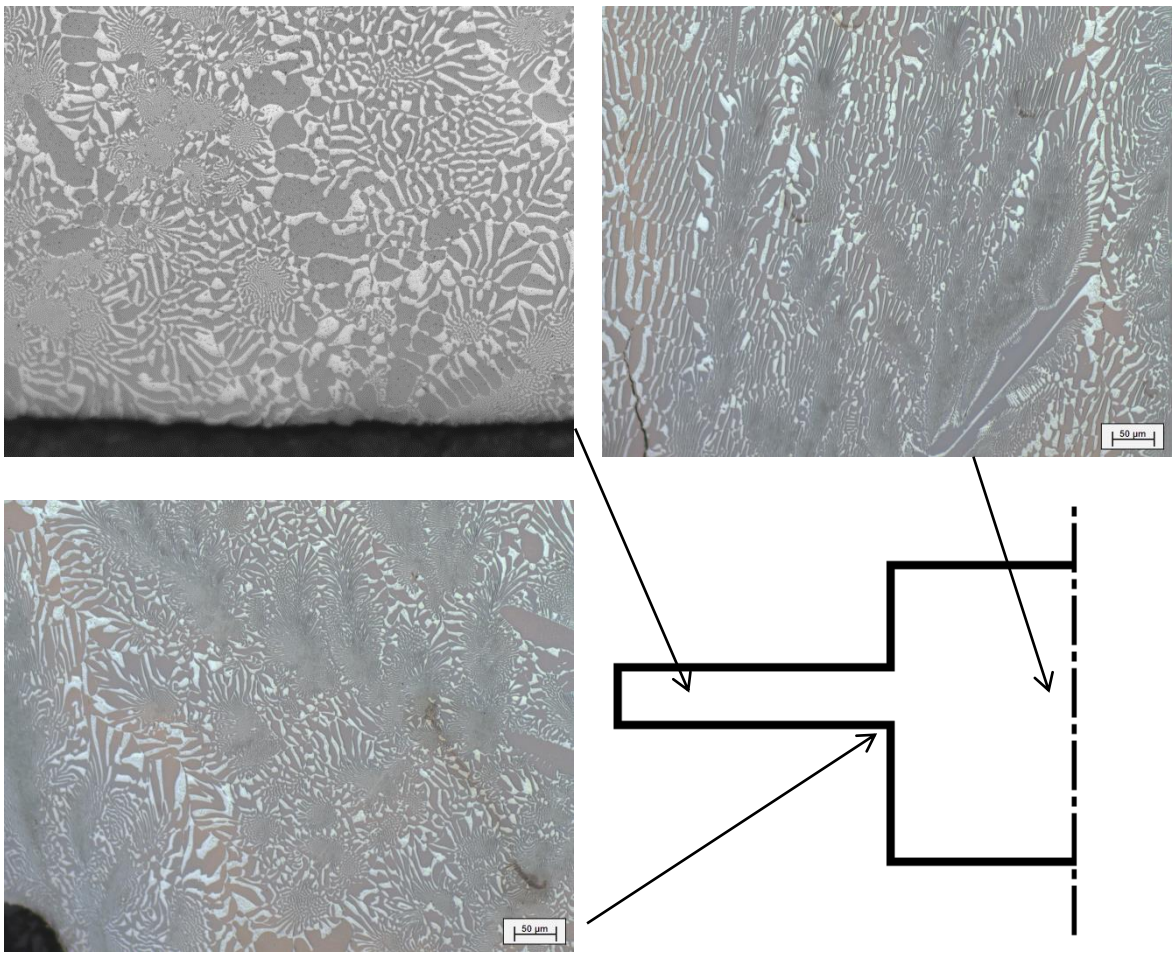

Figure 8-8: Struttura in diverse zone del provino, 200X

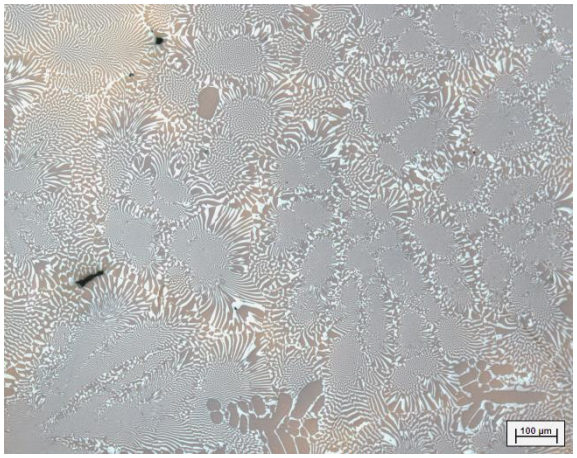

Figure 8-9: Sezione D del provino, 100X

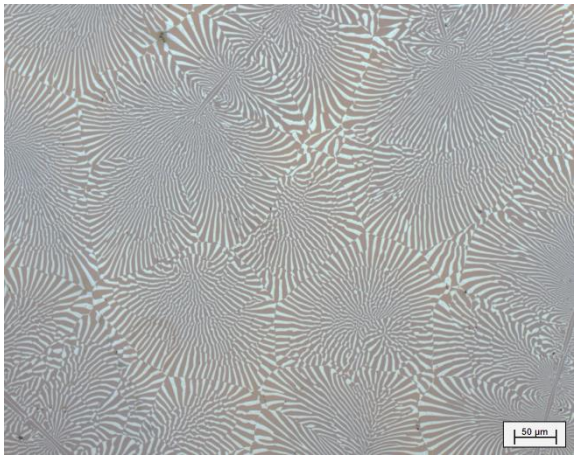

Figure 8-10: sezione A del provino, 200X

La sezione A è stata poi analizzata anche al microscopio elettronico, per avere una migliore visione a elevati ingrandimenti e analizzare le due fasi. Da quest'analisi si evince che le zone scure sono NiAl, mentre quelle chiare sono CrMo.

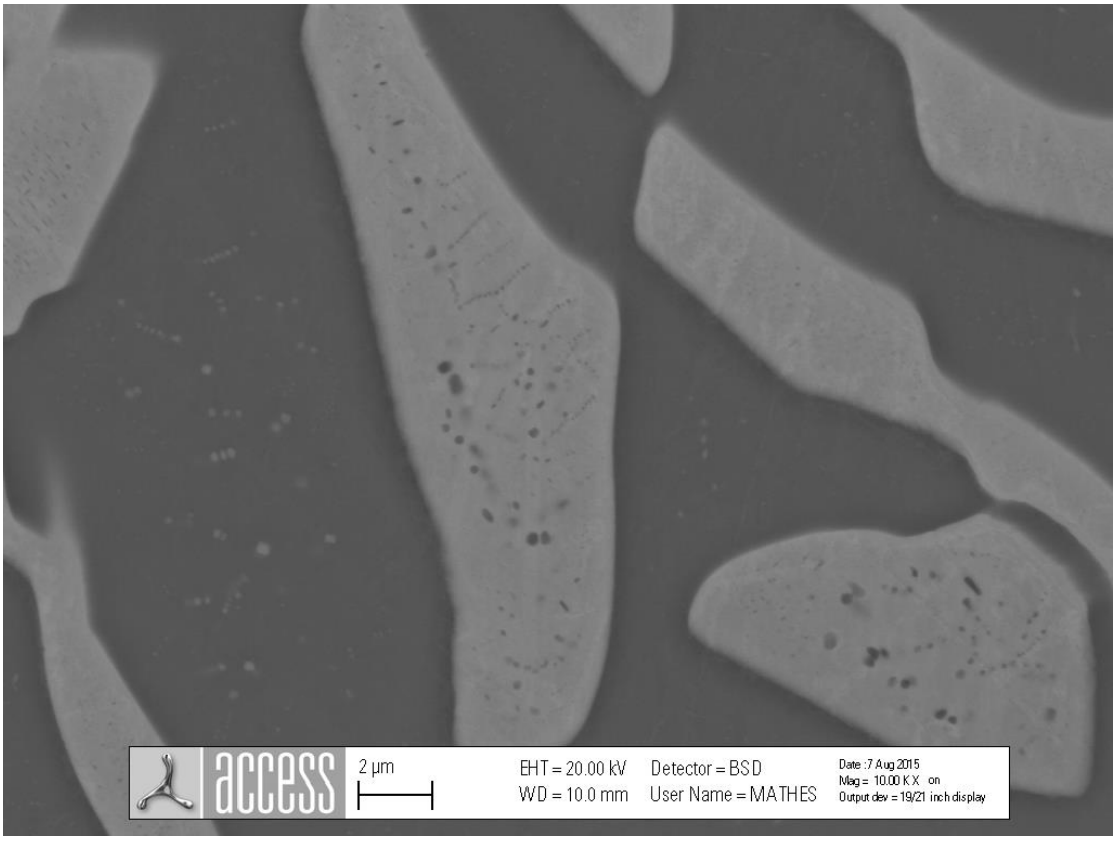

Figure 8-11: Struttura del taglio A visto al microscopio elettronico, ingrandimento 10000X

8.4.2 Simulazione

Con la simulazione saranno analizzate le temperature e la frazione solido/liquido durante la solidificazione del pezzo. La prima simulazione è stata condotta con gli stessi parametri della sperimentazione fisica, e attraverso l'analisi di questa saranno condotte altre simulazioni al fine di migliorare il processo.

Simulazione 1

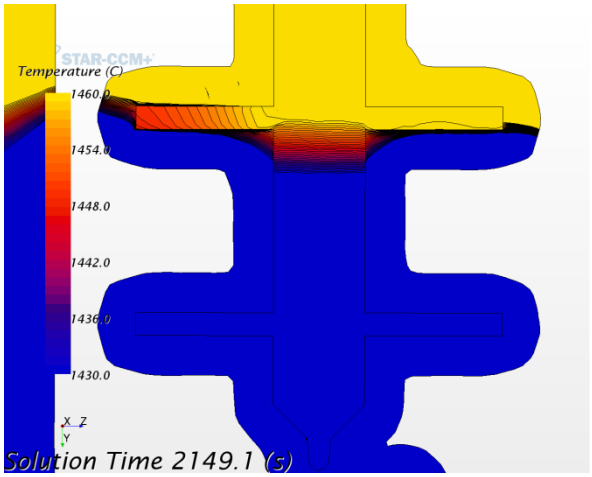

Figure 8-12: Campo di temperature durante la solidificazione

In questa prima simulazione è chiaro come la solidificazione nei bracci avvenga in direzione ortogonale a quella desiderata. Si nota dalla direzione delle isoterme in Figure 8-12. Nella parte centrale del provino invece il fronte di solidificazione è planare, anche se la mushy zone è piuttosto estesa e questo può portare a delle irregolarità della struttura. La differenza di raffreddamento tra il braccio destro e quello sinistro è dovuta alla presenza del riscaldatore sulla destra, e della colonna dello stampo sulla sinistra che porta a un effetto ombra che raffredda di più il braccio sinistro rispetto a quello destro.

Dopo questa simulazione, ne sono state condotte altre due mantenendo la stessa temperatura massima in camera calda ma variando la velocità di ritiro dello stampo, per verificare se utilizzando questo forno, era possibile migliorare il fronte di solidificazione. Questo non è stato possibile, sono state condotte quindi altre simulazioni con temperature nella camera calda più elevate. Tali prove sono quindi solo teoriche, dal momento che non è possibile effettuare un test fisico per verificare i risultati della simulazione.

Simulazione 2

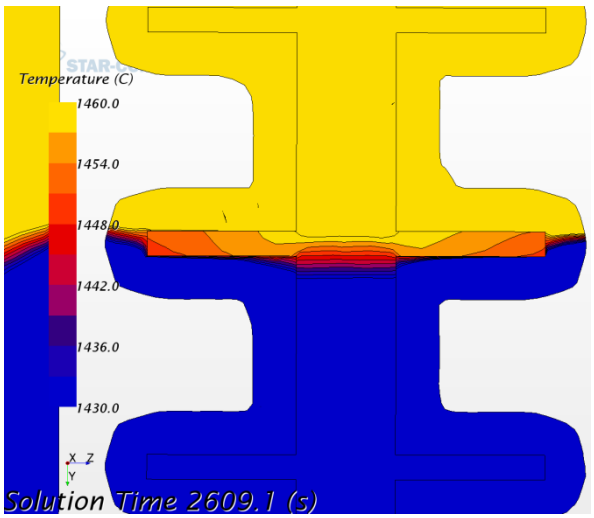

Figure 8-13: Simulazione condotta con temperatura massima di 1700 °C e velocità di ritiro di 3 mm/min

In questa seconda simulazione è stata utilizzata la stessa velocità di ritiro precedente, ma la temperatura è stata alzata da 1620 °C a 1700 °C. Come si vede dalla figura, il comportamento è già migliore, la mushy zone è più piccola e nei bracci si ha circa la stessa solidificazione sia a destra sia a sinistra. Anche se il comportamento è migliore, non è comunque quello desiderato e nei bracci non ci sarà sicuramente la struttura voluta.

Simulazione 3

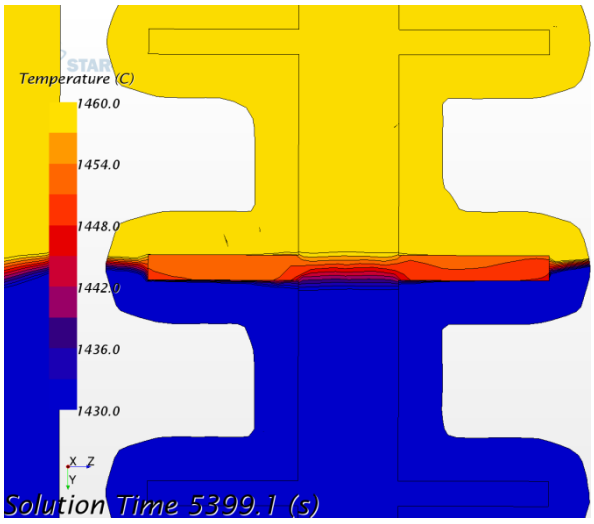

Figure 8-14: Simulazione condotta con temperatura massima di 1750 °C e velocità di ritiro di 1.5 mm/min

Per migliorare ancora il comportamento, la temperatura deve essere ulteriormente alzata. Facendo questo però si sposta anche la posizione del fronte di solidificazione rispetto al setto che divide la camera calda da quella fredda del forno. Più è alzata la temperatura della camera calda, e più la posizione di questo si abbassa, portando a un incurvamento del fronte di solidificazione. Per ottenerlo il più planare possibile, deve essere a metà tra le due camere. In questo caso, alzando la temperatura a 1750 °C, il fronte di solidificazione si abbassava troppo, la velocità di ritiro è stata così ridotta a 1.5 mm/min, per riportarlo nella posizione precedente. Il risultato è visibile in Figure 8-14, c'è un ulteriore miglioramento rispetto al caso precedente.

Simulazione 4

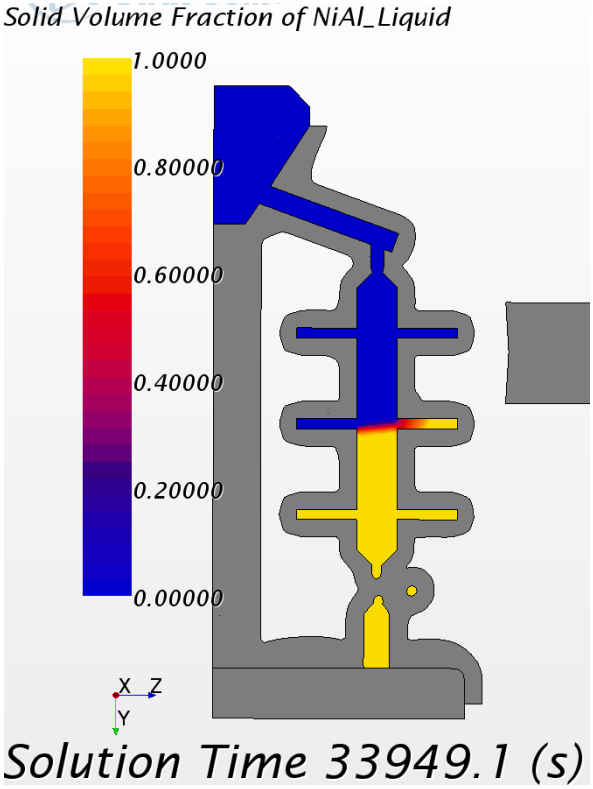

Figure 8-15: Simulazione ottenuta con temperatura massima di 2000 °C e velocità di ritiro di 0.3 mm/min

Come si nota il gradiente di temperatura nei bracci è molto più basso rispetto a quello nella zona centrale del provino, si nota perché la distanza tra due isoterme nei bracci è molto maggiore che nella parte centrale. Per migliorare questo comportamento, la mushy zone deve essere ridotta. In questa simulazione la temperatura massima allora viene alzata molto, portandola a 2000 °C, e di conseguenza anche la velocità di ritiro deve essere molto più bassa. È stata scelta una velocità di ritiro di 0.3 mm/min, ma come si vede dalla Figure 8-15 questa non è comunque sufficiente a garantire il posizionamento del fronte di solidificazione a metà tra le due camere. Per questo motivo, il fronte di solidificazione è anche notevolmente inclinato come si evince dalla figura.

8.5 Conclusioni e prospettive future

Test di sotto raffreddamento

È stato dapprima eseguito un test di sotto raffreddamento per valutare questa proprietà nel materiale. È stato trovato un valore medio di sottoraffreddamento di 23.9 ± 4.4 °C, valore piuttosto basso se comparato ad altre superleghe utilizzate per questo scopo. Questo non è altro che il livello di sottoraffreddamento cui può arrivare la lega prima di iniziare a nucleare. Un valore basso significa che se l'andamento delle temperature nel fronte di solidificazione è curvo, dove questo scende a valori inferiori al valore di sottoraffreddamento in quella zona può nucleare un nuovo cristallo. Si perde quindi il vantaggio di avere un materiale monocristallino.

Test di solidificazione direzionale

Scopo iniziale di questo lavoro era di ottenere un composito in-situ con una struttura lamellare perfettamente allineata nella direzione voluta. Per ottenere questo, sia il fronte di solidificazione a livello microscopico che quello a livello macroscopico avrebbero dovuto essere perfettamente planari. In realtà, dall'analisi al microscopio del provino si evince che il fronte di solidificazione a livello microscopico è del tipo cellulare, mentre quello macroscopico è planare nella zona centrale del provino, ma non lo è nei bracci. Questo porta a un certo curvamento delle lamelle, che quindi, anche se presentano una direzione preferenziale di crescita, non sono comunque perfettamente allineate come da requisito.

Simulazione e considerazioni finali

La prima simulazione conferma i risultati ottenuti dalla sperimentazione fisica, infatti, si vede chiaramente che nei bracci la solidificazione non avviene nella direzione voluta. Inoltre è presente una mushy zone elevata, che può portare a delle irregolarità nella struttura. Tramite le simulazioni successive, si è pensato che una possibile soluzione al problema sia di aumentare il gradiente di temperatura e di conseguenza diminuire la velocità di ritiro dello stampo. Sebbene questo possa portare a un miglioramento della struttura, ci sono due fattori da tenere in considerazione. Il primo è che un forno che possa garantire un elevato gradiente termico non esiste, per cui se queste leghe possono essere realizzate a livello industriale, servono maggiori sforzi nel campo della realizzazione di queste fornaci. Inoltre, la velocità di ritiro non può essere troppo bassa, perché se lo può essere in campo di ricerca per verificare la bontà delle assunzioni fatte, in campo industriale è richiesta una certa produttività che non può essere soddisfatta se il processo di realizzazione di questo materiale è troppo lungo.

Lo studio sarebbe molto più facile se a disposizione ci fosse un materiale perfettamente eutettico. In questo caso infatti la mushy zone non ci sarebbe, e probabilmente non sarebbe necessario troppo lavoro per raggiungere i giusti parametri di processo. Purtroppo, ottenere una composizione che sia perfettamente eutettica a livello industriale, è molto difficile ed è dovuto non solo al controllo della lega difficile quando le quantità di questa sono elevate, ma anche alla probabile presenza di impurità nel forno, negli stampi e all'interno della lega stessa.

Durante questo lavoro non sono stati compiuti test con differenti spessori dello stampo. Sperimentazioni di questo tipo possono essere molto interessanti, poiché uno spessore inferiore dello stampo significa un minore isolamento termico, per cui potrebbe essere più

facile raggiungere determinate condizioni senza grosse modifiche del processo. Un altro problema di questo processo è dovuto, come si nota dalle simulazioni, al differente gradiente termico presente nei bracci comparato a quello della parte centrale del provino. Inoltre, c'è da considerare che mentre nella parte centrale del provino la solidificazione avviene solo per crescita di un nucleo già solido, nei bracci si deve avere invece nucleazione e quindi crescita. Si può pensare di migliorare quest'aspetto raffreddando la parte inferiore dei bracci, potendoli così far nucleare in minore tempo. Uno stampo che contiene, però, un sistema di raffreddamento per la parte inferiore dei bracci è certamente molto costoso e laborioso da realizzare, ma potrebbe portare a dei vantaggi anche in termini di tempo di processo. Si tratta quindi di una possibile soluzione da studiare attentamente.